



TESIS DOCTORAL

**Aprendizaje automático para la predicción de
características de calidad de productos cárnicos
mediante técnicas de visión por computador en MRI**

JUAN PEDRO TORRES MUÑOZ

PROGRAMA DE DOCTORADO EN TECNOLOGÍAS INFORMÁTICAS (TIN)

Con la conformidad de los directores:

Andrés Caro Lindo

Maria Mar Ávila Vegas

Esta tesis cuenta con la autorización del director y codirectora de la misma y de la Comisión Académica del programa. Dichas autorizaciones constan en el Servicio de la Escuela Internacional de Doctorado de la Universidad de Extremadura

2024



TESIS DOCTORAL

**Aprendizaje automático para la predicción de
características de calidad de productos
cárnicos mediante técnicas de visión por
computador en MRI**

JUAN PEDRO TORRES MUÑOZ

PROGRAMA DE DOCTORADO EN TECNOLOGÍAS INFORMÁTICAS
(TIN)

2024

Agradecimientos institucionales

Este trabajo ha sido financiado con fondos de la Junta de Extremadura, Consejería de Economía e Infraestructuras, Fondo Europeo de Desarrollo Regional, mediante el Proyecto de Investigación IB16089: “Desarrollo de métodos no destructivos basados en ultrasonidos y algoritmos sobre Imágenes de Resonancia Magnética para evaluar la calidad de la carne de ternera y de cerdo ibérico”.

Agradecimientos personales

En primer lugar, agradecer al Grupo de Ingeniería de Medios, el cual ha hecho posible que empezara y terminara esta aventura. Gracias a todos los integrantes, tanto pasados como actuales con los que coincidí durante mi estancia como PCI. Gracias a todos ellos tanto por los ánimos, como por siempre mantener el buen humor. A mis directores de tesis Andrés y Mar, por conseguir que me embarcara en esta aventura y por confiar en que era posible llegar al final. Y no me olvido del amigo y vecino que no me dio la oportunidad de olvidarme del doctorado.

A mi familia, por apoyarme en todo momento y aguantarme durante mis mejores y peores momentos.

A la Escuela Politécnica de Cáceres, donde he pasado 9 años entre mi etapa en el grado, el máster y PCI. A todos los profesionales que despertaron en mí la curiosidad para seguir aprendiendo e investigando, aunque fuera por mi cuenta.

Y, por último, y mucho más importante, a mis amigos que me han acompañado durante todos estos años. Especialmente a Jorge y a Daniel, los que formamos un grupo en el que pese a cada uno seguir su camino, siempre hay tiempo para reunirse y planear alguna aventura juntos. Suerte para ellos también en sus respectivos doctorados, pues se puede llegar al final.

Y con esto se cierra el ciclo de estudiante, a ver qué depara el futuro...

ÍNDICE DE FIGURAS	IX
ÍNDICE DE TABLAS	X
RESUMEN	XII
1. INTRODUCCIÓN	14
1.1 Planteamiento y contextualización	14
1.2 Técnicas empleadas	17
1.2.1 Resonancia Magnética (MR)	17
1.2.2 Algoritmos de extracción de características de textura	17
1.2.2.1 Grey Level Co-occurrence (GLCM)	17
1.2.2.2 Neighboring Grey Level Dependence Matrix (NGLDM)	18
1.2.2.3 Level Run Length Matrix (GLRLM).....	19
1.2.2.4 Filtros de Gabor.....	21
1.2.2.5 Wavelets	21
1.2.2.6 One Point Fractal Texture Algorithm	22
1.2.2.7 Fractal Texture Algorithm (FTA).....	22
1.2.2.8 Classical Fractal Algorithm (CFA)	23
1.2.3 Algoritmos de aprendizaje automático.....	24
1.2.3.1 LM.....	24
1.2.3.2 Penalized	24
1.2.3.3 Support vector machine (SVM)	25
1.2.3.4 elmNNR	26
1.2.3.5 BART.....	26
1.2.3.6 BRNN.....	27
1.2.3.7 rqPen.....	28
1.2.3.8 Random Forest (RF)	29
1.2.3.9 M5P.....	29
1.2.3.10 Cubist.....	30
1.2.3.11 CForest.....	31
1.2.3.12 bagEarth.....	31

1.2.3.13 Earth.....	32
1.2.3.14 GAMBoost.....	33
1.3 Objetivos	34
1.4 Contribuciones. Justificación unitaria de la tesis doctoral.....	35
2. DISEÑO EXPERIMENTAL Y MATERIALES.....	41
2.1 Diseño experimental	41
2.2 Materiales.....	42
3. MÉTODOS	48
3.1 Artículo “A Computer-Aided Inspection System to Predict Quality Characteristics in Food Technology”	48
3.2. Artículo “MRI-computer vision on fresh and frozen-thawed beef: Optimization of methodology for classification and quality prediction”	62
3.3. Artículo “An experimental protocol to determine quality parameters of dry-cured loins using low-field Magnetic Resonance Imaging”	74
4. RESULTADOS Y DISCUSIÓN.....	83
4.1 Resultados del artículo “A Computer-Aided Inspection System to Predict Quality Characteristics in Food Technology”	83
4.2 Resultados del artículo “An experimental protocol to determine quality parameters of dry-cured loins using low-field Magnetic Resonance Imaging”	92
4.3 Resultados del artículo “MRI-computer vision on fresh and frozen-thawed beef: Optimization of methodology for classification and quality prediction”.....	100
5. CONCLUSIONES	108
REFERENCIAS.....	110

Índice de Figuras

Figura 1.1. Ejemplo filtros de Gabor. <i>Fuente: researchgate.</i>	21
Figura 2.1 Diseño experimental del sistema propuesto.....	42
Figura 2.2. Imagen MRI de un lomo de cerdo curado.	43
Figura 2.3. Región de interés de un lomo de cerdo curado.	43
Figura 2.4. Imagen MRI de un lomo de ternera fresco.	43
Figura 2.5. Imagen MRI de un lomo descongelado de ternera(izquierda) y cerdo(derecha).	44
Figura 4.1. Porcentaje de votos de cada regresor.	84
Figura 4.2. Distribución de los mejores regresores(a) y los mejores extractores(b).	88
Figura 4.3. Distribución de los mejores regresores(a) y los mejores extractores(b), de acuerdo a los grupos de extractores.....	89
Figura 4.4. Correlaciones para las mejores combinaciones.....	90
Figura 4.5. Implementación del protocolo experimental evaluado en este estudio.	93
Figura 4.6. Valores medios, desviación estándar y p-values entre los valores reales y GLCM y real y OPFTA.....	98
Figura 4.7. Biplot del análisis de componentes principales de los parámetros físico-químicos.	101
Figura 4.8. Imágenes MRI de un lomo de ternera fresco (A) y descongelado (B).	102
Figura 4.9. Coeficientes de correlación para las predicciones de parámetros fisicoquímicos en lomos frescos de ternera.	104
Figura 4.10. Coeficientes de correlación para las predicciones de parámetros fisicoquímicos, textura instrumental y parámetros sensoriales en lomos de ternera cocinados.....	107

Índice de Tablas

Tabla 1.1. Características GLCM.....	18
Tabla 1.2. Características NGLDM.....	19
Tabla 1.3. Características GLRLM.....	20
Tabla 1.4. Características OPFTA.....	22
Tabla 1.5. Características FTA.....	23
Tabla 1.6. Parámetros algoritmo LM.....	24
Tabla 1.7. Parámetros algoritmo Penalized.....	25
Tabla 1.8. Parámetros algoritmo SVM.....	25
Tabla 1.9. Parámetros algoritmo elmNNR.....	26
Tabla 1.10. Parámetros algoritmo BART.....	27
Tabla 1.11. Parámetros algoritmo BRNN.....	27
Tabla 1.12. Parámetros algoritmo rqPen.....	28
Tabla 1.13. Parámetros algoritmo RF.....	29
Tabla 1.14. Parámetros algoritmo M5P.....	30
Tabla 1.15. Parámetros algoritmo Cubist.....	30
Tabla 1.16. Parámetros algoritmo CForest.....	31
Tabla 1.17. Parámetros algoritmo bagEarth.....	32
Tabla 1.18. Parámetros algoritmo Earth.....	32
Tabla 1.19. Parámetros algoritmo GAMBoost.....	33
Tabla 2.1. Características de calidad de productos cárnicos.....	45
Tabla 2.2. Características computacionales.....	47
Tabla 4.1. Ranking de regresores.....	85
Tabla 4.2. Coeficientes de correlación para lomos de cerdo.....	86
Tabla 4.3. Coeficientes de correlación para lomos de ternera.....	86
Tabla 4.4. Mejores combinaciones de regresores-algoritmo extractor.....	87
Tabla 4.5. Correlaciones para las mejores combinaciones.....	90
Tabla 4.6. Correlaciones para las mejores combinaciones.....	91
Tabla 4.7. Comparación entre valores fisicoquímicos y los valores predichos de GLCM y OPFTA.....	94

Tabla 4.8. Comparación entre valores fisicoquímicos y los valores predichos de GLCM y OPFTA.....	95
Tabla 4.9. Ecuaciones de predicción de los parámetros de calidad para lomos usando el regresor LM.....	96
Tabla 4.10. Ecuaciones de predicción de los parámetros de calidad para lomos usando el regresor LM.....	99
Tabla 4.11. Resultados de la clasificación de los lomos frescos y descongelados por diferentes combinaciones de algoritmos.	103

Resumen

En las últimas décadas se ha puesto en evidencia la importancia de la investigación en técnicas no destructivas aplicadas a la industria alimentaria. Estas técnicas permiten evaluar propiedades relacionadas con la calidad de productos cárnicos sin causar daños ni efectos secundarios en los productos. Esto es fundamental en la industria cárnica, garantizando la seguridad en el consumo de las muestras en etapas posteriores. En esta tesis se propone un sistema para predecir las características físico-químicas, textura instrumental y características sensoriales sin destruir las piezas cárnicas, en este caso lomos de cerdo y de ternera. Además de la predicción, se realizará una clasificación de lomos según su procedencia.

Para ello, se han utilizado imágenes obtenidas mediante resonancia magnética utilizando un escáner de bajo campo. Los productos cárnicos utilizados para los experimentos incluyeron lomos de cerdo alimentados con pienso, lomos de cerdo alimentados con bellota y lomos de ternera. Además, se evaluó el efecto de congelar y descongelar dichos lomos. Se obtuvieron imágenes de resonancia magnética de los lomos frescos, de lomos tras ser congelados y descongelados (para evaluar el efecto de congelación y descongelación sobre los lomos), también tras cocinar los lomos y, en el caso de los lomos de cerdos, tras el proceso de curar los lomos.

Se han aplicado, varios métodos de extracción de características sobre las imágenes de resonancia magnética. En concreto, 8 métodos de análisis de textura agrupados en cuatro tipos (3 algoritmos clásicos, algoritmo de Gabor, algoritmo de Wavelet y 3 algoritmos de fractales). Y se han evaluado diferentes técnicas de aprendizaje automático, seleccionando los 14 regresores con mejor rendimiento en comparación con resultados obtenidos en investigaciones previas. Se obtuvieron diferentes combinaciones de algoritmo extractor – algoritmo de aprendizaje automático para cada una de las características de calidad.

Con la idea de realizar las predicciones de forma óptima con la mejor combinación para cada característica, se ha desarrollado un modelo *ensemble learning* que combina los métodos de extracción de características y las 14 técnicas de aprendizaje automático (regresores) para predecir cada una de las características de calidad de forma óptima, identificando la mejor combinación de algoritmo extractor – algoritmo de aprendizaje automático para cada característica de calidad.

Finalmente, se han obtenido resultados complementarios mediante la creación de volúmenes de interés (VOI) como paso previo a la aplicación de técnicas de análisis de imágenes y aprendizaje automático, explorando la posibilidad de obtener información adicional en el interior de estos volúmenes. O como la propuesta de un protocolo experimental para la adquisición óptima de las imágenes de resonancia magnética, dado que cuanto más optimizado sea el proceso de generar las imágenes sobre las que se aplican los algoritmos de extracción de características, mejores resultados se obtendrán en las predicciones y clasificación al aplicar las técnicas de aprendizaje automático.

Capítulo 1

1. Introducción

1.1 Planteamiento y contextualización

En las últimas décadas se ha puesto en evidencia la importancia de la investigación en técnicas no destructivas aplicadas a la industria de la alimentación en general, y a la cárnica en particular, desde múltiples puntos de vista [1][2][3][4]. En general, la investigación en técnicas no destructivas es interesante para garantizar la calidad y seguridad de los productos alimentarios. Estas técnicas pueden permitir evaluar propiedades relacionadas con la calidad de productos cárnicos sin causar daños ni efectos secundarios, lo que es especialmente importante en la industria cárnica, donde la integridad de los productos es fundamental para su posterior consumo. La posibilidad de estudiar productos cárnicos de forma inocua para la salud del consumidor, sin alterar la integridad física ni química de los productos estudiados, es un factor de interés a la hora de proponer alternativas no destructivas a los actuales procesos de evaluación de la calidad de productos cárnicos. A ello se une la reducción de muestras desechadas como consecuencia de la realización de pruebas destructivas. La posibilidad de disponer de técnicas de análisis no destructivo implicará una disminución considerable de muestras descartadas para la comercialización, evitando pérdidas significativas en la evaluación de productos cárnicos a la hora de realizar pruebas de calidad, por ejemplo.

Además de que las técnicas no destructivas pueden resultar de utilidad en cuanto al cumplimiento normativo relacionado con regulaciones, estándares de calidad y normativas de seguridad de la industria alimentaria, el hecho de emplear metodologías y procedimientos

objetivos implica que estas técnicas generarán datos precisos y confiables. Actualmente, las técnicas habituales de evaluación de características de calidad alimentaria son destructivas y suponen procesos bastante tediosos, monótonos y repetitivos, con tiempos de espera elevados hasta la obtención de resultados mediante pruebas físico-químicas y sensoriales [5][6]. Los métodos no destructivos generan datos objetivos, y pueden gestionar de forma efectiva y eficiente la obtención de parámetros de calidad. El hecho de proponer procedimientos no destructivos que permitan la monitorización y evaluación de los procesos de producción alimentaria, sin interferir en ellos, también puede permitir mejorar y optimizar la eficiencia en la producción de alimentos. Cuestiones como la mejora en la trazabilidad alimentaria también pueden verse mejoradas con la aplicación de técnicas no destructivas, dado que es posible realizar un seguimiento más preciso desde las fases de producción del producto hasta su consumo.

Desde principios del siglo XXI, el uso de imágenes de resonancia magnética (MRI) ha presentado un campo de estudio en investigaciones científicas, en combinación con técnicas de análisis de imagen aplicado a la industria cárnica [10][11][12][13][15][16][17]. La MRI, además de resultar una técnica no invasiva e inocua para el posterior consumo de los productos cárnicos, proporciona imágenes detalladas del interior de la carne sin dañarla, lo que permite evaluar la calidad de la carne en términos de textura, distribución de grasa, y otros aspectos relevantes.

La generación de datasets que contengan características de calidad en tecnología de los alimentos, generadas a partir de técnicas no destructivas (sobre imágenes MRI, por ejemplo) y que también contengan características obtenidas mediante técnicas tradicionales (destructivas) es un punto muy importante en cualquier investigación. Esto permite contrastar resultados obtenidos mediante técnicas no destructivas, en relación con los mismos resultados obtenidos mediante las técnicas habituales en tecnología de los alimentos. Cualquier algoritmo de aprendizaje automático precisa de estos datasets, en las versiones de algoritmos de aprendizaje supervisado. Por tanto, en investigación, la elaboración de conjuntos de datos que combinen datos obtenidos tanto de técnicas no destructivas como de técnicas tradicionales puede considerarse como un avance importante.

Para realizar la extracción de características sobre imágenes de productos cárnicos, existen diferentes técnicas, como son las basadas en algoritmos de texturas clásicos: Grey

Level Co-occurrence Matrix (GLCM) [18][19], Neighboring Grey Level Dependence Matrix (NGLDM) [20][21], y Level Run Length Matrix (GLRLM) [22][23]; las técnicas basadas en filtros Gabor [24] o en transformadas wavelets [25], o algoritmos basados en fractales [26], etc. De esta forma, es posible elaborar datasets generados mediante algoritmos de visión por computador. El hecho de usar diferentes algoritmos de extracción de características fomenta la diversidad de datos, ya que los datos generados por técnicas diferentes pueden tener características específicas y complejas. El uso de técnicas variadas de extracción de características permite obtener diferentes aspectos de los datos, mejorando la representación, la robustez y la generalización. Además, con ello también se reduce el sesgo y la variabilidad, algo inherente a cualquier enfoque específico, mejorando de este modo la robustez de los modelos y su capacidad para enfrentarse a situaciones diferentes.

De igual modo, la aplicación de diferentes algoritmos de aprendizaje automático también puede considerarse como un enfoque que permite diversificar los modelos aplicados, obteniendo resultados en base a distintos y muy diferentes algoritmos [7][8][9]. De nuevo, ello influye en la generación de resultados diversos, cuya coincidencia en las estimaciones realizadas por métodos distintos implicará una clara robustez en las conclusiones obtenidas, además de permitir una comparación de rendimiento en cuanto a la evaluación de las diferentes técnicas propuestas, permitiendo una selección de las técnicas más efectivas, eficientes y adecuadas a cada situación. Este aspecto es crucial en aplicaciones industriales, donde la elección de las mejores herramientas en aplicaciones prácticas en uno de los objetivos fundamentales. Disponer de varias técnicas de extracción de características y de aprendizaje automático puede redundar en un incremento de la eficiencia, en el sentido de que es posible que una combinación de técnicas funcione de manera óptima en términos de precisión, mientras que otra combinación sea más eficiente computacionalmente, por ejemplo. De nuevo, en aplicaciones industriales, la propuesta de una combinación de técnicas adecuadas puede depender de restricciones de recursos, de tiempo, de necesidades especiales, etc.

En esta tesis doctoral se presenta un estudio exhaustivo del rendimiento de conocidos algoritmos de extracción de características sobre imágenes MRI. Estos algoritmos se combinan con catorce algoritmos diferentes de aprendizaje automático, que incluyen los más habituales en la literatura científica y algunos otros seleccionados para estudiar su

rendimiento. Como se ha comentado, el objetivo sería identificar la mejor combinación de algoritmo extractor – algoritmo de aprendizaje automático para cada característica de calidad.

1.2 Técnicas empleadas

1.2.1 Resonancia Magnética (MR)

La resonancia magnética es una técnica no invasiva de obtención de imágenes médicas que utilizan un campo magnético y ondas de radio generadas por computadora para crear imágenes detalladas de los órganos y de los tejidos del cuerpo. La mayoría de los aparatos de resonancia magnética son grandes imanes en forma de tubo. Cuando se realiza una resonancia magnética, el campo magnético realinea temporalmente las moléculas de agua en tu cuerpo. Las ondas de radio hacen que los átomos alineados produzcan señales muy débiles, que se usan para crear imágenes transversales de resonancia magnética.

Es usada principalmente en medicina para observar alteraciones en los tejidos y detectar patologías. También es utilizada industrialmente para analizar la estructura de materiales tanto orgánicos como inorgánicos.

A diferencia de la tomografía axial computerizada (TAC), no usa radiación ionizante, sino campos magnéticos para alinear la magnetización nuclear de los núcleos de hidrógeno del agua en la muestra. Estos núcleos resuenan a una frecuencia proporcional al campo magnético ejercido de forma que se puede aplicar un campo de radiofrecuencia.

1.2.2 Algoritmos de extracción de características de textura

1.2.2.1 Grey Level Co-occurrence (GLCM)

Es un algoritmo de extracción de características clásico, que se basa en técnicas estadísticas que obtienen características estadísticas de segundo orden. GLCM [18], [19] considera la posibilidad de alcanzar el mismo nivel de gris a diferentes distancias y orientación (0° , 45° , 90° , 135° , 180° , 225° , 270° y 315°). De esta forma se extraen diez características de

texturas: Energía (ENE), Entropía (ENTR), Correlación (COR), Correlación de Haralick (HC), Momento diferencial inverso (IDM), Inercia (INE), Grupos de baja luminosidad (CS), Grupos de alta luminosidad (CP), Contraste (CON) y Disimilaridad (DIS).

Tabla 1.1. Características GLCM.

Característica	Estadísticas
Energía	$\sum_i \sum_j P(i,j)^2$
Entropía	$-\sum_i \sum_j P(i,j) \log(P(i,j))$
Correlación	$\frac{\sum_i \sum_j (i - \mu_x)(j - \mu_y)P(i,j)}{\sigma_x \sigma_y}$
Correlación de Haralick	$\frac{\sum_i \sum_j (i,j)P(i,j) - \mu_x \mu_y}{\sigma_x \sigma_y}$
Momento diferencial inverso	$\sum_i \sum_j \frac{P(i,j)}{1 + (i - j)^2}$
Inercia	$\sum_i \sum_j (i - j)^2 \cdot P(i,j)$
Grupos de baja luminosidad	$\sum_i \sum_j ((i - \mu_x) + (j - \mu_y))^3 \cdot P(i,j)$
Grupos de alta luminosidad	$\sum_i \sum_j ((i - \mu_x) + (j - \mu_y))^4 \cdot P(i,j)$
Contraste	$\sum_i \sum_j (i - j)^2 \cdot (P(i,j))^2$
Disimilaridad	$\sum_i \sum_j (i + 1) - (j + 1) \cdot P(i,j)$

1.2.2.2 Neighboring Grey Level Dependence Matrix (NGLDM)

Este algoritmo utiliza características angulares independientes, considerando la relación entre un elemento y todos los elementos vecinos de una vez. En este método, la vecindad es

un cuadrado, la dimensión del cuadrado es 3×3 y la distancia d ($d = 1$) entre los píxeles vecinos. Este proceso elimina la dependencia angular mientras que simultáneamente reduce el número de cálculos requeridos para procesar una imagen. Se basa en el supuesto de que la matriz de dependencia espacial de nivel de grises de una imagen puede especificar adecuadamente la información de textura de dicha imagen. De estos resultados se consideran cinco medidas: SNE (énfasis en números pequeños), LNE (énfasis en números grandes), NNU (No uniformidad de números), SM (Segundo momento) y ENT (Entropía).

Tabla 1.2. Características NGLDM.

Característica	Estadísticas
SNE	$\sum_j \sum_i \frac{R(j, i)}{i^2}$
LNE	$\sum_j \sum_i i^2 R(j, i)$
NNU	$\sum_j \left(\sum_i R(j, i) \right)^2$
SM	$\sum_j \sum_i (R(j, i))^2$
ENT	$-\sum_j \sum_i R(j, i) \log(R(j, i))$

1.2.2.3 Level Run Length Matrix (GLRLM)

Este algoritmo se basa en analizar la longitud y el nivel de gris de las hileras (secuencias) de píxeles homogéneas de la imagen, siendo una hilera una secuencia de píxeles consecutivos y colineales que tienen el mismo nivel de gris. Una gran cantidad de píxeles vecinos con el mismo nivel de gris representan una textura gruesa, un número pequeño indica una textura fina. Este algoritmo crea una matriz que cuenta el número de hileras de cada longitud y nivel de gris, y a partir de ella se calculan 11 características, que pueden darnos una idea de la distribución y la variación de las hileras en la imagen.

Tabla 1.3. Características GLRLM.

Característica	Estadísticas
LRE	$\frac{\sum_i \sum_j Q(i,j)j^2}{\sum_i \sum_j Q(i,j)}$
SRE	$\frac{\sum_i \sum_j \left(\frac{Q(i,j)}{j^2}\right)}{\sum_i \sum_j Q(i,j)}$
GLNU	$\frac{\sum_i (\sum_j Q(i,j))^2}{\sum_i \sum_j Q(i,j)}$
RLNU	$\frac{\sum_j (\sum_i Q(i,j))^2}{\sum_i \sum_j Q(i,j)}$
RPC	$\frac{\sum_j \sum_i Q(i,j)}{L}$
LGRE	$\frac{\sum_i \sum_j \left(\frac{Q(i,j)}{i^2}\right)}{\sum_i \sum_j Q(i,j)}$
HGRE	$\frac{\sum_i \sum_j i^2 Q(i,j)}{\sum_i \sum_j Q(i,j)}$
SRLGE	$\frac{\sum_i \sum_j \left(\frac{Q(i,j)}{i^2 j^2}\right)}{\sum_i \sum_j Q(i,j)}$
SRHGE	$\frac{\sum_i \sum_j \left(\frac{i^2 Q(i,j)}{j^2}\right)}{\sum_i \sum_j Q(i,j)}$
LRLGE	$\frac{\sum_i \sum_j \left(\frac{j^2 Q(i,j)}{i^2}\right)}{\sum_i \sum_j Q(i,j)}$
LRHGE	$\frac{\sum_i \sum_j i^2 j^2 Q(i,j)}{\sum_i \sum_j Q(i,j)}$

Las características son las siguientes: SRE (Énfasis de las hileras más cortas), LRE (Énfasis de las hileras más largas), GLNU (No uniformidad del nivel de gris de las hileras), RLNU (No uniformidad de longitud de hileras), RPC (Porcentaje de hileras), LGRE (Énfasis de hileras de bajo nivel de gris), HGRE (Énfasis de hileras de alto nivel de gris), SRLGE (Énfasis de bajos niveles de gris en hileras cortas), SRHGE (Énfasis de altos niveles de gris).

en hileras cortas), LRLGE (Énfasis de bajos niveles de gris en hileras largas) y LRHGE (Énfasis de altos niveles de gris en hileras largas).

1.2.2.4 Filtros de Gabor

Este algoritmo que se emplea se basa en una técnica espectral que utiliza 6 ángulos y 3 frecuencias diferentes para tratar las imágenes; una vez realizado el proceso se calcula la media y la varianza de dichas imágenes. Esto genera 36 características en cada dimensión, lo que proporciona 72 características para cada imagen.

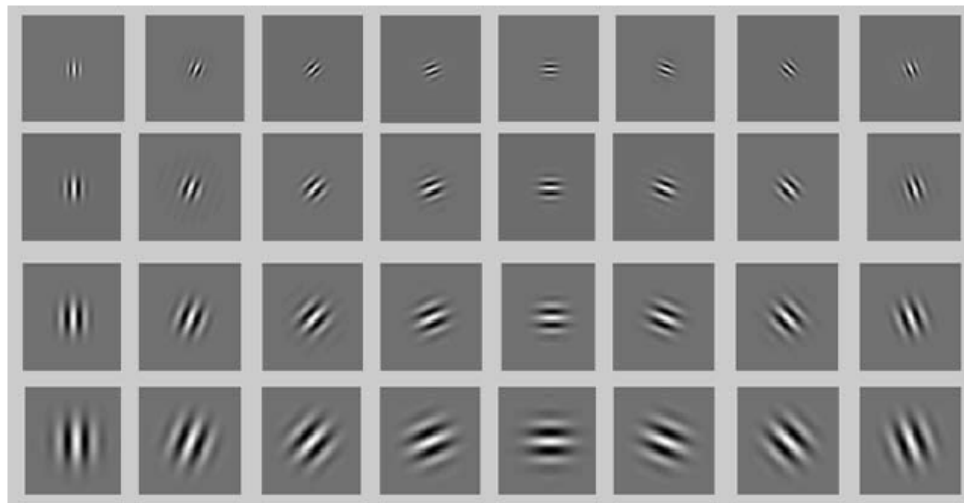


Figura 1.1. Ejemplo filtros de Gabor. *Fuente: researchgate.*

1.2.2.5 Wavelets

Se utiliza un algoritmo basado en las transformadas Wavelet, extrayendo características espectrales basadas en las Transformada Discreta Wavelet (DWI). Durante este proceso las imágenes son descompuestas utilizando filtros de paso bajo y paso alto aplicando filtros recursivamente sobre las imágenes. El algoritmo seleccionado para realizar la descomposición utiliza 3 escalas y 6 direcciones, considerando tres valores en cada escala (media, ángulo y varianza) obteniendo un total de 54 características de cada imagen.

1.2.2.6 One Point Fractal Texture Algorithm

Este algoritmo desarrollado en [61] refleja el número de veces que un patrón se replica en cada imagen, dependiendo del tamaño de la caja dentro de la imagen. Dado que este valor es representativo del contenido de la imagen se extraerán siete características computacionales de él.

Tabla 1.4. Características OPFTA.

Característica	Estadísticas
Uniformidad	$\sum_i \sum_j P(i,j)^2$
Entropía	$\sum_i \sum_j P(i,j) \cdot \log_{10}(P(i,j))$
Correlación	$\frac{\sum_i \sum_j (i - \mu_x)(j - \mu_y)P(i,j)}{\sigma_x \sigma_y}$
Homogeneidad	$\frac{\sum_i \sum_j P(i,j)}{1 + (i - j)^2}$
Inercia	$\sum_i \sum_j (i - j)^2 P(i,j)$
Contraste	$\sum_i \sum_j (i - j)^2 (P(i,j))^2$
Eficiencia	$\frac{\sigma_x}{\mu_x} + \frac{\sigma_y}{\mu_y}$

1.2.2.7 Fractal Texture Algorithm (FTA)

Este algoritmo se basa en las características que son obtenidas por una variante del algoritmo de Minkowski-Bouligand. Las características reflejan el número de veces que un patrón se repite en una imagen dependiendo del tamaño de la caja seleccionado. Para cada vector de características se calculan las diez características siguientes:

Tabla 1.5. Características FTA.

Característica	Estadísticas
Uniformidad	$\sum_{i=0}^n F_i^2$
Entropía	$\sum_i (F_i \cdot \log_{10}(F_i))$
Correlación	$\sum_i (i - \mu) \cdot F_i$
Momento diferencial inverso	$\sum_i \frac{F_i}{1 + i^2}$
Inercia	$\sum_i F_i \cdot i^2$
Contraste	$\sum_i F_i^2 \cdot i^2$
Énfasis	$\sum_i \frac{F_i}{i^2}$
Correlación de Jorna	$\sum_i (i - \mu)^2 \cdot F_i$
Grupos de baja luminosidad	$\sum_i (i - \mu)^3 \cdot F_i$
Grupos de alta luminosidad	$\sum_i (i - \mu)^4 \cdot F_i$

1.2.2.8 Classical Fractal Algorithm (CFA)

Este es el algoritmo clásico y más extendido para la extracción de características, el cual es una implementación del algoritmo de Minkowski-Bouligand. De la ejecución de este algoritmo se obtiene una única característica para cada tamaño de caja. En esta tesis se calcula para 9 tamaños de caja.

$$D = -\frac{\Delta \ln N}{\Delta \ln R}$$

1.2.3 Algoritmos de aprendizaje automático

Para el desarrollo de esta tesis se han utilizado 14 regresores para predecir características de calidad de los productos cárnicos.

1.2.3.1 LM

El regresor más básico que se puede encontrar, este regresor LM [43] genera un modelo lineal en el que contamos con una variable dependiente Y, y un conjunto de variables explicativas X: x, x, x, x, ... x. Siendo el objetivo de este modelo la obtención de una combinación lineal tal que:

$$Y = \beta_0 + \beta_1 x_1 + \beta_2 x_2 \dots \beta_k x_k$$

En este caso se ha utilizado la implementación en R, la cual nos permite configurar los siguientes parámetros:

Tabla 1.6. Parámetros algoritmo LM.

Parámetro	
formula	Fórmula que se utilizará para modelar la regresión.
data	Dataframe con todos los datos sobre los que se quiere realizar la regresión.
subset	Vector para especificar las observaciones para ajustar el modelo.
weights	Vector de pesos iniciales del modelo. Opcional.
offset	Usado para incluir a priori una componente en el modelo. Opcional.

1.2.3.2 Penalized

El regresor Penalized genera un modelo lineal en el que se cuenta con una variable Y, y un conjunto de variables explicativas X: x, x,...x, siendo el objetivo de este modelo la optimización de la función:

$$y = \text{probabilidad} + \text{penalización}$$

Este regresor actúa de forma diferente a los regresores anteriores, los cuales solamente optimizan la probabilidad de los resultados.

La implementación utilizada para los experimentos llevados a cabo en esta tesis utiliza la implementación en R, la cual tiene los siguientes parámetros:

Tabla 1.7. Parámetros algoritmo Penalized.

Parámetro	
response	Variable de respuesta que indicará el tipo de regresión.
penalized	Variable sobre la cual se realizarán las penalizaciones.
unpenalized	Variables sobre las que no se aplicarán las penalizaciones.
lambda1	Penalización L1, puede ser un valor positivo (aplicado a todas las variables) o un vector (penalizaciones individuales por variables).
lambda2	Penalización L2, puede ser un valor positivo (aplicado a todas las variables) o un vector (penalizaciones individuales por variables).
data	Dataframe con todos los datos a utilizar.
fusedl	Bandera para activar el tipo de regresión fussed lasso.

1.2.3.3 Support vector machine (SVM)

El regresor Support Vector Regression es un modo de ejecución del SVM, el cual se basa en el funcionamiento de las máquinas de vectores de soporte las cuales son un conjunto de algoritmos de aprendizaje supervisado.

Tabla 1.8. Parámetros algoritmo SVM.

Parámetro	
formula	Fórmula que se utilizará para realizar la regresión.
data	Dataframe con todos los datos que se van a utilizar.
type	Este regresor puede ser utilizado para regresiones, clasificaciones o detección de novedades. Este flag permite seleccionar el modo de ejecución.
kernel	Kernel utilizado a la hora de entrenar y predecir.
cross	Valor entero que indica el número de veces que se realizará la validación cruzada.

Para los experimentos se ha utilizado la implementación presente en el paquete e1071 disponible en el gestor de paquetes CRAN. Dicha implementación utiliza los parámetros mostrados en la tabla 1.8.

1.2.3.4 elmNNR

Extreme Learning Machine es un regresor que se basa en el funcionamiento de las redes neuronales de propagación hacia delante que pueden utilizarse para clasificación, regresión, agrupación y algunos usos más.

Para los experimentos se utilizó la implementación presente en el paquete elmNNRcpp de R, el cual es una reimplementación del paquete elmNN que fue descatalogado. Dicha implementación cuenta con los siguientes parámetros:

Tabla 1.9. Parámetros algoritmo elmNNR.

Parámetro	
x	Variables de entrada.
y	Matriz con los resultados.
nhid	Número de neuronas ocultas; debe ser mayor que 1. Debe ser especificado siempre; para los experimentos se utilizó el valor empírico de 500.
actfun	Cadena para indicar el tipo de activación de las neuronas. Debe ser una de las siguientes: “sig”(sigmoid), “sin”(sine), “radbas”(radial basis), “hardlim”(hard-limit), “hardlims”(symmetric hard-limit), “satlins”(satlins), “tansig”(tan-sigmoid), “tribas”(triangular basis), “relu”(rectifier linear unit) o “purelin”(linear).
Init_weights	Cadena para indicar la distribución de la que se tomarán los pesos iniciales y las bias. Deberá ser una de las siguientes: “normal gaussian”(rango [0,1]), “uniform positive”(rango [0,1]) o “uniform negative”(rango [-1,1]).
bias	Verdadero o Falso. En el caso de verdadero se añadirá un valor bias a las neuronas ocultas.
seed	Valor numérico para iniciar la semilla del generador de números aleatorios.

1.2.3.5 BART

El Regresor BartMachine (Bayesian Additive Regression Trees) de R, genera una regresión basada en árboles bayesianos. Se ha utilizado el paquete de R con el mismo nombre.

Este regresor es capaz de realizar tanto regresión, como clasificación, basándose en el tipo de datos de entrada a la hora de construir el modelo. En este experimento se ha utilizado la funcionalidad de regresión con los siguientes parámetros:

Tabla 1.10. Parámetros algoritmo BART.

Parámetro	
x	Variable que indica los valores sobre los que hacer la regresión.
y	Variable que indica los resultados de la regresión. Se emplea para decidir entre clasificación y regresión.
num_trees	Número de árboles a generar que se utilizarán a la hora de realizar la suma de resultados.
alpha	Base del hiperparámetro de los árboles para determinar si es un nodo hoja o no.
beta	Potencia del hiperparámetro de los árboles para determinar si es un nodo hoja o no.
k	Para regresiones, determina la probabilidad a priori de que $E(Y X)$ esté contenida en el intervalo (y_{min},y_{max}), basándose en una distribución normal. Para clasificación, determina la probabilidad a priori de que $E(Y X)$ este contenida en el intervalo (-3,3).
nu	Grados de libertad para la inversa de X^2 a priori. No se utiliza para clasificación.
seed	Es un parámetro opcional. Fija la semilla, tanto para R como para Java.

1.2.3.6 BRNN

El algoritmo Bayesian Regularization para feed-forward Neural Networks consiste en una red neuronal de dos capas descritas en [47], [48] y usa el algoritmo descrito en [49]. De esta forma se hacen pasar por la red los valores, lo cual nos genera unos resultados y un modelo ajustado a dichos datos que puede ser utilizado para predecir valores. La implementación utilizada para los experimentos está presente en el paquete *brnn* disponible en el gestor de paquetes CRAN para R. Los parámetros ajustables de este algoritmo son los siguientes:

Tabla 1.11. Parámetros algoritmo BRNN.

Parámetro	
formula	Fórmula que se utilizará para realizar la regresión.
data	Dataframe que contiene todos los datos a utilizar.
x	Dataframe con las variables independientes
y	Dataframe con los resultados de los datos de entrenamiento.
epochs	Entero positivo. Número de iteraciones para entrenar, por defecto 1000.
cores	Número de núcleos de la CPU utilizados para ejecutar el algoritmo. Solo para sistemas UNIX.
change	El algoritmo terminará si el máximo (en valor absoluto) de la diferencia de la función F en 3 iteraciones consecutivas es inferior a este valor.

1.2.3.7 rqPen

Este algoritmo se basa en la regresión por cuantil con LASSO (Least Absolute Shrinkage and Selection Operator). Esta implementación soporta un ancho margen de penalizaciones e incluye validación cruzada e información de criterio para la selección de los parámetros de ajuste. La capacidad de analizar grandes conjuntos de datos es uno de los principales atractivos de los métodos de regresión penalizada. Sin embargo, la programación lineal y la programación de conos de segundo orden se vuelven complicadas desde el punto de vista computacional para grandes conjuntos de datos. Para complicar aún más las cosas, la función de pérdida cuantil no es diferenciable, mientras que los algoritmos populares para funciones objetivas penalizadas confieren una función de pérdida diferenciable.

Para los experimentos se ha utilizado la implementación disponible en el paquete `rqPen` disponible en el gestor de paquetes CRAN para R.

Algunos de los parámetros ajustables para dicho algoritmo son los siguientes:

Tabla 1.12. Parámetros algoritmo `rqPen`.

Parámetro	
x	Dataframe con las variables independientes.
y	Dataframe con los resultados de los datos de entrenamiento.
tau	Cuantil de interés.
lambda	Parámetro para configurar el algoritmo. En nuestros experimentos es un valor empírico de 0.001.
weights	Pesos para inicializar la función objetivo.
intercept	Indica si el modelo incluirá un valor intercept o no.
method	Método a usar; se deberá elegir entre “br” y “fn”. Para regresiones penalizadas el recomendado es “br”.
penVars	Variables que deben ser penalizadas. Si no se especifica, serían todas.

1.2.3.8 Random Forest (RF)

El RandomForest [27,28] es un algoritmo de aprendizaje automático, cuyo funcionamiento se basa en crear una gran cantidad de árboles de decisión entrenados con subconjuntos diferentes de los datos de entrada. A la hora de realizar la regresión, en nuestros experimentos, el algoritmo tiene en cuenta los resultados de todos los árboles.

Este algoritmo se puede encontrar en el paquete randomForest, disponible en el gestor de paquetes CRAN para R. Dicha implementación cuenta con los siguientes parámetros:

Tabla 1.13. Parámetros algoritmo RF.

Parámetro	
formula	Fórmula que se utilizará para realizar la regresión.
data	Dataframe que contiene todos los datos a utilizar.
x	Dataframe con las variables independientes.
y	Dataframe con los resultados de los datos de entrenamiento.
mtry	Número de variables elegidas al azar a la hora de crear un conjunto de entrenamiento.
ntree	Número de árboles generados.
maxnodes	Número máximo de nodos permitidos en un árbol, en el caso de que no se especifique, se expandirá el árbol lo máximo posible.

1.2.3.9 M5P

El regresor M5 está basado en modelos de árboles y apoyado en reglas. Se ha utilizado la implementación disponible en Weka, por lo que se ha utilizado el paquete RWeka disponible en CRAN. El algoritmo fue desarrollado originalmente por R. Quinlan [41] y posteriormente perfeccionado por Yong Wang [40]. Dicha implementación utiliza los siguientes parámetros:

Tabla 1.14. Parámetros algoritmo M5P.

Parámetro	
formula	Fórmula que se utilizará para realizar la regresión.
data	Dataframe con todos los datos a utilizar.
N	Activa/Desactiva la poda. Activado para nuestros experimentos.
U	Activa/Desactiva el suavizado de predicciones. Activado en los experimentos.
R	Construir un árbol de regresión en lugar de un modelo clasificador. En los experimentos estuvo activado.
M	Número mínimo de instancias para considerar un nodo hoja.

1.2.3.10 Cubist

Cubist es un modelo basado en reglas que es una extensión del árbol modelo M5 de Quinlan. Se genera un árbol donde las hojas terminales contienen modelos de regresión lineal. Estos modelos se basan en los predictores utilizados en divisiones anteriores. Además, hay modelos lineales intermedios en cada paso del árbol. Se realiza una predicción usando el modelo de regresión lineal en el nodo terminal del árbol, pero se suaviza teniendo en cuenta la predicción del modelo lineal en el nodo anterior (que también ocurre recursivamente en el árbol). El proceso está explicado en [53]. Se ha utilizado la implementación disponible en el paquete Cubist presente en el gestor de paquetes CRAN.

Los principales parámetros que pueden configurarse para el algoritmo son los siguientes:

Tabla 1.15. Parámetros algoritmo Cubist.

Parámetro	
x	Dataframe con las variables independientes.
y	Dataframe con los resultados de los datos de entrenamiento.
committees	Entero. Número de committees que deben utilizarse.
control	Vector con los pesos iniciales para el entrenamiento. Opcional.

1.2.3.11 CForest

El algoritmo CForest es una implementación diferente del algoritmo randomForest. Difiere de la implementación clásica en el esquema de agregación utilizado a la hora de contabilizar los resultados obtenidos en todos los árboles, además de usar unas técnicas de aprendizaje diferentes.

Este algoritmo puede encontrarse en el paquete party, disponible en el gestor de paquetes CRAN para R. Dicha implementación cuenta con los siguientes parámetros:

Tabla 1.16. Parámetros algoritmo CForest.

Parámetro	
formula	Fórmula que se utilizará para realizar la regresión.
data	Dataframe con todos los datos a utilizar.
ntree	Número de árboles que se generarán.
mtry	Número de variables elegidas al azar a la hora de crear los conjuntos de entrenamiento.
weights	Vector opcional utilizado en la fase de predicción, cuya función es almacenar la probabilidad del resultado. Puede darse en forma de matriz en el caso de que sean muchos resultados.
cores	Número de cores en el que se ejecutará el algoritmo.

1.2.3.12 bagEarth

El algoritmo BagEarth es un wrapper de bagging para el cálculo de Splines de regresión adaptativa multivariable (MARS) [43] que usa la función Earth. Este algoritmo se puede encontrar en el paquete Caret, disponible en el gestor de paquetes CRAN para R. Este algoritmo utiliza los siguientes parámetros:

Tabla 1.17. Parámetros algoritmo bagEarth.

Parámetro	
x	Dataframe con las variables independientes.
y	Dataframe con los resultados de entrenamiento.
weights	Pesos para cada ejemplo, por defecto 1.
B	Número de muestras para el bootstrap
formula	Fórmula que se utilizará para realizar la regresión.
data	Dataframe con los datos a utilizar.

1.2.3.13 Earth

El algoritmo earth es un algoritmo para el cálculo de Splines de regresión adaptativa multivariante (MARS) [43, 44] que usa la función Earth. Este algoritmo se puede encontrar en el paquete earth, disponible en el gestor de paquetes CRAN para R.

Dicha implementación cuenta con los siguientes parámetros:

Tabla 1.18. Parámetros algoritmo Earth.

Parámetro	
formula	Fórmula que se utilizará para realizar la regresión.
data	Dataframe con todos los datos a utilizar.
nk	Número máximo de términos en el modelo antes de realizar una poda de los árboles.
trace	Valor numérico que indica el tipo de información que mostrará el algoritmo mientras se entrena.
degree	Grado máximo de interacción.
glm	Lista de argumentos opcional, utilizada para elegir si la respuesta es binaria o un valor.
nfold	Número de veces que se realizará la validación cruzada.

1.2.3.14 GAMBoost

Este algoritmo se utiliza para ajustar un modelo aditivo generalizado mediante potenciación basada en la probabilidad. Es especialmente adecuado para modelos con un gran número de predictores que pueden tener influencias no lineales. Proporciona estimaciones de funciones suaves relacionadas con las covariables, acompañadas de intervalos de confianza y grados de libertad aproximados.

La idea de potenciación basada en la probabilidad [53] se entiende más fácilmente para modelos con una respuesta gaussiana. Allí da como resultado un ajuste repetido de residuos (esta idea se transfiere luego al caso generalizado). Para obtener un modelo aditivo, GAMBoost utiliza una gran cantidad de pasos de impulso donde en cada paso se ajusta un B-spline penalizado [54] a una covariable, siendo la respuesta los residuos del último paso. La covariable que se actualizará se selecciona por desviación (o, en caso de aumento escaso, por algún criterio de selección de modelo). Las estimaciones del coeficiente B-spline en cada paso se ajustan bajo la restricción de una gran penalización en sus primeras diferencias (o de orden superior). Así que en cada paso solo se hace un pequeño ajuste. Sumando todos los pasos para cada covariable se obtiene una estimación de función suave. Cuando no se utiliza la expansión de la base, es decir, solo se actualizan los coeficientes de las covariables, se obtienen modelos lineales (generalizados).

Este algoritmo nos ofrece gran cantidad de parámetros para configurarlo, siendo algunos los siguientes:

Tabla 1.19. Parámetros algoritmo GAMBoost.

Parámetro	
x	Dataframe con las variables independientes.
y	Dataframe con los resultados de entrenamiento.
penalty	Valor de penalización para la actualización de la función de suavizado en cada etapa de mejora.
bdeg	Grado de la base de B-splines usada para crear funciones suaves y diferencia de las estimaciones del coeficiente a las que se debe aplicar la penalización.
weights	Vector opcional con pesos iniciales para el proceso de entrenamiento.
stepno	Número de etapas de mejora.

1.3 Objetivos

El principal objetivo de los trabajos de investigación realizados durante el desarrollo de esta Tesis Doctoral es el de predecir características de calidad de varios tipos de lomos, a partir de la extracción de características de imágenes MRI de los lomos, y empleando diferentes algoritmos de aprendizaje automático.

Este objetivo principal puede descomponerse en varios objetivos parciales, que se resumen en la siguiente relación:

a) En cuanto a la predicción de características de los lomos, se pretende clasificar:

- Lomos de cerdos alimentados con pienso
- Lomos de cerdos alimentados con bellota (montanera)
- Lomos de ternera
- El efecto de congelar y descongelar los lomos de los puntos anteriores

b) En cuanto a la predicción de características de calidad de los lomos, se pretende considerar:

- Las características de calidad físico-químicas
- Las características de calidad de texturas de tecnología de alimentos
- Las características de calidad sensoriales

c) En cuanto a los algoritmos de extracción de características de imágenes MRI de lomos, el objetivo es estudiar:

- A. Algoritmos clásicos de extracción de texturas clásicos: Grey Level Co-occurrence Matrix (GLCM), Neighboring Grey Level Dependence Matrix (NGLDM) y Level Run Length Matrix (GLRLM)
- B. Algoritmos basados en filtros Gabor
- C. Algoritmos basados en Wavelet

D. Algoritmos basados en fractales: One Point of Fractal curve Texture Algorithm (OPFTA), Fractal Texture Algorithm (FTA), Classical Fractal Algorithm (CFA)

d) En cuanto a algoritmos de aprendizaje automático, se pretende estudiar los algoritmos más habitualmente empleados en la literatura científica (Lm, penalized, SVM, elmNNR, BART, BRNN, rqPen, RF, M5P, CUBIST, CForest, bagEARTH, EARTH, GAMBOOST...).

e) Otros objetivos secundarios tienen que ver con:

1. La determinación del paralelepípedo de mayor volumen para realizar los estudios en el interior de esos volúmenes de interés (VOI)
2. La propuesta de un protocolo experimental que combine MRI con algoritmos de extracción y algoritmos de aprendizaje automático.

f) Finalmente, se pretende determinar la mejor combinación de algoritmo de extracción de característica con algoritmo de aprendizaje automático para la predicción de cada una de las características de calidad.

1.4 Contribuciones. Justificación unitaria de la tesis doctoral.

Esta tesis doctoral se presenta como el compendio de las siguientes publicaciones en revistas indexadas JCR, desarrolladas entre los años 2021 y 2023, como consecuencia de los trabajos de investigación realizados en el proyecto “Desarrollo de métodos no destructivos basados en ultrasonidos y algoritmos sobre Imágenes de Resonancia Magnética para evaluar la calidad de la carne de ternera y de cerdo ibérico”, financiado por la Consejería de Economía, Competitividad e Innovación de la Junta de Extremadura, desde el 02/02/2018 hasta el 10/07/2021.

Además, durante los años 2018, 2019 y 2022, también se han desarrollado trabajos presentados en congresos internacionales, que, sin formar parte del compendio de publicaciones, también se incluyen en este apartado al considerar que cubren parcialmente los objetivos propuestos en el apartado anterior.

Contribuciones en revistas indexadas JCR (incluidas en el compendio de publicaciones):

Los objetivos propuestos en la presente tesis se han ido cubriendo mediante las publicaciones aceptadas en revistas indexadas que forman parte del compendio. Se opta por presentar estas publicaciones no en orden cronológico, sino en orden de mayor a menor relación directa con la tesis. Así, la publicación I) resume casi todos los trabajos realizados y cubre prácticamente todos los objetivos propuestos en el apartado anterior, siendo la principal publicación de la tesis, dado que presenta y resume el volumen total de experimentos realizados (en total, 6160 modelos de aprendizaje automático realizados, cubriendo los objetivos a), b), c), d) y f) anteriores. Esta publicación data de 2022.

De entre los resultados expuestos en la publicación I), y por cuestiones de espacio y también de interés específico, se presenta una segunda publicación, la numerada como II). Esta publicación, fechada en 2023, se centra principalmente en el estudio del efecto de congelar y descongelar los productos cárnicos (particularmente el lomo de ternera) a la hora de realizar las clasificaciones mediante los algoritmos de aprendizaje automático en conjunción con los algoritmos de extracción de características sobre imágenes MRI.

Puede considerarse que las publicaciones I) y II) ya justifican la coherencia e importancia unitaria de las publicaciones para considerar la presentación de la presente tesis en formato de compendio. Pero, además, se han incluido dos nuevas publicaciones para terminar de cubrir algunos de los aspectos secundarios que han sido necesarios con carácter previo a los diseños experimentales realizados para las publicaciones I) y II), y que son los que se presenta en la publicación III).

En el caso de la publicación III), de 2022, se realiza un estudio sistemático de las combinaciones de adquisición de imágenes MRI, haciendo uso del dispositivo de bajo campo empleado en esta tesis. Así, esta publicación permite determinar y optimizar la mejor configuración para la adquisición de las imágenes de lomos curados, cuya experiencia y resultados se han tenido en cuenta en los experimentos llevados a cabo con posterioridad.

Finalmente, y dado que la extracción de características empleando los algoritmos de visión por computador deben llevarse a cabo en el interior de determinadas zonas de las imágenes, con carácter previo también fue necesario diseñar algoritmos que permitieran

circunscribir los cálculos a regiones de interés (2D) y volúmenes de interés (3D), algo que se resolvió en el algoritmo propuesto en 2021 en la publicación IV) del compendio.

Todo lo cual justifica la decisión de presentar la tesis en el formato de compendio de publicaciones, que se muestran a continuación:

I. A Computer-Aided Inspection System to Predict Quality Characteristics in Food Technology [69]. Juan P. Torres, Andrés Caro, Mar Ávila, Trinidad Pérez-Palacios, Teresa Antequera, Pablo García. IEEE Access, Volume 10, Pages 71496 – 71507, 2022. ISSN 2169-3536. DOI 10.1109/ACCESS.2022.3187404. Índice de impacto:

IF (2022): 3.9 (72/158) Q2 in COMPUTER SCIENCE, INFORMATION SYSTEMS

IF (2022): 3.9 (41/88) Q2 in TELECOMMUNICATIONS

IF (2022): 3.9 (100/275) Q2 in ENGINEERING, ELECTRICAL & ELECTRONIC

Esta publicación es la más completa de todas las propuestas, dado que consigue cubrir los objetivos a), b), c), d) y f)

II. MRI-computer vision on fresh and frozen-thawed beef: Optimization of methodology for classification and quality prediction [70]. Trinidad Pérez-Palacios, Mar Ávila, Teresa Antequera, Juan P. Torres, Alberto González-Mohino, Andrés Caro. Meat Science, Volume 197, Pages 109054, 2023. ISSN 0309-1740. DOI <https://doi.org/10.1016/j.meatsci.2022.109054>. Índice de impacto:

IF (2022): 7.1 (12/142) Q1 in FOOD SCIENCE & TECHNOLOGY

Esta publicación cubre parcialmente los objetivos a), b), c), d) y f), centrándose principalmente en el estudio de lomos de ternera y en el efecto de congelar y descongelar estos productos.

III. An experimental protocol to determine quality parameters of dry-cured loins using low-field Magnetic Resonance Imaging [71]. Daniel Caballero, Pablo García, Andrés Caro, Mar Ávila, Juan P. Torres, Teresa Antequera, Trinidad Pérez-Palacios. Journal of Food Engineering, Volume 313, Pages 110750, 2022. ISSN 0260-8774. DOI <https://doi.org/10.1016/j.jfoodeng.2021.110750>. Índice de impacto:

IF (2022): 5.5 (30/142) Q1 in FOOD SCIENCE & TECHNOLOGY

IF (2022): 5.5 (26/140) Q1 in ENGINEERING, CHEMICAL

Esta publicación cubre parcialmente el objetivo e2), así como los objetivos b), c) y d), también parcialmente.

Contribuciones en Congresos (no incluidas en el compendio de publicaciones):

A las publicaciones que forman parte del compendio de la tesis hay que sumar, además, las publicaciones presentadas en congresos internacionales que se presentan también como contribuciones de la tesis y que se muestran a continuación.

Las contribuciones i), ii) y iii) presentan estudios relacionados con otros datasets de imágenes MRI de productos cárnicos disponibles en el grupo de investigación en el que se ha desarrollado la tesis. Se trata de imágenes MRI de jamones, donde se estudia el comportamiento de los algoritmos cuando se comparan dispositivos MRI de alto y bajo campo, en la publicación i), en 2022. O la posibilidad de detectar productos en mal estado, en la publicación ii), también de 2022. O bien de realizar las primeras predicciones de características de calidad de productos cárnicos usando un escáner de bajo campo, en la publicación iii) de 2019. Por último, y más lejano en el tiempo, los resultados de combinar diferentes algoritmos extractores de características con regresores, en el caso de la publicación iv), realizados allá por el año 2018.

I. High-field vs. Low-field MRI scanners to analyse sensory attributes of dry-cured hams [108]. Teresa Antequera, Daniel Caballero, Juan Pedro Torres, Mar Ávila, Trinidad Pérez-Palacios. Pág. 65. International Conference on the applications of magnetic resonance in food science (MRFOOD). Aarhus (Dinamarca), 7-10 de junio, 2022

Esta publicación cubre parcialmente el objetivo e2)

II. Low Field MRI and computer vision to detect and characterize defective dry-cured hams [109]. Trinidad Perez-Palacios, Andrés Caro, Juan Pedro Torres, Mar Ávila, Teresa Antequera. Pág. 66. International Conference on the applications of magnetic resonance in food science (MRFOOD). Aarhus (Dinamarca), 7-10 de junio, 2022

Esta publicación cubre parcialmente los objetivos e1) y e2).

III. Non-destructively Prediction of Quality Parameters of Dry-Cured Ham by Applying Computer Vision and Low-Field MRI [88]. Juan Pedro Torres, Mar Ávila, Andrés Caro, Trinidad Pérez-Palacios, Daniel Caballero. 9th Iberian Conference on Pattern Recognition and Image Analysis, IbPRIA 2019. Madrid (España), 1–4 de julio de 2019. Springer Nature Switzerland AG 2019. IbPRIA 2019, LNCS 11867. Págs. 498–507. 2019. ISSN 0302-9743. DOI https://doi.org/10.1007/978-3-030-31332-6_43

Esta publicación cubre parcialmente los objetivos b), c) y d).

IV. Evaluation of different texture algorithms-regressors combinations to determine Iberian loin characteristics by MRI [107]. Mar Ávila, Dani Caballero, Manuel Fernández, Juan P. Torres, Andrés Caro. Pág. 82. 14th International Conference on the Applications of Magnetic Resonance in Food Science (MRFood 2018). Rennes (Francia), 17-21 de septiembre, 2018.

Esta publicación cubre parcialmente los objetivos b), c), d) y f).

V. Finding the largest volume parallelepipedon of arbitrary orientation in a solid
[72]. Rubén Molano, Daniel Caballero, Pablo G. Rodríguez, Mar Ávila, Juan P. Torres, Marisa Durán, José Carlos Sancho, Andrés Caro. IEEE Access, Volume 9, Pages 103600-103609, 2021. ISSN 2169-3536. DOI 10.1109/ACCESS.2021.3098234. Índice de impacto:

IF (2021): 3.476 (79/164) Q2 in COMPUTER SCIENCE, INFORMATION SYSTEMS

IF (2021): 3.476 (43/94) Q2 in TELECOMMUNICATIONS

IF (2021): 3.476 (105/276) Q2 in ENGINEERING, ELECTRICAL & ELECTRONIC

Esta publicación cubre el objetivo e1).

Capítulo 2

2. Diseño experimental y Materiales

2.1 Diseño experimental

Para la realización de esta tesis se han empleado como material de partida lomos de cerdo alimentados con pienso, lomos de cerdo alimentados con bellota y lomos de ternera, con lo que se generaron 5 conjuntos de datos: lomos frescos de cerdo, lomos frescos de ternera, lomos curados de cerdo, lomos cocinados de cerdo y lomos cocinados de ternera.

El diseño experimental se ha desarrollado siguiendo el esquema que se presenta en la figura 2.1.

En primer lugar, para todos los productos, se llevó a cabo la adquisición de las imágenes (MRI) (apartado 2.2.1) para realizar después los análisis físico-químicos, de textura instrumental y sensoriales (apartado 2.2.2), obteniéndose un dataset con características reales. Este conjunto de datos representa los valores utilizados como etiquetas para validar las predicciones realizadas por los modelos basados en los cuatro tipos de algoritmos de extracción de características.

Todas las MRI se analizaron mediante 8 métodos de análisis de textura agrupados en cuatro tipos (3 algoritmos clásicos, algoritmo de Gabor, algoritmo de Wavelet y 3 algoritmos de fractales), de los que se obtuvieron 138 características computacionales, conformando otro dataset con datos computacionales.

Sobre los datasets de características reales y características computacionales se aplicaron 14 algoritmos de aprendizaje automático para predecir las características de calidad de las piezas cárnicas, identificando la mejor combinación de algoritmo extractor – algoritmo de aprendizaje automático para cada característica de calidad.

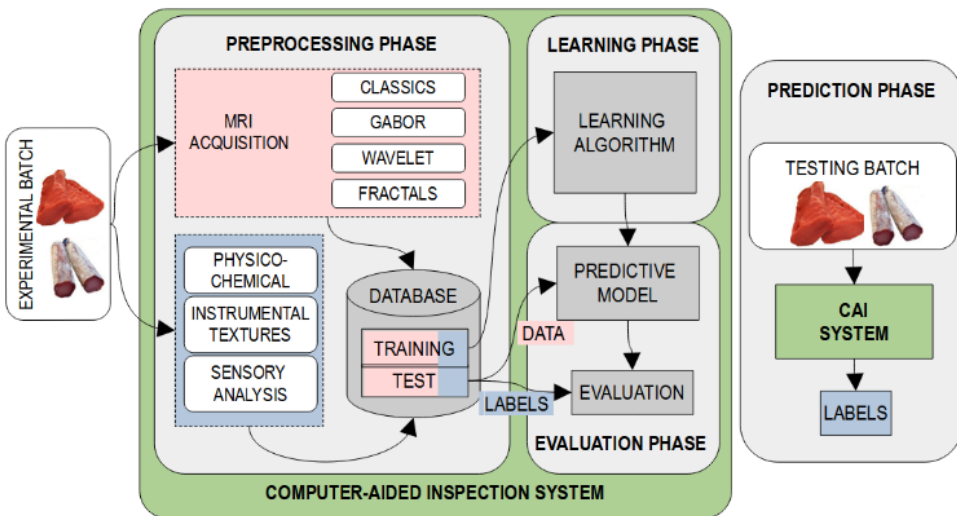


Figura 2.1 Diseño experimental del sistema propuesto.

2.2 Materiales

2.2.1. Imágenes de resonancia magnética

Para la adquisición de las imágenes se utilizó un dispositivo de resonancia magnética de campo bajo (ESAOTE VET-MR E-SCAN XQ 0.18 T) mediante una bobina de mano/muñeca, que fue financiado mediante una convocatoria competitiva (FEDER-MICIN UNEX10-1E-403). Se encuentra localizado en el Servicio de Análisis e Innovación en Productos de Origen Animal (SiPA) situado en la Facultad de Veterinaria de la Universidad de Extremadura (Cáceres, España). Según estudios previos [5], se utilizan secuencias ponderadas en T1 y Eco de gradiente (GE), y los siguientes parámetros: campo de visión (FOV): 160×160 mm²; Tiempo de eco (TE): 14 ms; espesor de corte: 4 mm; ángulo de giro: 75°; Tiempo de repetición (TR): 1450 ms; tamaño de matriz: 224×176 ; codificación de fase: 176. La adquisición de resonancia magnética se realiza a 23 °C, obteniendo un total de 13352 imágenes para los experimentos.

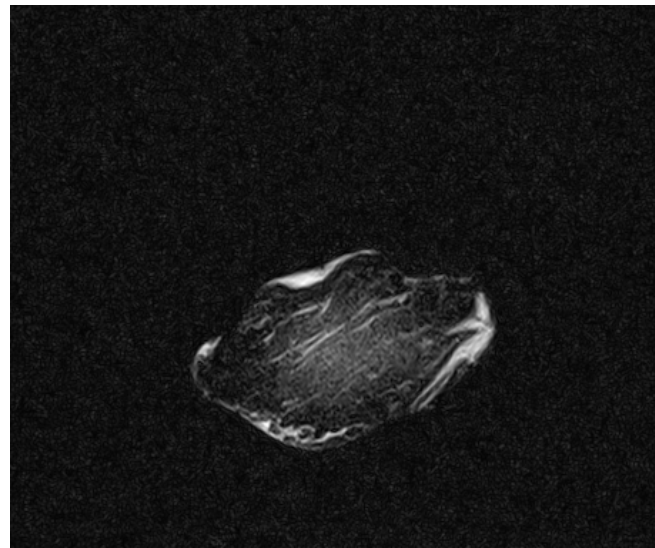


Figura 2.2. Imagen MRI de un lomo de cerdo curado.

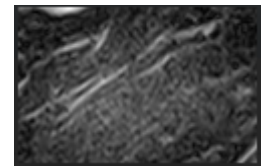


Figura 2.3. Región de interés de un lomo de cerdo curado.

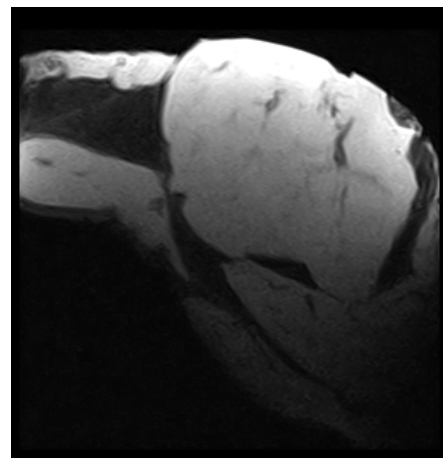


Figura 2.4. Imagen MRI de un lomo de ternera fresco.

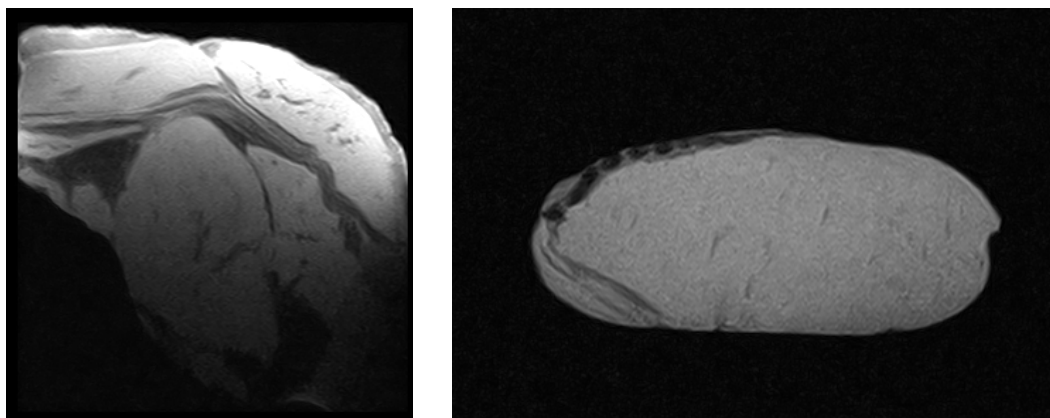


Figura 2.5. Imagen MRI de un lomo descongelado de ternera(izquierda) y cerdo(derecha).

2.2.2. Características físico-químicas, de textura instrumental y sensoriales

El sistema incluye la obtención de un conjunto de datos completo de características de calidad (tabla 2.1) obtenido mediante los métodos tradicionales (análisis físico-químico, análisis de textura instrumental y análisis sensorial). Este conjunto de datos se utiliza como etiquetas para validar las predicciones realizadas por los modelos basados en los cuatro tipos de algoritmos de extracción de características.

Los seis parámetros fisicoquímicos (PC) son obtenidos por expertos en tecnología de alimentos que analizan las muestras de carne por triplicado. La actividad del agua se obtiene mediante el sistema Lab Master-aw (NOVASINA AG, Suiza) después de la calibración a 20-22 °C. El color instrumental (L^* , a^* y b^*) se mide utilizando un colorímetro Minolta CR-300 (Minolta Camera Corp., Meter Division, Ramsey, NJ) con iluminancia D65, un observador estándar de 0° y un puerto/puerto de 2,5 cm. área de visualización. El colorímetro se estandariza antes de su uso con una baldosa blanca que tiene los siguientes valores: $L^* = 93,5$, $a^* = 1,0$ y $b^* = 0,8$. La humedad se determina a $102 \pm 2^\circ\text{C}$ mediante el método oficial (Association of Official Analytical Chemist, 2000; referencia 935.29). El contenido de lípidos de los lomos se determina gravimétricamente con cloroformo/metanol (2:1, v/v) [55].

Para determinar el conjunto de datos de textura instrumental (IT), se cortan porciones uniformes de las muestras en cubos de 1 cm³. Las muestras se comprimen axialmente hasta el 60% de su altura original con un émbolo plano de 50 mm de diámetro (P/50) a una velocidad de la cruceta de 2 mm/s a través de una secuencia de 2 ciclos. El análisis

instrumental se realiza en un analizador de textura TA.XT plus (Stable Micro Systems Ltd., Surrey, Reino Unido) [56].

Tabla 2.1. Características de calidad de productos cárnicos.

Físico-químicas	Instrumental	Sensorial (cocinado)	Sensorial (curado)
Wa Actividad del agua	Dureza	Intensidad de color	Intensidad de color
L* Brillo	Adhesividad	Brillo	Brillo
a* color rojo/verde	Pegajosidad	Intensidad del olor	Marmoleo
b* color amarillo/azul	Cohesión	Olor cocinado	Olor a paprika
MO humedad	Elasticidad	Sensibilidad	Intensidad del olor
LI grasa	Masticabilidad	Jugosidad	Dureza
	Resiliencia	Fibrosidad	Jugosidad
		Masticabilidad	Fibrosidad
		Intensidad de sabor	Masticabilidad
		Sabor a cocinado	Salado
			Sabor curado
			Sabor a paprika
			Intensidad de sabor
Total: 6	Total: 7	Total: 10	Total: 13

El conjunto de datos del Análisis Sensorial (SA) se basa en muestras de lomo cocinado y curado en seco, realizadas por catorce panelistas capacitados. Se degustan tres muestras por sesión, valorándose cada vez el lomo por triplicado. Después de la cocción (en horno a 180 °C durante 45 min), las muestras cocidas se refrigeran durante 24 h hasta su evaluación

sensorial. Luego, los lomos se cortan con una máquina cortadora de carne TGI 300 OMS S.r.l. (muestras en rodajas de 2 mm y alrededor de 5 g). Justo antes de la evaluación, las muestras se calientan durante 10 segundos en un horno microondas de 600 W. Los lomos curados también se cortan en lonchas (3 mm) antes de degustar. Las muestras (una rebanada por plato) se sirven en platos de vidrio con agua mineral y un trozo de galleta sin sal para seguir el protocolo de enjuague entre muestras. Las evaluaciones se desarrollan en salas de cata diseñadas según la norma UNE-EN-ISO 8589:2010. Todas las sesiones son realizadas a temperatura ambiente (20–22 °C) en una sala sensorial equipada con luz fluorescente blanca. El orden de servicio de las muestras es aleatorio según el diseño de cuadrado latino de Williams. Para recopilar los datos se utiliza el software FIZZ versión 2.20 C (Análisis sensorial y gestión de pruebas informáticas). Los atributos utilizados en este estudio se seleccionan en base a la experiencia previa en evaluación sensorial de productos cárnicos [57]. Se utiliza una escala no estructurada de 10 cm para calificar los atributos, y los anclajes verbales se fijan como "poco" a "mucho" para todos los atributos evaluados.

2.2.3. Conjunto de datos

Con todos los datos obtenidos anteriormente se generaron cinco datasets, lomos frescos tanto ternera como cerdo, lomos curados de cerdo, lomos cocinados tanto cerdo como ternera.

En la tabla 2.2 se puede observar la cantidad de características obtenidas para cada uno de los dataset utilizando los cuatro tipos de algoritmos extractores de características (Clásicos, fractales, wavelets y filtros de Gabor).

Se adquieren 138 características, 26 obtenidas mediante los algoritmos clásicos de textura, 22 conseguidas a través de los algoritmos de fractales, 54 extraídas con el algoritmo de wavelets y 36 derivadas de aplicar los filtros de Gabor sobre las imágenes de resonancia magnética.

Tabla 2.2. Características computacionales.

Grupo	Algoritmo de texturas	Características	Número total
Clásico	GLCM	ENE, ENT, COR, HC, IDM, INE, CS, CP, CON, DIS	10
	GLRLM	LRE, SRE, GLNU, RLNU, RPC, LGRE, HGRE, SRLGE, SRHGE, LRLGE, LRHGE	11
	NGLDM	SNE, LNE, NNU, SM, ENT	5
Wavelets	DT-CWT	e1d1-mean, e1d1-angle, e1d1-var, ... e3d6-mean, e3d6-angle, e3d6-var	54
Gabor	GABOR FILTER	a1f1-mean, a1f1-var a6f3-mean, a6f3-var	36
Fractales	OPFTA	UNI, ENT, COR, HOM, INE, CON, EFI	7
	FTA	UNI, ENT, COR, HOM, INE, CON, EMP, CC, CS, CP	10
	CFA	box2, box3, box4, box5, box6	5
TOTAL			138

Capítulo 3

3. Métodos

Esta tesis doctoral se presenta como el compendio de las siguientes publicaciones, desarrolladas entre los años 2021 y 2023, como consecuencia de los trabajos de investigación realizados en el proyecto “Desarrollo de métodos no destructivos basados en ultrasonidos y algoritmos sobre Imágenes de Resonancia Magnética para evaluar la calidad de la carne de ternera y de cerdo ibérico”, financiado por la Consejería de Economía, Competitividad e Innovación de la Junta de Extremadura, desde el 02/02/2018 hasta el 10/07/2021.

3.1 Artículo “A Computer-Aided Inspection System to Predict Quality Characteristics in Food Technology”

• **Autores:** Juan P. Torres, Andrés Caro, Mar Ávila, Trinidad Pérez-Palacios, Teresa Antequera, Pablo García

• **Publicación:** IEEE Access, Volume 10, Pages 71496 – 71507, 2022

• **ISSN:** 2169-3536

• **DOI:** 10.1109/ACCESS.2022.3187404

• **Índice de impacto:**

IF (2022): 3.9 (72/158) Q2 in COMPUTER SCIENCE, INFORMATION SYSTEMS

IF (2022): 3.9 (41/88) Q2 in TELECOMMUNICATIONS

IF (2022): 3.9 (100/275) Q2 in ENGINEERING, ELECTRICAL & ELECTRONIC

Las características de calidad que se obtienen a partir de muestras de alimentos habitualmente se determinan mediante análisis fisicoquímicos y sensoriales en las industrias alimentarias. Estos métodos son tediosos, laboriosos, producen residuos químicos e implican la destrucción de las muestras. Para las industrias cárnica, en este trabajo se propone un sistema de inspección asistido por ordenador no invasivo y no destructivo, basado en visión por ordenador y técnicas de aprendizaje automático. El trabajo presenta todas las posibilidades para el desarrollo de un sistema de inspección, haciendo una comparación exhaustiva de diferentes algoritmos utilizados para extraer características de las imágenes de las muestras, y varios enfoques de aprendizaje automático, estudiando hasta 6160 modelos diferentes, y seleccionando los 110 mejores para la propuesta. El sistema es capaz de determinar todas las características de calidad fisicoquímicas, texturales y sensoriales de lomos de cerdo y ternera en cuatro estados cárnicos (carne fresca, carne descongelada, carne cocida y carne curada) con buena precisión, siendo una alternativa real a los métodos habituales para la industria alimentaria.

Received 9 June 2022, accepted 26 June 2022, date of publication 30 June 2022, date of current version 11 July 2022.

Digital Object Identifier 10.1109/ACCESS.2022.3187404

RESEARCH ARTICLE

A Computer-Aided Inspection System to Predict Quality Characteristics in Food Technology

JUAN P. TORRES^{ID1}, ANDRÉS CARO^{ID1}, MARÍA DEL MAR ÁVILA^{ID1}, TRINIDAD PÉREZ-PALACIOS², TERESA ANTEQUERA², AND PABLO GARCÍA RODRÍGUEZ¹

¹Department of Computer and Telematics Systems Engineering, Universidad de Extremadura, 10003 Cáceres, Spain

²Institute of Meat and Meat Products (IProCar), Food Technology, Universidad de Extremadura, 10003 Cáceres, Spain

Corresponding author: Andrés Caro (andresc@unex.es)

This work was supported by the Junta de Extremadura through the European Regional Development Fund, Consejería de Economía, Ciencia y Agenda Digital, under Project GR21099 and Project GR21186. The work of Trinidad Pérez-Palacios was supported by the Spanish Government through the Ministerio de Ciencia e Innovación for the Ramón y Cajal under Contract RYC-2017-21842.

ABSTRACT Physicochemical and sensory analyses are commonly used to determine the quality characteristics of food samples in Food Industries. These methods are tedious, laborious, produce chemical residues, and involve the destruction of the samples. For the meat industries, this work proposes a non-invasive and non-destructive computer-aided inspection system, based on computer vision and ensemble machine learning techniques. The paper presents all the possibilities for the development of the system, making an exhaustive comparison of different algorithms used to extract features from the images of the samples, and various machine learning approaches, studying up to 6160 different models, and selecting the top 110 for the ensemble proposal. The system determines all the physicochemical, textural, and sensory quality characteristics of pork and beef loins in four meat states (fresh, thawed, cooked, and cured) with good precision, being a real alternative to the usual methods for the Food Industry.

INDEX TERMS Computer-aided system, feature extraction, loin, magnetic resonance imaging, quality parameters, regressor.

I. INTRODUCTION

Computer-Aided Inspection (CAI) has acquired great importance today, in different fields, such as mechanical and aerospace industry, textile industry, electrical and electronic industry... These systems have also generated interest in the food industry [1]–[4], mainly in the quality assurance step of the manufacturing process. The possibility of inspecting samples and predicting quality characteristics of the products, in a reliable and non-destructive way, is a great advance for the food industry.

The usual inspection techniques to determine quality parameters in meat industry are tedious, expensive, and involve the destruction of the samples by chemical substances. In addition, these techniques generate chemical waste that must be recycled.

The associate editor coordinating the review of this manuscript and approving it for publication was Joanna Kołodziej^{ID}.

Physicochemical analysis is one of the methods used to estimate quality characteristics [5]. This analysis determines the lipid and salt content, water activity and attributes related to the color of meat samples. Other analyses are related to meat textures, determining factors such as hardness, adhesiveness, strickiness, chewiness, etc. Besides, acceptance by consumers is related to sensory characteristics such as color, odor intensity, tenderness, juiciness, fibrousness... which are determined by expert tastings [6]. It is note that sensory analyses can produce subjective values. Through these three types of analysis (physicochemical, instrumental, and sensory) it is possible to create datasets with real values of the quality characteristics of meat products.

CAI system provides a new option for an automated, non-destructive and objective quality determination. The typical stages of CAI system consist of an image acquisition procedure for food samples, the application of feature extraction algorithms on the images, and the evaluation algorithms. Systems based on hyperspectral imaging and machine learning

were developed for different applications in food technology. Backpropagation Artificial Neural Networks were used to evaluate chicken meat [7]. Adaboost and Backpropagation Artificial Neural Network were also used to evaluate pork meat [8]. Regression models were proposed to predict the fat and moisture content of ground meat samples in [9]. Several works use Magnetic Resonance Imaging (MRI) as image acquisition technique [6], [10]–[13]. The acquisition of MRI is carried out in a non-invasive, non-intrusive, non-ionizing and innocuous way, so samples of analyzed meat can be marketed and consumed safely, since they are not destroyed or contaminated at all [14]. The content of lean meat in pork is evaluated in [15] and the distribution of intramuscular fat in beef is determined in [16]. Although MRI scanners produce high-quality images, they are very expensive, and low-field MRI devices are proposed to analyze meat products in recent years [17].

To perform the analysis of the meat product images, different techniques are used to extract features from images, through the classic texture algorithms: Grey Level Co-occurrence Matrix (GLCM) [18], [19], Neighboring Grey Level Dependence Matrix (NGLDM) [20], [21], and Level Run Length Matrix (GLRLM) [22], [23]; Gabor filters [24]; wavelets [25]; algorithms based on fractals [26], etc. In this way, it is possible to form datasets calculated by computer vision algorithms. A comparison of different approaches was presented in [6] although only multiple linear regression was used to predict the quality features.

Regarding the evaluation models in CAI systems, many machine learning models are presented in the scientific literature, being Random Forest (RF) [27], [28], Conditional Random Forest (CFOREST) [27] and Support Vector Machines (SVM) [29], [30] some of the most used. Bayesian models or Neural Networks (NN) are also common, which implies a need for studying and comparing the performance of the different techniques [31].

A right election of the predictive model is critical for a CAI system. Multiple regressors may be needed to predict various attributes, as the numerical distributions of features may produce better predictions in some models than in others. The same algorithm does not necessarily produce the best predictions for all the characteristics. Ensemble models combine several algorithms to form a better model. Each single model produces a different prediction. The predictions of the partial models are combined to obtain a final prediction. As each model works differently, their errors tend to compensate. This results in a better generalization error.

Similarly, feature selection algorithms also influence predictions, and some predictions are better when classic texture algorithms are used, others when fractals are used... However, the reviewed papers use the same algorithm as regressor or feature extractors to predict all the features, which can reduce the quality of the predictions.

In this paper, an exhaustive study of the performance of well-known image feature extraction algorithms (classical, instrumental, and sensory analyses) is carried out. These

algorithms are combined with fourteen different regressors, including the most commonly used and some others to check their performance. The main objective is to identify the best combination of regressor-feature extractor algorithm for each of the quality features, to propose an ensemble CAI system. No previous work proposed a selection of the best combination of regressor and feature extractor algorithm, for each of the features.

This paper illustrates the construction of a CAI model to predict quality parameters related to pork and beef loins. The CAI system is designed to receive batches of meat products as input and provide as output a complete report with all the quality characteristics. The system considers various states of the meat: fresh meat, meat that has been thawed, cooked meat, and, in the case of pork, loin at the end of the ripening process. The aim is to build an ensemble CAI system to predict quality characteristics as complete as possible to offer the meat industry an alternative solution to physicochemical and sensory methods.

The system complied with the secure software development guidelines specified in [32] and the considerations on security risk estimations presented in [33]. This implies the development of a secure system, especially considering the importance and significance of research related to food technology in relation to food safety. It should be noted that no previous works have proposed a system based on different machine learning models and different feature extraction algorithms to predict or classify all the usual quality parameters of meat products.

The main contributions of this paper can be summarized as follows: I) the construction of a generic ensemble CAI model is presented, particularized to predict up to 26 quality characteristics of meat products in various states (fresh, thawed, cooked and cured meat); II) four well-known extraction algorithms and fourteen regressors are compared, to determine the best combination of regressor and feature extraction algorithm for the predictions; and III) a practical application of CAI system to the meat industry is proposed.

The remaining parts of this paper have been organized as follows. Section 2 provides a brief survey of datasets and methods included for the determination of quality parameters of meat products, and the quality features used in the food industry. Section 3 describes the proposed system. Section 4 presents the results obtained by the CAI system, and the performance evaluation. Finally, Section 5 draws the conclusion.

II. MATERIALS AND METHODS

This paper presents a CAI system to predict the quality features used in food technology for pork and beef. Fig. 1 shows the design of the model.

The system is fed with several datasets, to train and evaluate the predictive models. Experts in food technology generate the datasets corresponding to the quality characteristics of the experimental batch, used as labels to train and validate

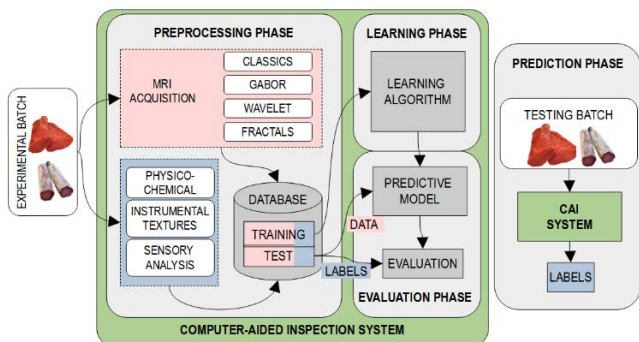


FIGURE 1. Experimental design of the proposed system.

TABLE 1. Quality features of the meat products used in food technology.

PC Physicochemical	IT Instrumental	SA Sensory (cooked)	SA Sensory (cured)
Wa Water activity	HD Hardness	Color intensity	Color intensity
L* Lightness	AD Adhesiveness	BR Brightness	BR Brightness
a* red/green color	ST Stickiness	OI Odor intensity	MB Marbling
b* yellow/blue color	CS Cohesiveness	CO Cooked odor	PO Paprika odor
MO Moisture	SP Springiness	TD Tenderness	OI Odor intensity
LI Lipid	CH Chewiness	JC Juiciness	HD Hardness
Total: #6	RE Resilience	FB Fibrousness	JC Juiciness
	Total: #7	CH Chewiness	FB Fibrousness
		FI Flavor intensity	CH Chewiness
		CF Cooked flavor	ST Salty
		Total: #10	CF Cured flavor
			PF Paprika flavor
			FI Flavor intensity
			Total: #13

the predictive models (in blue, in Fig. 1). Table 1 summarizes the quality features of meat products.

Variables based on computer vision are generated on MRI images (in pink, in Fig. 1), using four feature extraction algorithms (fractals, Wavelet, Gabor filters and classic textures). These variables are then used to predict the quality features of food technology.

Besides, the system is implemented to determine the quality parameters in four different stages: (I) in an initial stage (fresh meat); (II) freezing the meat and then thawing it weeks later, to observe the influence of the defrosting process on the quality characteristics; (III) cooking the meat and inspecting the characteristics after this; and (IV) in the case of pork loin, performing the ripening process and computing the labels at the end of this process. Then, both the acquisition of images and the analysis of samples are carried out in these four different stages.

TABLE 2. Number of trained models.

Meat Product	Meat stage	Trained models	PC	IT	SA
Pork	Fresh	6	6	-	-
	Thawed	13	6	7	-
	Cooked	23	6	7	10
	Cured	26	6	7	13
Total		68			
Beef	Fresh	6	6	-	-
	Thawed	13	6	7	-
	Cooked	23	6	7	10
Total		42			

Number of trained models needed in the system to predict any of the quality features in any of the stages of the meat (110 models in total). PC – Physicochemical analysis, IT – instrumental textures, SA – sensory analysis.

The CAI system is trained to predict the quality parameters of Table 1 considering the four stages of the meat. The prediction of each quality feature requires an appropriate model. Then, as 110 quality attributes are predicted, 110 trained models are needed for the system, 68 for pork and 42 for beef meat (Table 2).

A. IMAGE DATASET

MRI acquisition is performed at the University of Extremadura (Cáceres, Spain) using a Low Field-MRI scanner (ESAOTE VET-MR E-SCAN XQ 0.18 T) with a hand/wrist coil.

According to previous studies [5], T1-weighted and Gradient Echo (GE) sequences are used, and the following parameters: field-of-view (FOV): 160×160 mm²; Echo Time (TE): 14 ms; slice thickness: 4 mm; flip angle: 75°; Repetition Time (TR): 1450 ms; matrix size: 224 × 176; phase encode: 176. The MRI acquisition is performed at 23 °C, obtaining a total of 13352 images for the experiments.

B. QUALITY PARAMETERS IN FOOD TECHNOLOGY

A complete dataset of quality features is included in the system. This dataset is computed by performing the traditional methods. This dataset is used as labels to validate the predictions carried out by the models based on the four algorithms of feature extraction.

The six Physicochemical (PC) parameters of Table 1 are obtained by experts in food technology which analyze the meat samples in triplicate. Water activity is obtained by means of the system Lab Master-aw (NOVASINA AG, Switzerland) after calibration at 20–22 °C. Instrumental color (L*, a*, and b*) is measured using a Minolta CR-300 colorimeter (Minolta Camera Corp., Meter Division, Ramsey, NJ) with illuminance D65, a 0° standard observer and a 2.5 cm port/viewing area. The colorimeter is standardized before use with a white tile having the following values: L* = 93.5, a* = 1.0, and b* = 0.8. Moisture is determined at 102 ± 2 °C by the official method (Association of Official Analytical Chemist, 2000; reference 935.29). The lipid

content of loins is determined gravimetrically with chloroform/methanol (2:1, v/v) [34].

For determination of the Instrumental Texture (IT) dataset, uniform portions of the samples are cut into 1 cm³ cubes. Samples are axially compressed to 60% of their original height with a flat plunger 50 mm in diameter (P/50) at a crosshead speed of 2 mm/s through a 2-cycle sequence. The instrumental analysis is performed in a TA.XT plus Texture Analyzer (Stable Micro Systems Ltd., Surrey, UK) [35].

The Sensory Analysis (SA) dataset is based on cooked and dry-cured loin samples, performed by fourteen trained panelists. Three samples are tasted per session, evaluating each time loin in triplicate. After cooking (in oven at 180 °C for 45 min), the cooked samples are refrigerated for 24 h until sensory evaluation. Then, loins are sliced using a slicer meat machine TGI 300 OMS S.r.l. (slice samples of 2mm and around 5 g). Just before the evaluation, samples are heated for 10 seconds in a 600W microwave oven. The dry-cured loins are also sliced (3 mm) before tasting. Samples (one slice per plate) are served on glass plates with mineral water and a piece of unsalted cracker to follow the rinsing protocol between samples. Evaluations are developed in tasting rooms designed according to the UNE-EN-ISO 8589:2010 regulation. All sessions are conducted at room temperature (20–22 °C) in a sensory room equipped with white fluorescent light. The serving order of the samples is randomized according to the Williams Latin square design. FIZZ software 2.20 C version (Sensory Analysis and Computer Test Management) is used for collecting the data. Attributes used in this study are selected based on the previous experience in sensory evaluation of meat products [36]. A 10 cm unstructured scale is used for attributes scoring, and verbal anchors are fixed as ‘little’ to ‘very much’ for all evaluated attributes.

C. COMPUTATIONAL METHODS

Four feature extraction algorithms and fourteen regressors are evaluated for the predictions. This study allows deciding the best combination of regressor-feature extraction algorithm to include in the ensemble CAI system.

1) FEATURE EXTRACTION ALGORITHMS

The system focuses on four texture-based feature extraction algorithms: classic texture algorithms, Wavelet transform based algorithm, Gabor filter-based algorithm, and fractal-based algorithms. Most of them have been widely used and validated in previous studies [5], [6].

- Classic texture algorithms consider the statistical techniques that extract second-order statistical features. **GLCM** [18], [19] considers the probability of obtaining the same grey level at different distances and orientations (0°, 45°, 90°, 135°, 180°, 225°, 270°, and 315°) extracting ten textural features: Energy (ENE), Entropy (ENTR), Correlation (COR), Haralick’s Correlation (HC), Inverse Difference Moment (IDM), Inertia (INE), Cluster Shade (CS), Cluster Prominence (CP), Contrast

(CON), and Dissimilarity (DIS). **NGLDM** [21], uses angular independent features based on the grey-level spatial dependence matrix, considering five measures: SNE (Small Number Emphasis), LNE (Large Number Emphasis), NNU (Number Non-Uniformity), SM (Second Moment), and ENT (Entropy). **GLRLM** [22] includes sets of consecutive pixels with the same grey level values, in different directions (0°, 45°, 90°, 135°, 180°, 225°, 270°, and 315°), computing eleven features: SRE (Short Run Emphasis), LRE (Long Run Emphasis), GLNU (Grey Level Non-Uniformity), RLU (Run Length Non-Uniformity), RPC (Run Percentage), LGRE (Low Grey-level Run Emphasis), HGRE (High Grey-level Run Emphasis), SRLGE (Short Run Low Grey-level Emphasis), SRHGE (Short Run High Grey-level Emphasis), LRLGE (Long Run Low Grey-level Emphasis), and LRHGE (Long Run High Grey-level Emphasis).

- Algorithm based on **Wavelet** transform [37], [38], consists of spectral characteristics based on the Discrete Wavelet Transform (DWT), where images are decomposed into low-pass and high-pass frequency band by applying filters recursively. The selected wavelet algorithm uses 3 scales and 6 directions, considering 3 values in each scale (mean, angle, and variance) computing a total of 54 features.
- Algorithm based on **Gabor** filters [39], as a spectral technique which uses 6 angles, and 3 different frequencies, calculating the mean and the variance. Thus, 36 characteristics are obtained in each of the two dimensions considered (72 features in total).
- Fractal-based algorithms includes fractal-based statistical methods. One Point of Fractal curve Texture Algorithm (**OPFTA**) [26] extracts seven texture features by applying second order statistics: Uniformity (UNI), Entropy (ENT), Correlation (COR), Homogeneity (HOM), Inertia (INE), Contrast (CON), and Efficiency (EFI) [40], [41]. Fractal Texture Algorithm (**FTA**) [40] is based on the repetitions of patterns in boxes, gathering the fractal characteristics in vectors to compute ten second order statistics: Uniformity (UNI), Entropy (ENT), Correlation (COR), Inverse Difference Moment (IDM), Inertia (INE), Contrast (CON), Emphasis (EMP), Correlation Coefficient (CC), Cluster Shade (CS) and Cluster Prominence (CP) [40], [41]. Classical Fractal Algorithm (**CFA**) [26] studies the pattern of repetition by computing the so-called local exponent with different box sizes, computing nine fractal dimensions: BOX1-BOX9.

Table 3 shows all the algorithms used to extract features from the images, forming a vector of 178 texture features.

Table 4 (for classic textures) and 5 (for fractals) shows how to compute some of the 178 texture features.

Classic texture algorithms are statistical methods based on the relationship between pairs of pixels, neighboring pixels,

TABLE 3. Feature extraction algorithms.

Group	Texture Algorithm	Features	# of features
CLASSICS	GLCM	ENE, ENT, COR, HC, IDM, INE, CS, CP, CON, DIS	10
	GLRLM	LRE, SRE, GLNU, RLNU, RPC, LGRE, HGRE, SRLGE, SRHGE, LRLGE, LRHGE	11
	NGLDM	SNE, LNE, NNU, SM, ENT	5
WAVELET	DT-CWT	e1d1-mean, e1d1-angle, e1d1-var	54
		e3d6-mean, e3d6-angle, e3d6-var	
GABOR	GABOR FILTER	a1f1-mean, a1f1-var a6f3-mean, a6f3-var	72
FRACTALS	OPFTA	UNI, ENT, COR, HOM, INE, CON, EFI	7
	FTA	UNI, ENT, COR, IDM, INE, CON, EMP, CC, CS, CP	10
	CFA	box1, box2, box3, box4, box5, box6, box7, box8, box9	9
TOTAL			178

TABLE 4. Classic texture algorithms.

GLCM	GLRLM	NGLDM
$ENE = \sum_i \sum_j P(i,j)^2$	$LRE = \frac{\sum_i \sum_j Q(i,j)j^2}{\sum_i \sum_j Q(i,j)}$	$SNE = \sum_j \sum_i \frac{R(j,i)}{i^2}$
$ENT = - \sum_i \sum_j P(i,j) \log(P(i,j))$	$SRE = \frac{\sum_i \sum_j Q(i,j)}{\sum_i \sum_j Q(i,j)j^2}$	$LNE = \sum_j \sum_i i^2 R(j,i)$
$COR = \frac{\sum_i \sum_j (i - \mu_x)(j - \mu_y)P(i,j)}{\sigma_x \sigma_y}$	$GLNU = \frac{\sum_i (\sum_j Q(i,j))^2}{\sum_i \sum_j Q(i,j)}$	$NNU = \sum_i (\sum_j R(j,i))^2$
$HC = \frac{\sum_i \sum_j (i,j)P(i,j) - \mu_x \mu_y}{\sigma_x \sigma_y}$	$RLNU = \frac{\sum_i (\sum_j Q(i,j))^2}{\sum_i \sum_j Q(i,j)}$	$SM = \sum_j \sum_i (R(j,i))^2$
$IDM = \sum_i \sum_j \frac{P(i,j)}{1 + (i-j)^2}$	$RPC = \frac{\sum_j \sum_i Q(i,j)}{L}$	$ENT = - \sum_i \sum_j R(j,i) \log(R(j,i))$
$INE = \sum_i \sum_j (i-j)^2 P(i,j)$	$LGRE = \frac{\sum_i \sum_j \frac{Q(i,j)}{i^2}}{\sum_i \sum_j Q(i,j)}$	
$CS = \sum_i \sum_j ((i - \mu_x) + (j - \mu_y))^3 P(i,j)$	$HGRE = \frac{\sum_i \sum_j i^2 Q(i,j)}{\sum_i \sum_j Q(i,j)}$	
$CP = \sum_i \sum_j ((i - \mu_x) + (j - \mu_y))^4 P(i,j)$	$SRLGE = \frac{\sum_i \sum_j \frac{Q(i,j)}{i^2 j^2}}{\sum_i \sum_j Q(i,j)}$	
$CON = \sum_i \sum_j (i-j)^2 (P(i,j))^2$	$SRHGE = \frac{\sum_i \sum_j \frac{i^2 Q(i,j)}{j^2}}{\sum_i \sum_j Q(i,j)}$	
$DIS = \sum_i \sum_j (i+1) - (j+1) P(i,j)$	$LRLGE = \frac{\sum_i \sum_j \frac{i^2 Q(i,j)}{i^2}}{\sum_i \sum_j Q(i,j)}$	
	$LRHGE = \frac{\sum_i \sum_j i^2 j^2 Q(i,j)}{\sum_i \sum_j Q(i,j)}$	

and also measure runs of gray levels in an image. The computational cost for GLCM is $O(n^2)$, $O(n^3)$ for NGLDM, and $O(n^2)$ for GLRLM [6]. In contrast, Wavelet transform is only computed in $O(n)$.

TABLE 5. Fractals algorithms.

OPFTA	FTA	CFA
$UNI = \sum_i \sum_j P(i,j)^2$	$UNI = \sum_{i=0}^n F_i^2$	$D = - \frac{\Delta \ln N}{\Delta \ln R}$
$ENT = \sum_i \sum_j P(i,j) * \log_{10}(P(i,j))$	$ENT = \sum_i (F_i * \log_{10}(F_i))$	
$COR = \frac{\sum_i \sum_j (i - \mu_x)(j - \mu_y)P(i,j)}{\sigma_x \sigma_y}$	$COR = \sum_i (i - \mu) * F_i$	
$HOM = \frac{\sum_i \sum_j P(i,j)}{1 + (i - j)^2}$	$IDM = \sum_i \frac{F_i}{1 + i^2}$	
$INE = \sum_i \sum_j (i - j)^2 P(i,j)$	$INE = \sum_i F_i * i^2$	
$CON = \sum_i \sum_j (i - j)^2 (P(i,j))^2$	$CON = \sum_i F_i^2 * i^2$	
$EFI = \frac{\sigma_x}{\mu_x} + \frac{\sigma_y}{\mu_y}$	$EMP = \sum_i \frac{F_i}{i^2}$	
	$CC = \sum_i (i - \mu)^2 * F_i$	
	$CS = \sum_i (i - \mu)^3 * F_i$	
	$CP = \sum_i (i - \mu)^4 * F_i$	

Gabor features are based on the Gabor filter responses to given input images. A set of filters tuned to various orientations and frequencies is used to calculate the responses to the image. For a point, the complexity of calculating the filter response is $O(M^2)$, where M represents the width and height of the mask. For an entire image of $N \times N$ size, it becomes $O(M^2 N^2)$ [42]. In the case of fractals features, according to [6], the computational complexity is $O(N^2)$ for OPFTA, $O(N^2 \log(n))$ for FTA is, and $O(N^3)$ for CFA.

2) REGRESSION MODELS

Fourteen regressors are compared in this paper. The programming language R was used in our experiments. As they are well known regressors, a brief description is presented below, including bibliographic references:

- lm (Linear Models), classical linear regression, for multivariate linear regression [43].
- penalized linear regression. The model fits generalized linear models with L1 (lasso and fused lasso) and/or L2 (ridge) penalties, or a combination of the two [44].
- SVM, Support Vector Machine for regression, included in the package e1071. The function was configured to perform a k-fold cross validation on the training data to assess the quality of the model, optimizing the Mean Squared Error [29].
- elmNRR, Extreme Learning Machine (ELM) neural network but with Gaussian kernel, defined in the package elmNNRcpp
- BART, Bayesian Additive Regression Tree [45], [46].
- BRNN, Bayesian Regularized Neural Network. The brnn function fits a two-layer neural network [47], [48] and uses the algorithm defined in [49].

- rqPen, quantile regression with LASSO (Least Absolute Shrinkage and Selection Operator) penalty. Algorithm is similar to LASSO code presented in [50].
- RF, Random Forest (RF) ensemble of random regression trees. The randomForest function implements Breiman's random forest algorithm based on the code presented in [27].
- M5P (P stands for 'prime') generates M5 model trees using the M5 algorithm introduced in [51] and enhanced in [52].
- CUBIST fits the M5 rule-based M5 model [52] with additional corrections based on nearest neighbors in the training set, as described in [53].
- CForest, is an implementation of the random forest and bagging ensemble algorithms using conditional inference trees as base learners [27].
- bagEARTH, is the bagged Multivariate Adaptive Regression Spline (MARS), a bagging ensemble of MARS [54].
- EARTH, is the Multivariate Adaptive Regression Spline (MARS) [54], [55].
- GAMBOOST, is the boosted generalized additive model where the regressor fits a generalized additive model by likelihood-based boosting.

Regarding the computational complexity of the models, it depends on the number of training examples (n) and the number of features (m).

For linear regressions (LM, penalized), train time complexity is $O(n^*m^2 + m^3)$, while test time complexity is $O(m)$ [56]. For random forest and M5P, train time is $O(n^*\log(n)^*m)$, and test time is $O(m)$. In the case of CForest, where M represents the number of trees, train complexity is $O(M^*n^*\log(n)^*m)$, and test complexity is $O(m^*M)$ [28], [56]. In SVM, as the number of training vectors increases, the time and space requirements also increase. Standard SVMs reach a computing time of $O(n^3)$ [30].

In elmNRR, complexity of model selection is determined by the number of parameters (weight variance, number of hidden units...) and the ranges used for them. The complexity is $O(H^3)$, where H is the number of hidden units [57]. CUBIST is a rule-based model that is an extension of Quinlan's M5 model tree. The train time complexity is $O(n^*\log(n)^*m)$, and the test time complexity is $O(m)$ [56].

III. THE ENSEMBLE CAI SYSTEM

In the pre-processing phase (Fig. 2), a batch of pork and beef loins is available. The feature extraction process is repeated at different times (fresh, thawed, cooked, and cured), to develop a complete CAI system.

The extraction of computer vision features is based on MRI and four computer vision algorithms. The feature vector of computer vision is made up of 178 variables: classic textures (26) + Gabor filter (72) + Wavelet (54) + fractals (26).

Methods of food technology (physicochemical, instrumental textures, and sensory analyses), allows obtaining the label

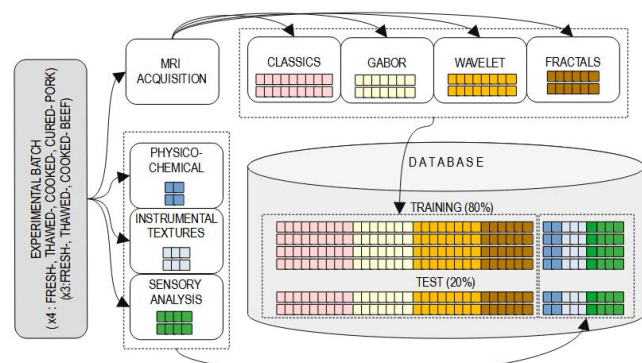


FIGURE 2. Pre-processing phase.

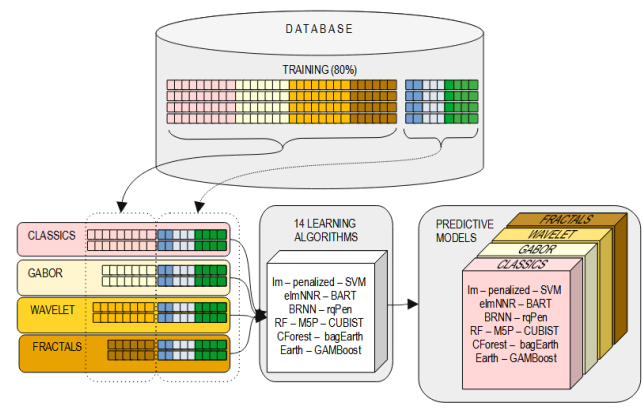


FIGURE 3. Learning phase.

dataset. Depending on the state of the meat, the size of the label vector is the following (Table 2): Fresh meat (6 labels from PC); thawed meat (13 labels from PC and IT); cooked meat (23 labels from PC, IT and SA); and cured loin (26 labels from PC, IT, and SA).

When all the feature extraction tasks are completed, the usual scaling, feature selection, dimensionality reduction and sampling procedures are carried out in the preprocessing stage. Finally, the dataset is divided into two sets: training and test datasets, following the percentage division: 80% training and 20% testing.

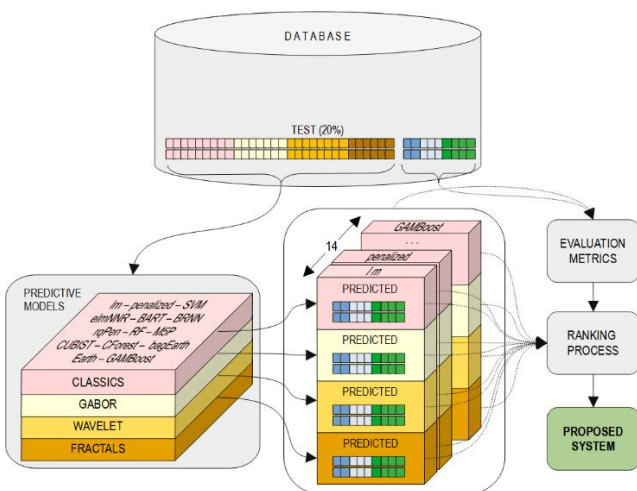
The training phase (Fig. 3) compares the performance of the four feature extraction algorithms and the fourteen learning algorithms. The features corresponding to the four sets of textures are considered separately and are the input to the fourteen learning algorithms.

The total number of trained models to estimate the food technology quality labels considering all the combinations based on the four feature algorithms and on the fourteen different learning algorithms is summarized in table 6.

A total of 6160 models are trained (3808 models for pork meat and 2352 models for beef meat). Of these 6160 approaches, only the top 110 models are integrated in the final system, the best combinations for any of the feature quality at any of the stages of the meat (as Table 2 shown).

TABLE 6. Models trained in learning phase.

Meat Product	Meat Stage	Trained models	Feature algorithms	Learning algorithms	Food technology
Pork	Fresh	336	4	14	6
	Thawed	728	4	14	13
	Cooked	1288	4	14	23
	Cured	1456	4	14	26
TOTAL		3808			
Beef	Fresh	336	4	14	6
	Thawed	728	4	14	13
	Cooked	1288	4	14	23
	TOTAL	2352			

**FIGURE 4.** Evaluation phase.

This stage also includes the cross-validation, and hyperparameter optimization procedures [58].

When the predictive models are trained, the test set of the database (20%) is used as input for the predictive models in the evaluation phase (Fig. 4).

The model performance is evaluated through some quantitative metrics. Pearson's correlation coefficient r between real and predicted labels is used, and other error measures as MSE (Mean Square Error), RMSE (Root Mean Squared Error), MAE (Mean Absolute Error), and MAPE (Mean Absolute Percentage Error). Denoting the actual value of the quality parameters as y_i , the average value as \bar{y} and the predicted value as f_i , where $i = 1, 2, \dots, n$ indicates the number of samples, the four measures are defined as follows:

$$r = \sqrt{\frac{\sum_{i=1}^n (f_i - \bar{y})^2}{\sum_{i=1}^n (y_i - \bar{y})^2}}$$

$$RMSE = \sqrt{\frac{1}{n} \sum_{i=1}^n (f_i - y_i)^2}$$

$$MAE = \frac{1}{n} \sum_{i=1}^n |f_i - y_i|$$

$$MAPE = \frac{1}{n} \sum_{i=1}^n \left| \frac{f_i - y_i}{y_i} \right|$$

These measures can give a thorough evaluation of the model performance. The correlation coefficient r measures the linear relation between the predicted values and actual values, which is better if closer to 1. Indeed, this coefficient was defined in [59] as follows: 0 – 0.25, negligible or not correlated; 0.25 – 0.50, fair correlation; 0.50 – 0.75, moderate-to-good correlation and >0.75, very good-to-excellent correlation. RMSE, MAE and MAPE measure the relative errors (first-order and second-order) between the predicted value and actual value, which are better when lower.

The proposed system estimates all the quality food technology labels, based on the 6160 predictive models. Then, the estimations are compared with the real labels stored in the test dataset, and the performance metrics are obtained (“evaluation metrics” module of Fig. 4).

The ensemble CAI system integrates the top 110 models, by examining the metrics of all 6160 models. For each of the quality parameters, all models are ranked, considering the best correlations obtained by the 6160 combinations of regressor-feature extraction algorithm.

IV. RESULTS AND DISCUSSION

The participation of the regressors in the final model could be interesting to the scientific community. Then, a ranking of the regressors is firstly presented, based on the correlations obtained in the experiments.

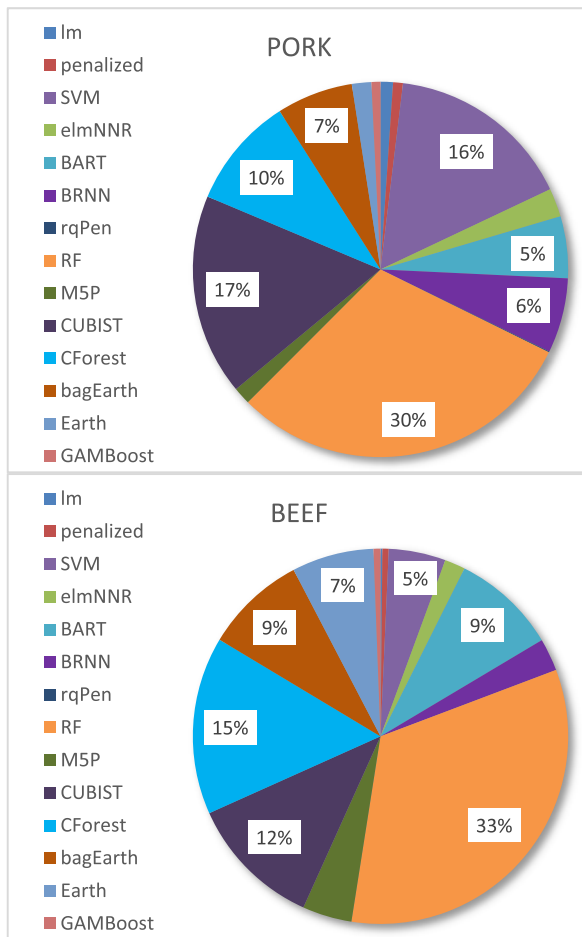
The ranking procedure rewards regressors with coefficient r higher than the average of correlations, also forcing this correlation to be greater than 0.5 (moderate to excellent correlation). Fig. 5 shows the percentage of votes received by each regressor in all the experiments, separated by batches.

In the case of pork, RF received 30 % of the votes, being the majority option. CUBIST (17 %) and SVM (16 %) together also present approximately 1/3 of the votes. Of the rest, CFOREST received 10 % of votes, and M5P 7 %. The rest of regressors obtained a small representation.

Results on beef meat were quite similar. A third of the votes were for RF, being CFOREST (15%) the second-best option. CUBIST went down a bit, going to 12%. Slightly below 10% were bagEARTH (9%), BART (9%) and EARTH (7%) regressors. It should be noted that SVM had an importance of only 5%.

Table 7 shows the ranking of the best 7 regressors, out of the 14 studied, as well as their influence according to the votes received, for pork, beef, and for both types mixed. As can be seen, with half of the regressors, approximately 90% participation is obtained in the final learning model, according to the votes.

Table 8 (for pork) and Table 9 (for beef) show the average correlations obtained when the regressors of Table 7 are considered to calculate all the attributes of each of the four feature extractor algorithms. Average correlations obtained are not very good. According to Colton's indications [59],

**FIGURE 5.** Percentage of votes for the regressors.**TABLE 7.** Ranking of regressors.

PORK		BEEF		PORK & MEAT	
Regressor	%	Regressor	%	Regressor	%
RF	30.21%	RF	33.21%	RF	31.71%
CUBIST	17.35%	CForest	15.31%	CUBIST	14.44%
SVM	16.05%	CUBIST	11.54%	CForest	12.47%
CForest	9.64%	BART	9.06%	SVM	10.48%
BagEarth	6.56%	BagEarth	8.73%	BagEarth	7.65%
BRNN	6.45%	EARTH	7.06%	BART	7.20%
BART	5.34%	SVM	4.91%	BRNN	4.63%
TOTAL	91.60%	TOTAL	89.82%	TOTAL	88.58%

there are hardly any correlations that can be considered in the “very good-to-excellent” group. Some of the features of the same algorithm reach high values, but others get low values, which means that the average is not as high as it would be desirable. Numerical distributions are not homogeneous for all features of the same model, which penalizes the use of a single method for predictions. This proves that it is not a good option to consider the same regressor to calculate all the features according to the same extractor algorithm. Instead,

TABLE 8. Correlation coefficients for pork loin.

	Algorithm	RF	Cubist	SVM	CForest	bagEarth	BRNN	BART
Fresh	Classics	0.6274	0.6200	0.5715	0.5822	0.5454	0.4912	0.5509
	Gabor	0.6657	0.6491	0.6595	0.6613	0.5989	0.5867	0.5815
	Wavelet	0.5163	0.5055	0.4190	0.4899	0.5068	0.4515	0.4977
	Fractals	0.7995	0.8362	0.5193	0.6256	0.4994	0.4442	0.5997
Thawed	Classics	0.6603	0.5922	0.6740	0.5970	0.5371	0.5188	0.5550
	Gabor	0.5827	0.5399	0.5729	0.5781	0.4931	0.4921	0.4683
	Wavelet	0.3629	0.3806	0.2635	0.3332	0.3782	0.1687	0.3379
	Fractals	0.5767	0.5148	0.5148	0.5282	0.4407	0.5767	0.4744
Cooked	Classics	0.6433	0.5895	0.5857	0.5962	0.5381	0.5178	0.5495
	Gabor	0.5600	0.5203	0.5459	0.5269	0.4984	0.4378	0.4780
	Wavelet	0.3307	0.3814	0.2010	0.2796	0.3631	0.2495	0.2972
	Fractals	0.5968	0.3814	0.3814	0.5754	0.4975	0.4059	0.5314
Cured	Classics	0.6185	0.5865	0.6437	0.5947	0.5315	0.5340	0.5723
	Gabor	0.6856	0.6668	0.6959	0.6719	0.5342	0.5253	0.5911
	Wavelet	0.4751	0.4738	0.3391	0.4052	0.4226	0.2532	0.3985
	Fractals	0.2896	0.2584	0.2841	0.2896	0.2419	0.3044	0.2635

TABLE 9. Correlation coefficients for beef loin.

	Algorithm	RF	Cubist	SVM	CForest	bagEarth	BRNN	BART
Fresh	Classics	0.7179	0.6766	0.6852	0.6563	0.6704	0.6414	0.6383
	Gabor	0.6294	0.5940	0.5923	0.5607	0.5603	0.4806	0.6026
	Wavelet	0.5636	0.5607	0.5378	0.5496	0.5238	0.4982	0.4597
	Fractals	0.6266	0.6310	0.5991	0.6021	0.5381	0.5874	0.5132
Thawed	Classics	0.7118	0.7503	0.7646	0.7328	0.6712	0.5492	0.6507
	Gabor	0.6907	0.6679	0.6171	0.6047	0.5746	0.5262	0.6028
	Wavelet	0.5286	0.5100	0.5545	0.5191	0.5391	0.5381	0.3063
	Fractals	0.6373	0.6360	0.6123	0.5946	0.4648	0.5739	0.4788
Cooked	Classics	0.7474	0.7149	0.7249	0.6941	0.7114	0.6747	0.6489
	Gabor	0.6896	0.6413	0.5954	0.5898	0.6038	0.5560	0.5701
	Wavelet	0.5094	0.4567	0.4499	0.496	0.4913	0.4145	0.2924
	Fractals	0.5532	0.5560	0.5119	0.5024	0.3500	0.5074	0.4278

it is convenient to study the best combination regressor-feature extraction algorithm, attribute-by-attribute.

The final correlation of the system following this approach is 0,712379883 for pork loin and 0,745761477 for beef loin, computed as an average of the best combinations showed in bold in Tables 8 and 9.

As shown in Table 6, all the combinations of regressors-feature extraction algorithms represent a total of 6180 different models. In the context of proposing a meat industry solution, integrating all these models into an ensemble system can pose a challenge. In order to overcome this limitation, only 110 models were integrated into the proposed CAI ensemble system. Specifically, the models that provided the best results.

Table 10 shows the best combinations for the 110 trained models, based on the ranking proposed in the methodology.

Fig. 6.a shows that RF is the best regressor for more than half of the predicted quality characteristics, being SVM the second most repeated option for approximately one third of the characteristics. CUBITS and CForest are the third and fourth options, respectively.

Regarding the extractor algorithms (Fig. 6.b), the classic algorithms are used in half of the features, while a third of the features are based on Gabor. Fractals are the third option, and it is noted that Wavelet is not used in any of the combinations.

TABLE 10. Best combination regressor-feature extraction algorithm.

	PORK							
	FRESH		THAWED		COOKED		CURED	
Wa	RF	FR	BRNN	GA	RF	CL	svm	GA
L*	Cubist	FR	RF	CL	RF	CL	svm	GA
a*	Cubist	FR	RF	CL	RF	GA	svm	GA
b*	Cubist	FR	svm	CL	Cubist	CL	svm	GA
MO	Cubist	FR	svm	CL	CForest	FR	svm	GA
LI	RF	FR	svm	CL	RF	FR	RF	GA

	BEEF							
	FRESH		THAWED		COOKED			
Wa	RF	CL	RF	CL	BRNN	CL		
L*	CForest	FR	RF	CL	RF	CL		
a*	RF	CL	RF	CL	bagEarth	CL		
b*	RF	CL	RF	CL	RF	CL		
MO	svm	GA	CForest	CL	M5P	CL		
LI	RF	CL	CForest	CL	RF	CL		

a)

	PORK				BEEF					
	THAWED		COOKED		CURED		TAWED		COOKED	
HD	svm	GA	RF	GA	svm	GA	RF	CL	RF	CL
AD	svm	CL	svm	GA	Cubist	GA	RF	CL	BRNN	CL
ST	svm	CL	RF	FR	RF	GA	RF	CL	RF	CL
CS	RF	CL	RF	FR	svm	GA	RF	CL	RF	CL
SP	svm	GA	svm	CL	svm	GA	RF	CL	CForest	CL
CH	bart	FR	RF	CL	svm	GA	RF	CL	RF	CL
RE	RF	GA	RF	FR	svm	GA	RF	CL	RF	CL

b)

	CI	BR	OI	CO	TD	JC	FB	CH	FI	CF
PORK	svm	Cubist	RF	svm	svm	RF	RF	RF	RF	RF
	CL	CL	FR	CL	CL	GA	GA	GA	FR	CL

| | RF |
|------|----|----|----|----|----|----|----|----|----|----|
| BEEF | CL |

c)

	CI	BR	MB	PO	OI	HD	JC	FB	CH	ST	CF	PF	FI
	svm	svm	svm	RF	Cubist	svm	svm	svm	svm	RF	RF	RF	RF
	GA	GA	GA	GA	GA	GA	GA	GA	GA	GA	GA	GA	GA

d)

Best combination regressor – feature extraction algorithm, for the quality parameters based on a) physicochemical analysis (42 models), b) instrumental textures (35 models), c) sensory analysis for cooked meat (20 models), and d) sensory analysis for para cured pork (13 models).

CL - Classics; GA - Gabor; WA - Wavelet; FR - Fractals.

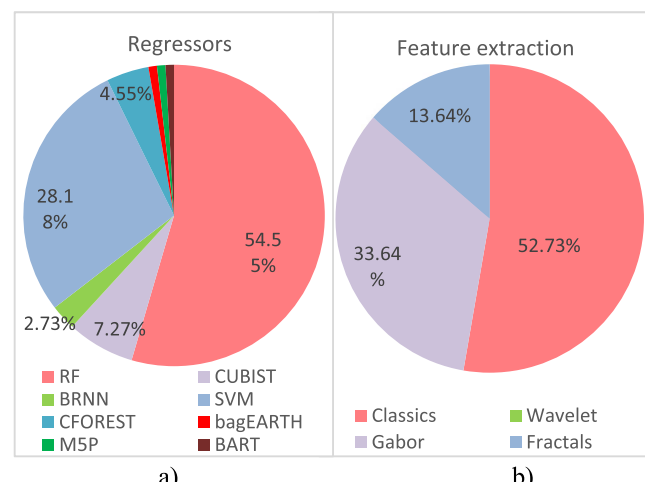
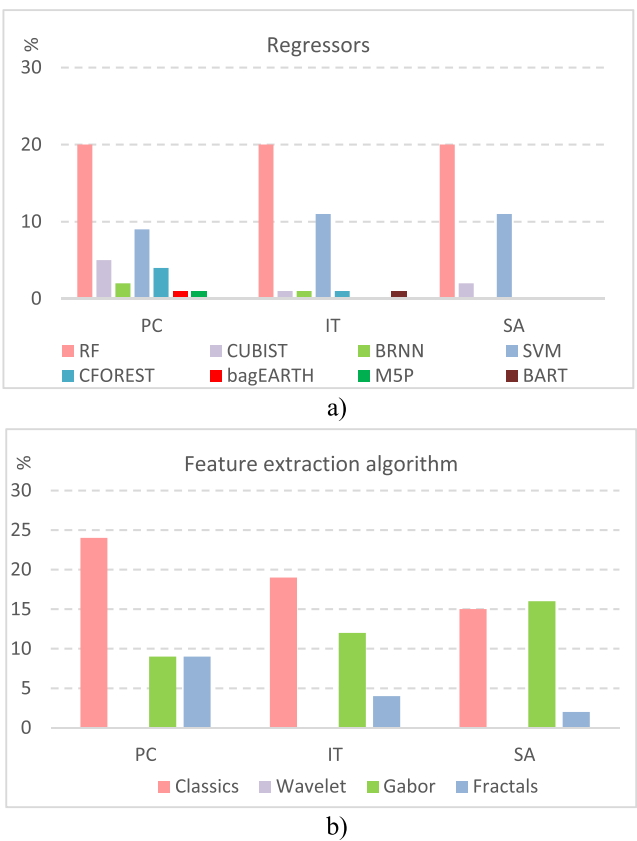
**FIGURE 6.** Distribution of a) the best regressors, and b) the best feature extraction algorithms.

Fig. 7.a shows the participation of each regressor and extractor algorithm in the different subsets of quality cate-

gories. RF is the most used regressor and SVM the second one to predict the three sets of characteristics (both PC, IT and SA). Up to 7 different regressors are involved in the prediction of PC features, which implies features with heterogeneous distributions. Thus, some features are better predicted with tree-based methods (RF, CUBIST, M5P), others with SVM and some with ensemble models (CFOREST, bagEARTH). As for the IT features, most are predicted with RF and SVM, and other regressors are practically hardly used. Finally, for sensory attributes, most are predicted using trees (mainly RF, and CUBIST) and a third using SVM. Note that the Bayesian models (BRNN and BART) are only useful for a few PC and IT features.

As for extractor algorithms (Fig. 7.b), classic textures reach the best results for more than half of the PC and IT characteristics, being the Gabor and fractal features the best options for the other half. In the sensory features, Gabor is the most repeated, closely followed by classic algorithms. Again, Wavelet does not appear for any of the features.

Finally, Table 11 shows the correlations obtained by the combination of the best regressors and feature extraction algorithms, for each of the predicted quality features.

Fig. 8 shows the quality of the predictions, noting that in Fig. 8.a almost half of the characteristics (specifically 40% of

TABLE 11. Correlations for the best combination.

	Meat	Wa	L*	a*	b*	MO	LI
Pork	Fresh	0.8603	0.8308	0.9289	0.8515	0.8737	0.7883
	Thawed	0.6744	0.7103	0.6649	0.6774	0.7277	0.6711
	Cooked	0.6238	0.6770	0.6336	0.6437	0.6640	0.6752
	Cured	0.7070	0.7646	0.6651	0.6700	0.6839	0.6954
Beef	Fresh	0.7489	0.7518	0.8814	0.6840	0.7291	0.6244
	Thawed	0.6691	0.7375	0.8504	0.7761	0.8232	0.7946
	Cooked	0.8516	0.6685	0.6800	0.8470	0.7682	0.7426

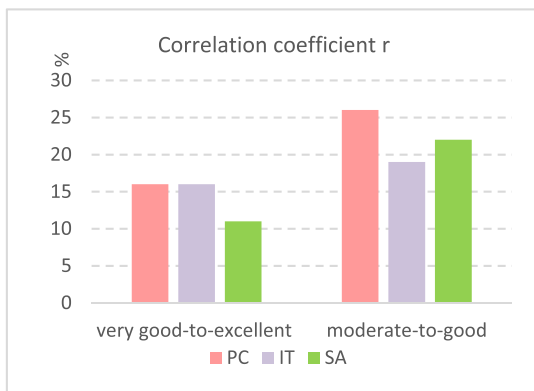
	a)							
	Meat	HD	AD	ST	CS	SP	CH	RE
Pork	Thawed	0.6786	0.7406	0.7683	0.7441	0.6648	0.6334	0.6372
	Cooked	0.5902	0.7012	0.7711	0.7185	0.6421	0.6849	0.7527
	Cured	0.7510	0.7129	0.7875	0.7266	0.7261	0.7274	0.7040
Beef	Thawed	0.8698	0.7237	0.7992	0.8591	0.8610	0.8512	0.7518
	Cooked	0.6726	0.8530	0.8139	0.8104	0.7393	0.7692	0.7901

	b)											
	Meat	CI	BR	OI	CO	TD	JC	FB	CH	FI	CF	
Pork	0.525	0.657	0.634	0.658	0.587	0.655	0.613	0.645	0.707	0.679		
Beef	0.744	0.820	0.791	0.727	0.753	0.738	0.849	0.767	0.785	0.836		

	c)												
	CI	BR	MB	PO	OI	HD	JC	FB	CH	ST	CF	PF	FI
0.7	0.7	0.7	0.6	0.7	0.7	0.7	0.7	0.7	0.7	0.7	0.6	0.6	0.7
40	28	21	81	22	51	81	54	27	50	69	87	25	

d)

Correlations for the best combination of regressor and feature extraction algorithm, for the quality features of a) physicochemical analysis, b) instrumental textures, c) sensory analysis for cooked meat, and d) sensory analysis for cured pork.

**FIGURE 8.** Distribution of the correlation coefficient r of the proposed model, for the different quality parameter subsets (PC—PhysicoChemical analysis, IT—Instrumental Textures; SA—Sensory Analysis).

them) obtain a prediction from “very good-to-excellent”, and high percentages in the “moderate-to-good” category. IT features obtain the most precision as a whole (Fig. 8.b), followed by the PC characteristics. The sensory ones obtain the worst correlations, although obtaining good results. Nonetheless the developed CAI system predicts most of the quality characteristics with high accuracy.

The final correlation of the system following this approach is 0.7346 for pork loin and 0.7746 for beef loin, computed as an average of the best combinations showed in Tables 8 and 9. The correlations have been improved from 0.7124 to 0.7346 for pork loin, and from 0.7458 to 0.7746 for beef loin, considering an attribute-by-attribute selection

TABLE 12. Results of the performance metrics.

Meat	Metric	Wa	L*	a*	b*	MO	LI
FRESH	R	0.8898	0.9491	0.9435	0.8974	0.8489	0.7620
	RMSE	0.0020	0.6900	0.4448	0.4828	0.6794	0.7857
	MAE	0.0013	0.5106	0.3128	0.3281	0.5153	0.6083
	MAPE	0.0014	0.0116	0.0308	0.0937	0.0073	0.0974
BEEF	R	0.7264	0.6911	0.8641	0.6381	0.7730	0.6506
	RMSE	0.0034	1.1521	1.4890	1.6137	1.2970	1.6860
	MAE	0.0025	0.8871	0.9781	1.1381	0.9496	1.1136
	MAPE	0.0025	0.0213	0.0576	0.1662	0.0130	0.3383

of the best combinations, instead of considering the best combinations grouped by extractor algorithms.

Finally, as an example, Table 12 shows the results obtained by the different performance metrics considered for the case of fresh pork and beef.

V. CONCLUSION

In this paper, the performance of four feature extraction algorithms (classic textures, Gabor filters, Wavelet, and fractals) on MRI of pork and beef loin has been studied. In addition, fourteen regressors have been tested to predict the quality characteristics of pork and beef loins at various meat states (fresh, thawed, cooked, and cured). A total of 6160 models have been studied, and the best combinations of regressor – feature extraction algorithm for each of the quality parameters have been included in a new CAI system developed in this paper. The proposed CAI system determines all the quality attributes of pork and beef loin, in the four states of meat with an average correlation of 0.74 for pork loin, and 0.76 for beef loin. This is the first CAI system proposed to predict quality parameters of different types of loins and could be considered as an alternative to the traditional methods for the inclusion in the meat industry.

REFERENCES

- [1] L. Shrestha, S. O. J. Crichton, B. Kulig, B. Kiesel, O. Hensel, and B. Sturm, “Comparative analysis of methods and model prediction performance evaluation for continuous online non-invasive quality assessment during drying of apples from two cultivars,” *Thermal Sci. Eng. Prog.*, vol. 18, Aug. 2020, Art. no. 100461.
- [2] S. M. Fowler, D. Wheeler, S. I. Mortimer, and D. L. Hopkins, “Partial least squares and machine learning for the prediction of intramuscular fat content of Lamb loin,” *Meat Sci.*, vol. 177, Jul. 2021, Art. no. 108505.
- [3] P. Cortez, M. Portelinha, S. Rodrigues, V. Cadavez, and A. Teixeira, “Lamb meat quality assessment by support vector machines,” *Neural Process. Lett.*, vol. 24, no. 1, pp. 41–51, Aug. 2006.
- [4] H. A. Neto, W. L. F. Tavares, D. C. S. Z. Ribeiro, R. C. O. Alves, L. M. Fonseca, and S. V. A. Campos, “On the utilization of deep and ensemble learning to detect milk adulteration,” *BioData Mining*, vol. 12, no. 1, pp. 1–13, Dec. 2019.
- [5] T. Pérez-Palacios, D. Caballero, T. Antequera, M. L. Durán, M. Ávila, and A. Caro, “Optimization of MRI acquisition and texture analysis to predict physico-chemical parameters of loins by data mining,” *Food Bioprocess Technol.*, vol. 10, no. 4, pp. 750–758, Apr. 2017.
- [6] D. Caballero, A. Caro, A. B. Dahl, B. K. Ersbøll, J. M. Amigo, T. Pérez-Palacios, and T. Antequera, “Comparison of different image analysis algorithms on MRI to predict physico-chemical and sensory attributes of loin,” *Chemometric Intell. Lab. Syst.*, vol. 180, pp. 54–63, Sep. 2018.

- [7] U. Khulal, J. Zhao, W. Hu, and Q. Chen, "Intelligent evaluation of total volatile basic nitrogen (TVB-N) content in chicken meat by an improved multiple level data fusion model," *Sens. Actuators B, Chem.*, vol. 238, pp. 337–345, Jan. 2017.
- [8] H. Li, Q. Chen, J. Zhao, and M. Wu, "Nondestructive detection of total volatile basic nitrogen (TVB-N) content in pork meat by integrating hyperspectral imaging and colorimetric sensor combined with a nonlinear data fusion," *LWT Food Sci. Technol.*, vol. 63, no. 1, pp. 268–274, Sep. 2015.
- [9] M. Zhao, C. Esquerre, G. Downey, and C. P. O'Donnell, "Process analytical technologies for fat and moisture determination in ground beef—A comparison of guided microwave spectroscopy and near infrared hyperspectral imaging," *Food Control*, vol. 73, pp. 1082–1094, Mar. 2017.
- [10] P. Fantazzini, M. Gombia, P. Schembri, N. Simoncini, and R. Virgili, "Use of magnetic resonance imaging for monitoring parma dry-cured ham processing," *Meat Sci.*, vol. 82, no. 2, pp. 219–227, Jun. 2009.
- [11] T. Antequera, A. Caro, P. G. Rodríguez, and T. Pérez, "Monitoring the ripening process of Iberian ham by computer vision on magnetic resonance imaging," *Meat Sci.*, vol. 76, no. 3, pp. 561–567, Jul. 2007.
- [12] L. Manzocco, M. Anese, S. Marzona, N. Innocente, C. Lagazio, and M. C. Nicoli, "Monitoring dry-curing of S. Daniele ham by magnetic resonance imaging," *Food Chem.*, vol. 141, no. 3, pp. 2246–2252, Dec. 2013.
- [13] T. Pérez-Palacios, D. Caballero, A. Caro, P. G. Rodríguez, and T. Antequera, "Applying data mining and computer vision techniques to MRI to estimate quality traits in Iberian hams," *J. Food Eng.*, vol. 131, pp. 82–88, Jun. 2014.
- [14] R. Molano, D. Caballero, P. G. Rodriguez, M. D. M. Avila, J. P. Torres, M. L. Duran, J. C. Sancho, and A. Caro, "Finding the largest volume parallelepipedon of arbitrary orientation in a solid," *IEEE Access*, vol. 9, pp. 103600–103609, 2021.
- [15] M. Bernau, P. V. Kremer, E. Lauterbach, E. Tholen, B. Petersen, E. Pappenberg, and A. M. Scholz, "Evaluation of carcass composition of intact boars using linear measurements from performance testing, dissection, dual energy X-ray absorptiometry (DXA) and magnetic resonance imaging (MRI)," *Meat Sci.*, vol. 104, pp. 58–66, Jun. 2015.
- [16] S. Lee, S. Lohumi, H. Lim, T. Gotoh, T. Goto, B. Cho, and S. Jung, "Determination of intramuscular fat content in beef using magnetic resonance imaging," *J. Fac. Agricult., Kyushu Univ.*, vol. 60, no. 1, pp. 157–162, 2015.
- [17] D. Caballero, T. Pérez-Palacios, A. Caro, M. Ávila, and T. Antequera, "Optimization of the image acquisition procedure in low-field MRI for non-destructive analysis of loin using predictive models," *PeerJ Comput. Sci.*, vol. 7, p. e583, Jun. 2021, doi: 10.7717/peerj-cs.583.
- [18] R. M. Haralick, K. Shanmugam, and I. Dinstein, "Textural features for image classification," *IEEE Trans. Syst., Man, Cybern.*, vol. SMC-3, no. 6, pp. 610–621, Nov. 1973.
- [19] R. M. Haralick and L. G. Shapiro, *Computer and Robot Vision*. Chicago, IL, USA: Addison-Wesley, 1993.
- [20] M. Sonka, V. Hlavac, and R. Boyle, *Image Processing, Analysis and Machine Vision*. Stanford, CA, USA: International Thomson Publishing, 1999.
- [21] C. Sun and W. G. Wee, "Neighbouring gray level dependence matrix for texture classification," *Comput. Vis., Graph., Image Process.*, vol. 23, no. 3, pp. 341–352, 1983, doi: 10.1016/0734-189X(83)90032-4.
- [22] M. M. Galloway, "Texture classification using gray level run length," *Comput. Graph. Image Process.*, vol. 4, no. 2, pp. 172–179, 1975.
- [23] L. H. Siew, R. M. Hodgson, and E. J. Wood, "Texture measures for carpet wear assessment," *IEEE Trans. Pattern. Anal. Mach. Intell.*, vol. PAMI-10, no. 1, pp. 10–92, Jan. 1988.
- [24] S. Minhas and M. Y. Javed, "Iris feature extraction using Gabor filter," in *Proc. Int. Conf. Emerg. Technol.*, Oct. 2009, pp. 252–255.
- [25] S. G. Mallat, "A theory for multiresolution signal decomposition: The wavelet representation," *IEEE Trans. Pattern Anal. Mach. Intell.*, vol. 11, no. 7, pp. 674–693, Jul. 1989.
- [26] B. B. Mandelbrot, *The Fractal Geometry of Nature*. New York, NY, USA: W. H. Freeman and Company, 1983.
- [27] L. Breiman, "Random forests," *Mach. Learn.*, vol. 45, pp. 5–32, Oct. 2001.
- [28] K. Hassine, A. Erbad, and R. Hamila, "Important complexity reduction of random forest in multi-classification problem," in *Proc. 15th Int. Wireless Commun. Mobile Comput. Conf. (IWCMC)*, Jun. 2019, pp. 226–231.
- [29] C. C. Chang and C. J. Lin, *LIBSVM: A Library for Support Vector Machines*. Accessed: Jun. 2022. [Online]. Available: <https://www.csie.ntu.edu.tw/~cjlin/libsvm/>
- [30] I. W. Tsang, J. T. Kwok, and P.-M. Cheung, "Core vector machines: Fast SVM training on very large data sets," *J. Mach. Learn. Res.*, vol. 6, pp. 363–392, Apr. 2005.
- [31] A. C. Lorena, L. F. O. Jacintho, M. F. Siqueira, R. D. Giovanni, L. G. Lohmann, A. C. P. L. F. de Carvalho, and M. Yamamoto, "Comparing machine learning classifiers in potential distribution modelling," *Expert Syst. Appl.*, vol. 38, no. 5, pp. 5268–5275, May 2011.
- [32] J. C. S. Nunez, A. C. Lindo, and P. G. Rodriguez, "A preventive secure software development model for a software factory: A case study," *IEEE Access*, vol. 8, pp. 77653–77665, 2020.
- [33] J. C. Sancho, A. Caro, M. Ávila, and A. Bravo, "New approach for threat classification and security risk estimations based on security event management," *Future Gener. Comput. Syst.*, vol. 113, pp. 488–505, Dec. 2020.
- [34] T. Pérez-Palacios, J. Ruiz, D. Martín, E. Muriel, and T. Antequera, "Comparison of different methods for total lipid quantification," *Food Chem.*, vol. 110, pp. 1025–1029, Oct. 2008.
- [35] TTC (Texture Technologies Company). *Overview of Texture Profile Analysis*. Accessed: Jun. 2022. [Online]. Available: <https://texturetechnologies.com/resources/texture-profile-analysis/#settings-and-standards>
- [36] A. González-Mohino, T. Antequera, S. Ventanas, D. Caballero, J. Mir-Bel, and T. Pérez-Palacios, "Near-infrared spectroscopy-based analysis to study sensory parameters on pork loins as affected by cooking methods and conditions," *J. Sci. Food Agric.*, vol. 98, no. 11, pp. 4227–4423, 2018.
- [37] J. S. Walker, *A Primer on Wavelets and Their Scientific Applications*. Boca Raton, FL, USA: CRC Press, 2008.
- [38] A. Laine and J. Fan, "Texture classification by wavelet packet signatures," *IEEE Trans. Pattern Anal. Mach. Intell.*, vol. 15, no. 11, pp. 1186–1191, Nov. 1993.
- [39] T. Randen and J. H. Husøy, "Filtering for texture classification: A comparative study," *IEEE Trans. Pattern Anal. Mach. Intell.*, vol. 21, no. 4, pp. 291–310, Apr. 1999.
- [40] N. Aggarwal and R. K. Agrawal, "First and second order statistics features for classification of magnetic resonance brain images," *J. Signal Inf. Process.*, vol. 3, no. 2, pp. 146–153, 2012.
- [41] S. Peckingpaugh, "An improved method for computing gray-level co-occurrence matrix-based texture measured," *Comput. Vis., Graph. Image Process.*, vol. 53, pp. 574–580, Nov. 1991.
- [42] G. Amayeh, A. Tavakkoli, and G. Bebis, "Accurate and efficient computation of Gabor features in real-time applications," in *Proc. 5th Int. Symp. Vis. Comput. (ISVC)*, Las Vegas, NV, USA, 2019, pp. 243–252.
- [43] J. M. Chambers, "Linear models," in *Statistical Models in S* (Wadsworth & Brooks/Cole), J. M. Chambers and T. J. Hastie, Eds., Sacramento, CA, USA, 1992, ch. 4.
- [44] J. J. Goeman, " L_1 penalized estimation in the Cox proportional hazards model," *Biometrical J.*, vol. 52, pp. 70–84, Feb. 2010.
- [45] A. Kapelner and J. Bleich, "BartMachine: Machine learning with Bayesian additive regression trees," *J. Stat. Softw.*, vol. 70, no. 4, pp. 1–40, 2016.
- [46] H. A. Chipman, E. George, and R. E. McCulloch, "BART: Bayesian additive regression trees," *Ann. Appl. Statist.*, vol. 4, no. 1, pp. 266–298, 2010.
- [47] D. J. C. MacKay, "Bayesian interpolation," *Neural Comput.*, vol. 4, no. 3, pp. 415–447, May 1992.
- [48] F. Dan Foresi and M. T. Hagan, "Gauss-Newton approximation to Bayesian learning," in *Proc. Int. Conf. Neural Netw. (ICNN)*, 1997, pp. 1930–1935.
- [49] D. Nguyen and B. Widrow, "Improving the learning speed of 2-layer neural networks by choosing initial values of the adaptive weights," in *Proc. ICNN*, vol. 3, 1990, pp. 21–26.
- [50] R. Koenker and I. Mizera, "Convex optimization in R," *J. Stat. Softw.*, vol. 60, pp. 1–23, Sep. 2014.
- [51] Y. Wang and I. H. Witten, "Induction of model trees for predicting continuous classes," in *Proc. Eur. Conf. Mach. Learn.*, 1997, pp. 1–13.
- [52] R. Quinlan, "Learning with continuous classes," in *Proc. Austral. Joint Conf. Artif. Intell.*, 1992, pp. 343–348.
- [53] R. Quinlan, "Combining instance-based and model-based learning," *Proc. 10th Int. Conf. Mach. Learn.*, 1993, pp. 236–243.
- [54] J. H. Friedman, "Multivariate adaptive regression splines (with discussion)," *Ann. Statist.*, vol. 19, no. 1, pp. 1–141, 1991.
- [55] J. H. Friedman, "Fast MARS," Dept. Statist., Stanford Univ., Tech. Rep. LCS110, 1993.

- [56] Kaggle. *Computational Complexity of Machine Learning Models*. Accessed: Jun. 2022. [Online]. Available: <https://www.kaggle.com/general/263127>
- [57] E. Parviainen and J. Riihimäki, "A connection between extreme learning machine and neural network kernel," in *Knowledge Discovery, Knowledge Engineering and Knowledge Management*, vol. 272. Valencia, Spain: Springer, 2013, pp. 122–135.
- [58] A. Dag, K. Topuz, A. Oztekin, S. Bulur, and F. M. Megahed, "A probabilistic data-driven framework for scoring the preoperative recipient-donor heart transplant survival," *Decis. Support Syst.*, vol. 86, pp. 1–12, Jun. 2016.
- [59] T. Colton, *Statistical in Medicine*. New York, NJ, USA: Little Brown and Co, 1974.



TRINIDAD PÉREZ-PALACIOS received the Veterinary and Ph.D. degrees from the University of Extremadura, in July 2004 and 2009, respectively. She got grants for stay in Gent, Belgium, and Porto, Portugal. She is currently a member of the Institute of Meat and Meat Products (IPoCar). She has participated in several research projects, and has achieved several papers in high quality journals, conferences, and book chapters. Her research interests include food technology, meat and meat products, and MRI.



JUAN P. TORRES received the B.Sc. degree in computer engineering from the University of Extremadura, Spain, in 2017. Currently, he is a Researcher in the research and development project focused in MRI and image and data analysis applied to meat products in order to extract and predict quality parameters. His research interests include MRI, image processing, data mining, prediction techniques, data analysis, and computer systems.



ANDRÉS CARO received the B.Sc., M.Sc., and Ph.D. degrees in computer science from the University of Extremadura, Spain, in 1993, 1998, and 2006, respectively. He has been an Associate Professor with the Department of Computer and Telematics Systems Engineering, University of Extremadura, since 1999, where he is currently the Laboratory Head of the Media Engineering Group. He has participated in the management of both national and international research and development projects and private financing. He is the coauthor of numerous research SCI journal articles and book chapters. His research interests include cybersecurity, big data, machine learning, and pattern recognition.



MARÍA DEL MAR ÁVILA received the B.Sc. and M.Sc. degrees in computer science from the University of Extremadura, in 1997 and 1999, respectively, and the Ph.D. degree in computer science, in 2018. She has been an Assistant Professor with the Department of Computer and Telematics Systems Engineering, University of Extremadura, since 2002. She has participated in several research projects, being the coauthor of several SCI journal articles. Her research interests include pattern recognition, data mining and machine learning, information retrieval, and cybersecurity.



TERESA ANTEQUERA received the Ph.D. degree in chemistry from the University of Extremadura, in 1990. She is currently a Full Professor with the Department of Animal Production and Food Science, University of Extremadura. She leads the research line on applications of nondestructive techniques, mainly magnetic resonance imaging (MRI) to find issues that may affect the quality of Iberian pig products and their classification. She has participated in more than 40 projects and research contracts and the coauthor of more than 200 articles in journals included in SCI, technical journals, and conference contributions.



PABLO GARCÍA RODRÍGUEZ received the Doctor (Ph.D.) degree in computer science, in 2000. He was the Director of the School of Technology, Cáceres, from 2017 to 2019, where his engineering studies are teaching in civil, building, computing, and telecommunications. He is currently the General Director of the Digital Agenda of the Government of the Autonomous Community of Extremadura, Spain. His teaching was mainly centered on subjects of programming and information systems in computer engineering. His research interests include the Internet of Things (IoT), bigdata and pattern recognition, and image analysis.

3.2. Artículo “MRI-computer vision on fresh and frozen-thawed beef: Optimization of methodology for classification and quality prediction”

• **Autores:** Trinidad Pérez-Palacios, Mar Ávila, Teresa Antequera, Juan P. Torres, Alberto González-Mohino, Andrés Caro

• **Publicación:** Meat Science, Volume 197, Pages 109054, 2023

• **ISSN:** 0309-1740

• **DOI:** <https://doi.org/10.1016/j.meatsci.2022.109054>

• **Índice de impacto:**

IF (2022): 7.1 (12/142) Q1 in FOOD SCIENCE & TECHNOLOGY

En este trabajo se evalúa la capacidad de las técnicas de resonancia magnética (MRI) y visión por computador para clasificar carne cruda de ternera fresca y carne cruda congelada-descongelada. También se realiza un estudio para predecir características de textura, características físico-química y características sensoriales mediante la optimización de la metodología de análisis de imágenes (algoritmo) y análisis de datos (regresor), probando diferentes combinaciones algoritmo-regresor. La precisión de los resultados de clasificación y predicción depende especialmente del algoritmo. En el trabajo se determinan diferentes combinaciones óptimas para la clasificación (fractales con cforest, random forest o SVM) y predicción de parámetros de calidad de muestras de carne cruda de ternera congelada-descongelada (fractales-cforest o fractal-random forest) y cocidas (texturas clásicas-random forest). El algoritmo para analizar la imagen puede fijarse en función del objetivo (clasificación o predicción) y del tipo de muestra (cruda o cocida), sin que la característica analizada sea relevante. Este estudio muestra, en primer lugar, la capacidad de la resonancia magnética para clasificar la carne de ternera (carne cruda de ternera fresca frente a carne cruda de ternera fresca congelada-descongelada) y determinar las características de calidad de forma no destructiva.



MRI-computer vision on fresh and frozen-thawed beef: Optimization of methodology for classification and quality prediction

Trinidad Perez-Palacios ^{a,*}, Mar Ávila ^b, Teresa Antequera ^a, Juan Pedro Torres ^b, Alberto González-Mohino ^a, Andrés Caro ^b

^a Institute of Meat and Meat Products (IProCar), Food Technology, University of Extremadura, Cáceres, Spain

^b Institute of Meat and Meat Products (IProCar), Computer Systems and Telematics Engineering, University of Extremadura, Cáceres, Spain



ARTICLE INFO

Keywords:

Beef
Freezing-thawing
Quality parameters
MRI
Algorithm
Regressor

ABSTRACT

This study aims to evaluate the capability of Magnetic Resonance Imaging (MRI) and computer vision techniques to classify fresh (raw F) ($n = 12$) and frozen-thawed (FT) ($n = 12$) beef and predict physico-chemical, texture and sensory characteristics by optimization the methodology for image analysis (algorithm) and data analysis (regressor), testing different algorithm-regressor combinations. The accuracy of the classification and prediction results especially depend on the algorithm. Different optimum combinations were found for classification (Fractal with CForest, RF or SVM) and prediction of quality parameters of raw FT (Fractal-CForest or Fractal-RF) and cooked FT samples (Classic-RF). Thus, the computational analysis of MRI, especially the algorithm to analyze the image, may be set as a function of the aim (classification or prediction) and of the type of sample (raw or cooked), while the analysed characteristic is not relevant. This study firstly showed the capability of MRI to classify beef (raw F vs. raw FT) and to determine quality characteristics in a non-destructive way.

1. Introduction

Beef can be considered a primary food source, due to its content of high-quality protein, essential amino acids, minerals (Fe, Ca, Mg and P) and vitamins, such as B-complex (Cabrera & Saadoun, 2014; Oh et al., 2016) and vitamin E, which is especially abundant in beef from animals fed extensively. This is the case of the beef included in the Protected Geographical Indication (PGI) "Ternera de Extremadura" (ORDEN APA/2423/2002, 2022; BOE n° 237) that guarantees compliance with the production and processing conditions of beef from Extremadura (in the southwest of Spain). Production requirements are mainly related to the system, feeding, area, breed, and age at slaughter, among other characteristics, and specify the prohibition of freezing of carcasses and meat pieces.

The restriction of freezing is related to the high-quality characteristics required in beef from the PGI "Ternera de Extremadura" and to the potential impact of the freezing-thawing process (Leygonie, Britz, & Hoffman, 2012). The formation of extracellular ice crystals influences physico-chemical (moisture losses, lipid oxidation, protein denaturation) and sensory characteristics (changes in colour and texture), which also depend on the quality of the fresh meat and the freezing-thawing

conditions (Carballo & Jiménez, 2001). In fact, differentiation between fresh and frozen-thawed meat has long been a need in the food industry to guarantee consumers assurance in both economic and food quality terms (Evans, Nott, Kshirsagar, & Hall, 1998).

Physico-chemical parameters and sensory attributes of meat and meat products have been traditionally analysed by means of destructive methods that also are tedious, time and solvent consuming and require, in the case of the sensory analysis, a trained panel to evaluate the samples. Several studies have been focused on evaluating the potential of different techniques, based on images and/or spectra, for determining quality characteristics of meat in a non-destructive way. Digital cameras, computed tomography, Near-Infrared Spectroscopy, Hyperspectral Imaging, Nuclear Magnetic Resonance and Magnetic Resonance Imaging (MRI) have been the most evaluated methods (Antequera, Caballero, Grassi, Uttaro, & Perez-Palacios, 2021). Among these techniques, MRI may be best suited for the analysis of meat samples since it is non-destructive, non-invasive, non-intrusive, nonionizing, innocuous and gets information from the interior of the sample (Caballero, Perez-Palacios, Caro, & Antequera, 2021).

Since 2000, the number of publications about MRI studies in meat have experienced a notable increase. In most studies, the procedure

* Corresponding author at: Avda. de las Ciencias s/n, University Institute building, 10003 Cáceres, Spain.

E-mail address: triny@unex.es (T. Perez-Palacios).

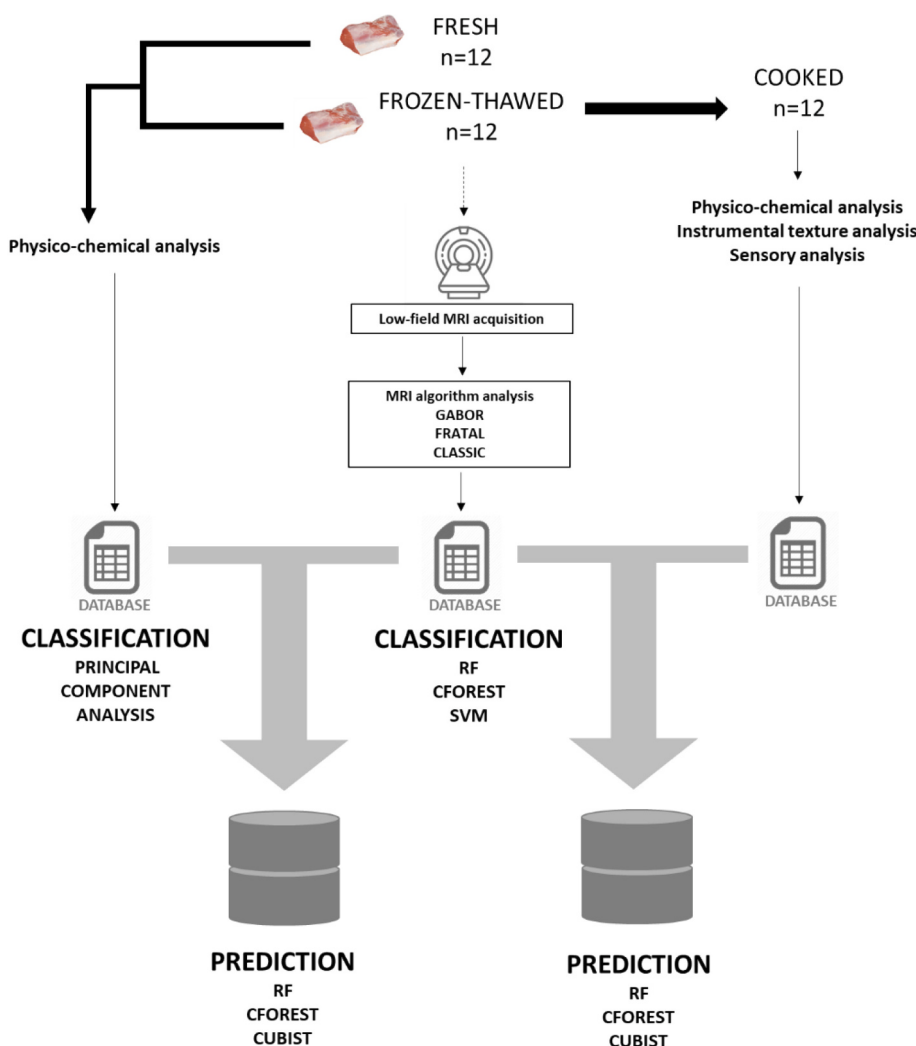


Fig. 1. Overall experimental procedure.

consists of the image acquisition, followed by the image analysis and the data analysis. Spin echo T1-weighted sequence has been preferably used for the image acquisition; Classic texture algorithms are normally applied for the image analysis; and for the data analysis, traditional statistical techniques, such as Principal Component Analysis, Partial Least Square and Multiple Linear Regression are mostly used, as reviewed by Caballero et al. (2021).

As well as the procedure, the validation of the results is also of great importance in MRI studies, which has usually been done by cross-validation methodology (Kohavi, 1995), with training set and test sets. According to Ávila et al. (2019), this protocol could be much too optimistic, because the test set would be the only one available to evaluate the performance of the model for each hyperparameter value, and the performance of the final model for the value of the selected hyperparameter. These authors suggested dividing the data set into training, validation and test partitions, where the validation set will fix the adjustable hyperparameters.

Hams and dry-cured loins have been the most analysed food by means of MRI with the aims of classifying samples (i.e. depending on the animal breed, feeding, lipid composition) and/or predicting quality parameters (Caballero, Antequera, Caro, Durán, & Pérez-Palacios, 2016; Pérez-Palacios et al., 2017). Recently, MRI has been used to evaluate the effect of freezing/thawing on chicken (Frelka et al., 2019) and beef (Cheng et al., 2019), finding some visual differences between unfrozen and frozen-thawed samples and modifications in the signal intensity and

percentage of pixels of the MRI images. However, no image analysis or data analysis, to classify samples or predict quality characteristics, have been carried out in beef. In this kind of meat, MRI was applied to determine the water content in samples cooked under jets of hot air for the development of a crust in the meat surface (Portanguen, Ikonik, Clerjon, & Kondjoyan, 2014).

Considering all these premises, the main goal of the present work was to evaluate the capability of MRI and computer vision techniques to differentiate between fresh and frozen-thawed beef samples from the PGI “Ternera de Extremadura” and to predict physico-chemical parameters and sensory attributes in these meat samples. A secondary goal was to determine optimum procedures for image analysis, and data analysis were also aimed. This study was expected to provide new knowledge about the use of MRI as technique for analysis of meat.

2. Material and methods

2.1. Overall experimental procedure

Fig. 1 shows the overall experimental procedure followed in the present study. Twenty-four fresh beef loins from PGI “Ternera de Extremadura” were purchased in a local market. All of them came from the same group of animals, male or females feeding extensively, and slaughtered at 11 months old, according to the requirements of the PGI. The average weigh was 7500 kg. Half of them were immediately

analysed as fresh samples (raw F), and the other half were vacuum packaged, frozen at -20°C and thawed after 30 days (FT). The thawing process was carried out at $5\text{--}7^{\circ}\text{C}$ over 36–48 h.

The two batches (raw F and raw FT) were firstly MRI scanned and then physico-chemical analysed for moisture, water activity and instrumental colour coordinates (L^* , a^* , b^*). The obtained MRI images were analysed applying three algorithms (Gabor, Fractal and Classic), transforming each image in a vector of computational characteristics.

The raw FT loins were then oven cooked (180°C for 45 min) (cooked FT) and analysed for physico-chemical, instrumental texture and sensory analyses.

Thus, three individual databases were obtained: i) from physico-chemical analysis of raw F and raw FT samples; ii) from MRI analysis of raw F and raw FT samples; and iii) from physico-chemical, instrumental texture and sensory analysis of cooked FT samples. All these datasets were normalized to the range 0–1.

Classification raw F vs. raw FT samples was tried by means of i) physico-chemical data, applying Principal Component Analysis and of ii) computational characteristics of MRI, from Gabor, Fractal and Classic algorithms, applying three classification methods (Random Forest (RF), CFOREST and Super Vector Machine (SVM)). Each algorithm was used in combination with each classification method, resulting in nine combinations in total.

Prediction of physico-chemical parameters of raw F and raw FT beef samples was carried out by different regressors (RF, CFOREST and CUBIST), which were applied to the dataset composed of physico-chemical and computational data from raw F and raw FT batches.

Prediction of physico-chemical, instrumental texture and sensory analysis of cooked FT beef samples as a function of computational data from raw FT samples was also tried. In this case, a dataset with physico-chemical, instrumental texture and sensory analysis of cooked FT samples and computational data from raw FT batch was constructed. Again, the regressors RF, CFOREST and CUBIST were applied.

As occurred in the classification trial, in the prediction analysis, each class of MRI algorithm was used in combination with each regressor, resulting in nine algorithm-regressor combinations.

2.2. Physico-chemical analysis

Beef samples from raw F, raw FT and cooked FT batches were analysed for moisture, water activity and instrumental colour coordinates. The moisture was determined at $102 \pm 2^{\circ}\text{C}$ by the official method (AOAC, 2000; reference 118,935.29). For measuring the water activity, the system Lab Master-aw (NOVASINA AG, Switzerland) was used after calibration at $20\text{--}22^{\circ}\text{C}$. Instrumental colour was measured in the inner part, after the loin being cut transverse to the longitudinal axis and allowed to bloom for 45–60 min. It was done by using a Minolta CR-300 colorimeter (Minolta Camera 125 Corp., Meter Division, Ramsey, NJ), which was standardized with a white tile. The selected light source was D65, with SCE (specular component excluded), a 0° standard observer and a 2.5 cm port/viewing area. In this study, lightness (L^*), redness-greenness (a^*) and yellowness-blueness (b^*) were the measured colour coordinates. Each sample was analysed in triplicate.

2.3. Instrumental texture analysis

Texture analysis was carried out in cooked FT samples, by using a TA XT plus Texture Analyser (Stable Micro Systems Ltd., Surrey, UK), performing a Texture Profile Analysis (TPA). Firstly, the samples were cut into ten uniform portions of 1 cm^3 , which were axially compressed to 60% of their original height with a flat plunger 50 mm in diameter (P/50) at a crosshead speed of 2 mm/s through a 2-cycle sequence. The following texture parameters were measured from the force deformation curves according to the Texture Technologies protocol (<https://texturetechnologies.com/resources/texture-profile-analysis#tpa-measurements>): hardness, adhesiveness, springiness,

cohesiveness, gumminess, chewiness, resilience.

2.4. Sensory analysis

Cooked FT samples were also subjected to quantitative-descriptive analysis of sensory attributes. Trained panellists (14) were staff at the Meat and Meat Products Research Institute (IPoCar) of the University of Extremadura. Three loins were tasted per session, evaluating each sample in triplicate. After cooking (in oven at 180°C for 45 min), the cooked samples were refrigerated for 24 h until sensory evaluation. Then, cooked loins were sliced using a slicer meat machine TGI 300 OMS S.r.l. (TGI, Jerago con Orago, Italy) (slice samples of 2 mm and around 5 g). Just before the evaluation, samples were heated for 10 s in a 600 W microwave oven. Samples (one slice per plate) were served on glass plates with mineral water and a piece of unsalted cracker to follow the rinsing protocol between samples. Evaluations were developed in tasting rooms designed according to the UNE-EN-ISO 8589:2010 regulation. All sessions were performed at room temperature ($20\text{--}22^{\circ}\text{C}$) in a sensory room equipped with white fluorescent light. The serving order of the samples was randomized according to the Williams Latin square design. FIZZ software 2.20C version (Biosystèmes, Couternon, France, 2002) was used for collecting the data.

Panellist training and attribute selection were carried out in different sessions. To start the panel training, various attributes were suggested, based on the previous experience of the authors in sensory evaluation of meat products (Caballero et al., 2018; González-Mohino, Antequera, Caballero, Mir-Bel, & Perez-Palacios, 2018). In addition, panellists were asked to generate terms to describe the samples. Then, redundant attributes were removed and ballot anchors were established for each selected descriptive term. A 10 cm unstructured scale was used for attribute scoring, and verbal anchors were fixed as 'little' to 'very much' for all evaluated attributes. The following sensory attributes were chosen: colour intensity, brightness, odour intensity, cooked odour, tenderness, juiciness, fibrousness, chewiness, flavour intensity and cooked flavour. Finally, the ballots were tested by panellists in individual booths with unknown representative samples.

2.5. Acquisition of MRI

Beef samples from raw F and raw FT batches were analysed by a low field-MRI scanner (ESAOTE VET-MR E-SCAN XQ 0.18 T) at the Faculty of Veterinary of the University of Extremadura (Cáceres, Spain), with a body coil. The Spin Echo T1-weighted sequence was applied with the following parameters: field-of-view: $240 \times 240\text{ mm}^2$; echo time: 29 ms; repetition time: 910 ms; slice thickness: 4 mm; flip angle: 90° . A total of 13,352 images were obtained for the experiments. The MRI acquisition was performed at 23°C . All images were acquired in DICOM format with 512×512 resolution and 256 Gy levels.

2.6. MRI analysis

Three types of texture-based algorithms were applied to the MRI images obtained from beef samples to extract computational features of the images: Gabor filter-based algorithm, Fractal-based algorithms and Classic texture algorithms.

- Algorithms based on Gabor filters (Randen & Husøy, 1999) were implemented with a spectral technique. This uses 6 angles ($\pi/6$) and 3 different frequencies and calculates the mean and the variance, obtaining 36 characteristics in each of the two dimensions considered. Thus, this algorithm gives 72 computational features (a1f1-mean, a1f1-var, ..., a6f3-mean, a6f3-var).
- Fractal-based algorithms applied in the present study have included three fractal-based statistical methods: one point of fractal curve texture algorithm (OPFTA), fractal texture algorithm (FTA) and classical fractal algorithm (CFA).

OPFTA ([Caballero et al., 2017](#)) is based on a two-dimensional variation of the Minkowski-Bouligand algorithm ([Mandelbrot, 1982](#)). Firstly, it achieves local exponents with different box sizes (powers of 2) and a matrix with the values of the most representative local exponent is generated. Then, second order statistics are applied to finally extract seven texture features: Uniformity, Entropy, Correlation, Homogeneity, Inertia, Contrast and Efficiency ([Aggarwal & Agrawal, 2012](#)).

FTA ([Caballero, Caro, et al., 2017](#)) is also based on a variation of Minkowski-Bouligand algorithm ([Mandelbrot, 1982](#)) and considers the repetitions of patterns in boxes. A vector of ten fractal characteristics is computed after applying second order statistics: Uniformity, Entropy, Correlation, Inverse Difference Moment, Inertia, Contrast, Emphasis, Correlation coefficient, Cluster shade and Cluster Prominence ([Aggarwal & Agrawal, 2012](#)).

CFA ([Mandelbrot, 1982](#)) also studies the pattern of repetition in boxes of different sizes and computes the so-called local exponent, obtaining nine fractal dimensions (BOX1-BOX9) as computational features.

Classic texture algorithms applied in this study were gray level cooccurrence matrix (GLCM), gray level run length matrix (GLRLM) and neighborhood gray-level different matrix (NGLDM). They employ statistical techniques to extract second-order statistical features.

GLCM ([Haralick, Shanmugam, & Dinstein, 1973](#)) evaluates the probability of obtaining the same gray level at different distances and orientations (0°, 45°, 90°, 135°, 180°, 225°, 270°, and 315° in the present study) and accumulates the co-occurrences into a single matrix, to ten texture features: Energy, Entropy, Correlation, Haralick's correlation, Inverse Difference Moment, Inertia, Cluster Shade, Cluster Prominence, Contrast and Dissimilarity.

GLRLM ([Galloway, 1975](#)) considers sets of consecutive pixels with the same gray level values in different directions (0°, 45°, 90°, 135°, 180°, 225°, 270° and 315°) and computes eleven features: Short Run Emphasis, Long Run Emphasis, Gray Level Non-Uniformity, Run Length Non-Uniformity, Run Percentage, Low Gray-Level Run Emphasis, High Gray-Level Run Emphasis, Short Run Low Gray-Level Emphasis, Short Run High Gray-Level Emphasis, Long Run Low Gray-Level Emphasis and Long Run High Gray-Level Emphasis.

NGLDM ([Sun & Wee, 1982](#)) uses angular independent features of the gray-level spatial dependence matrix and extracts the five computational features: Small Number Emphasis, Large Number Emphasis, Number Non-Uniformity, Second Moment and Entropy.

Thus, three vectors, from Gabor, Fractal and Classic algorithms, with 72, 26 and 26 computational texture features, respectively, were obtained after the MRI analysis.

2.7. Data analysis

Four different Machine Learning regressors were applied to carry out the data analysis of the present work. RF, CForest, CUBIST and SVM were selected based on a previous trial with several regressors (data not shown). In the present work these regressors have been implemented in R, using the packages randomForest, party, Cubist, and e1071, respectively.

- RF is a collection of random regression trees. It is implemented in the Breiman's random forest algorithm and is based on the code presented by [Breiman \(2001\)](#).
- CFOREST is a forest ensemble of conditional inference trees. It has been implemented based on the random forest and bagging ensemble algorithms and uses, as base learners, conditional inference trees ([Breiman, 2001](#)).
- SVM is the support vector machine for regression. It is included in the package e1071. The function of SVM performs a k-fold cross validation on the training data to calculate the model and optimize the Mean Squared Error ([Chang & Lin, 2021](#)). The cross-validation parameter (cross) was set to four repetitions, the insensitive-loss

function (epsilon) and the cost of constraints violation (the 'C'-constant of the regularization term in the Lagrange formulation) were 0, 0.2, 0.01 and 4, 8, 16, 32, 64, 128, respectively.

- CUBIST is based on a M5 rule model with corrections on the nearest neighbors in the training set ([Quinlan, 1993](#)). The committee models (boosting iterations) were fixed to 10.

RF, CForest and SVM were applied as classifiers and RF, CForest and CUBIST were used for prediction purposes. Each regressor was applied on each vector of computational features, having in total nine combinations for classification (Gabor-RF, Gabor-CForest, Gabor-SVM, Fractal-RF, Fractal-CForest, Fractal-SVM, Classic-RF, Classic-CForest, Classic-SVM) and another nine for prediction (Gabor-RF, Gabor-CForest, Gabor-CUBIST, Fractal-RF, Fractal-CForest, Fractal-CUBIST, Classic-RF, Classic-CForest, Classic-CUBIST).

2.8. Validation

Results on classification of raw F vs. raw FT samples based on computational characteristics of MRI (from Gabor, Fractal and Classic algorithms) and three classification methods (RF, CFOREST and SVM) were evaluated by means of measures of precision, recall and F-score.

Precision is the proportion of correctly predicted positive cases, and it is calculated from the equation:

$$\text{Precision} = \frac{TP}{TP + FP}$$

Recall is the proportion of correctly identified positive cases, and it is calculated from the equation:

$$\text{Recall} = \frac{TP}{TP + FN}$$

F-score is defined as the harmonic mean of precision and recall and it is calculated from the equation:

$$F\text{-score} = \frac{\text{Precision} \times \text{Recall}}{\text{Precision} + \text{Recall}}$$

Where TP (True Positive) is the total number of positive cases that are correctly classified by the diagnostic model, FP (False Positive) is defined as the total number of negatively identified cases that are classified wrongly by the diagnostic model and FN (False Negative) is the total number of cases that are positively identified but classified as wrong by the diagnostic model.

Precision or recall cannot describe the efficiency of a classifier because high results in one of these indices does not necessarily imply good performance on the other. For this reason, F-score, a popular combination, is commonly used as a single metric to evaluate classifier performance ([Vafeiadis, Diamantaras, Sarigiannidis, & Chatzisavvas, 2015](#)). Values closer to one imply better combined precision and recall for the classifier ([Fawcett, 2006](#)).

In the case of the prediction assays, the dataset was divided into training (80%) and testing (20%) tests. The aim of the training set aim is comparing the performance of the algorithms for MRI analysis and of the regressor. The three vectors of computational features, from Gabor, Fractal and Classic algorithms, were the input to each of the three Machine learning regressors to predict the quality parameters of the beef samples, carrying out cross-validation and procedures of hyper-parameter optimization. The set was divided into 10 sub-sets, selecting the models based on the average/median prediction performance across 10 non-overlapping test. A 10-fold cross validation reduce the variation between the training and tests performance ([Dag, Topuz, Oztekin, Bulur, & Megahed, 2016](#)).

Once all the predictive models are available, the testing set of the database (20%) is used as input. Particularly, Pearson's correlation coefficient (r) between predicted and real values of the quality parameters was studied in each algorithm-regressor combination. Correlation

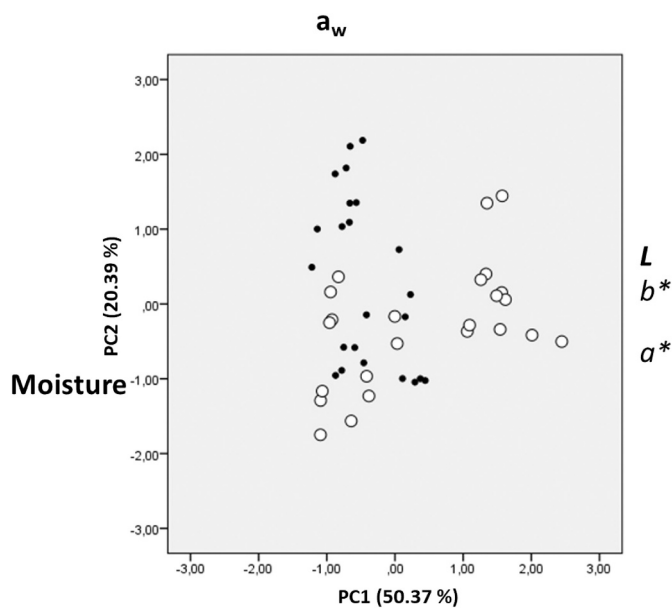


Fig. 2. Biplot of Principal Components Analysis of physico-chemical parameters from fresh (●) and frozen-thawed (○) beef loins.

Table 1
Results (mean \pm standard deviation) of physico-chemical parameters of fresh and frozen-thawed beef sample.

	Fresh	Frozen-Thawed	p-value
Moisture (%)	72.58 ± 2.27	67.81 ± 5.44	>0.05
Water activity	0.98 ± 0.00	0.97 ± 0.00	>0.05
<i>L</i> *	41.31 ± 1.78	49.73 ± 8.84	>0.05
<i>a</i> *	16.12 ± 3.19	16.52 ± 3.42	>0.05
<i>b</i> *	7.16 ± 2.25	7.30 ± 2.76	>0.05

coefficients were defined according to Colton (1974): 0–0.25, negligible or not correlated; 0.25–0.50, fair correlation; 0.50–0.75, moderate-to-good correlation and > 0.75, very good-to-excellent correlation.

In addition, the model performance was also evaluated through error measures as RMSE (root mean squared error), MSE (mean square error), MAE (mean absolute error), and MAPE (mean absolute percentage error). Denoting the actual value of the quality parameters as y_i , the average value as \bar{y} and the computed value as f_i , where $i = 1, 2, \dots, n$ indicates the number of samples, the measures are defined as follows:

$$RMSE = \sqrt{\frac{1}{n} \sum_{i=1}^n (f_i - y_i)^2}$$

$$MSE = \frac{1}{n} \sum_{i=1}^n (f_i - y_i)^2$$

$$MAE = \frac{1}{n} \sum_{i=1}^n |f_i - y_i|$$

$$MAPE = \frac{1}{n} \sum_{i=1}^n \left| \frac{f_i - y_i}{y_i} \right|$$

3. Results and discussion

3.1. Classification of fresh and frozen-thawed beef samples

Classification of raw F and raw FT samples have been tried by means of physico-chemical parameters (moisture, water activity, *L**, *a**, *b**) and MRI-computer vision techniques. Fig. 2 shows PCA-biplot of

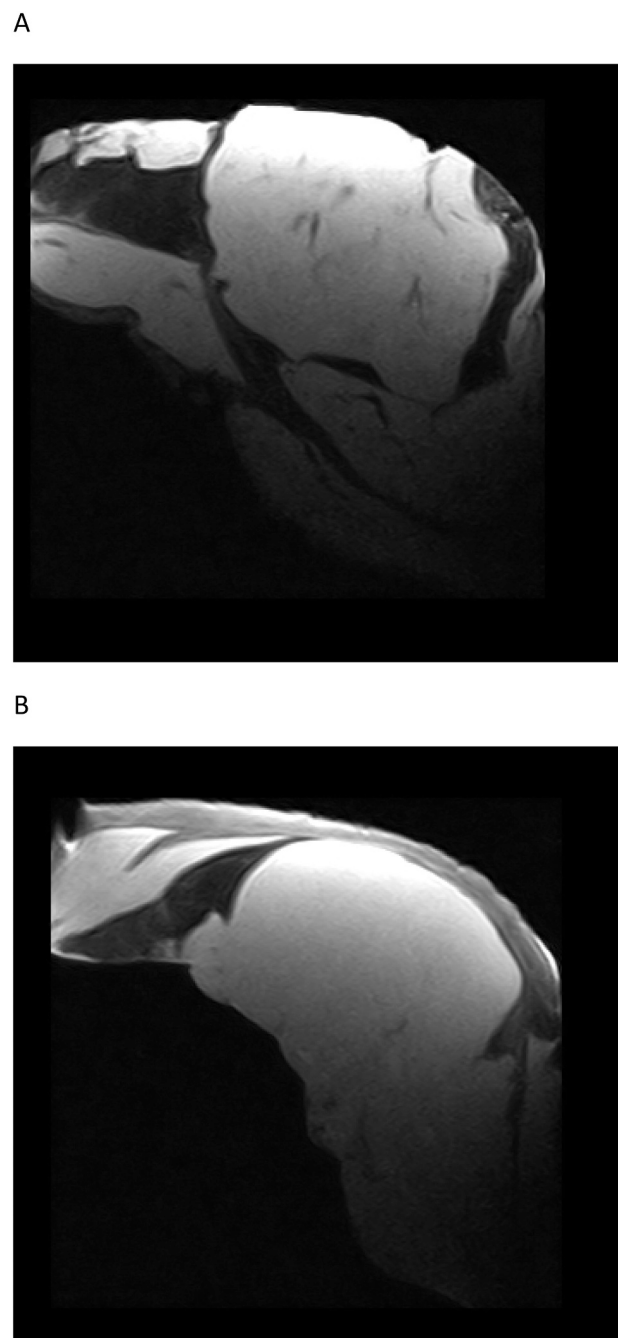


Fig. 3. MRI images from fresh (A) and frozen-thawed (B) beef loins (light gray colour: lean part; dark gray colour: fat).

physico-chemical parameters of raw F and raw FT samples. Two principal components accounted for 70.76% of the total variance (50.37% for PC1 and 20.39% for PC2). Raw F and raw FT samples were located in the four quadrants, and were not well separated. This may be explained by the absence of significant differences ($p > 0.05$) in the physico-chemical parameters between raw F and raw FT batches (Table 1). However, it is worth mentioning the notable differences in the mean values of moisture and *L** between raw F and raw FT although they did not differ significantly, which may be explained by the high statistical deviation in these two parameters. In fact, differences in the percentage of moisture and some colour coordinates have previously been described between fresh and frozen-thawed hams (Perez-Palacios, Ruiz, Martín, Barat, & Antequera, 2011) and was ascribed to the water release during the thawing process. This aspect may also be related to the variability in

Table 2

Results of fresh and frozen-thawed beef sample classification by means of different combinations of MRI algorithms and regressors.

		CLASSIC		FRACTAL		GABOR	
		Fresh	Frozen-Thawed	Fresh	Frozen-Thawed	Fresh	Frozen-Thawed
CFOREST	Precision	0.683	0.745	0.988	1.000	0.682	0.738
	Recall	0.755	0.672	1.000	0.988	0.758	0.652
	F-score	0.717	0.707	0.994	0.994	0.718	0.693
RF	Precision	0.685	0.776	1.000	1.000	0.684	0.752
	Recall	0.748	0.736	1.000	1.000	0.789	0.665
	F-score	0.715	0.751	1.000	1.000	0.732	0.710
SVM	Precision	0.657	0.778	0.964	1.000	0.780	0.648
	Recall	0.788	0.644	1.000	0.963	0.528	0.854
	F-score	0.717	0.704	0.982	0.981	0.630	0.737

the values of moisture and L^* , because it is not easy to hold the water from the interior at the surface of the frozen-thawed samples. In the present study, values of physico-chemical parameters seemed not be able to classify raw F and raw FT beef samples properly.

Fig. 3 shows MRI images of raw F and raw FT samples. The light gray colour illustrates the lean part of the meat piece, while the dark gray colour represents the fat. It is difficult to discern any visual difference between raw F and raw FT images. At the most, it may be pointed out a lighter gray colour of the lean in the raw FT samples in comparison to raw F ones. This may be explained by the release of water during the freezing-thawing, since MRI T1-weighted sequences detect Hydrogen and other features like fat fluidity and water retention, which increase the T1 relaxation time (Lufkin, 1998).

Table 2 describes quality measures (precision, recall, F-score) of classification results between raw F and raw FT samples by means of different combinations of algorithms applied on the MRI (Gabor, Fractal and Classic), and regressors used (RF, CFOREST and SVM). The highest values for precision, recall and F-score were found when applying Fractal algorithms in combination with any of the regressors. The best ones were obtained with the RF regressor (1.000 in all cases). The Classic and Gabor algorithms offered lower values for these quality classification measures. These results point out the capability of MRI-computation analysis (Fractal-RF) to differentiate raw F from raw FT beef samples. The high values for precision, recall and F-score obtained with Fractal may indicate that raw FT beef samples have much larger influence on the pattern of repetitions of the MRI than in the gray levels or spatial distribution analysed by the Classic and Gabor algorithms, respectively. According to Caballero et al. (2017), in pork loins, the instrumental colour coordinates are more related to the pattern of

repetitions than to the gray levels, while the latter are more strongly related to the moisture related parameters.

As well as quality classification measures, the computational cost should be also considered to select the most suitable combination of MRI algorithm and regressor. The computational cost for the different fractal algorithms is $O(N^3)$ for CFA, $O(N^2 \log n)$ for FTA, and $O(N^2)$ for OPFTA. Classical algorithms are statistical methods based on the relationship between pairs of pixels, neighboring pixels, and also measure runs of gray levels in an image. Combined, these algorithms have a computational cost of $O(N^3)$ (Caballero et al., 2018). Gabor features are based on the Gabor filter responses to a given input image. The responses on the image are calculated for a set of filters tuned at various orientations and frequencies. The simplest technique to perform the filtering operation is to implement the convolution in the spatial domain. The complexity of the convolution directly depends on the size of the convolution mask (in this case, the mask is the Gabor filter). The complexity of calculating the filter response for a point is $O(M^2)$, where M is the width and height of the mask. If filtering is done on the entire $N \times N$ size image, the complexity becomes $O(M^2 N^2)$ (Amayeh, Tavakkoli, & Bebis, 2019).

Analyzing the computational cost of the 3 regressors, RF implies a time cost of $O(M m n \log(n))$, with "M" being the number of trees, "m" the number of features and "n" the number of data samples in the training set (Hassine, Erbad, & Hamila, 2019). As CForest is a type of RF implementation, the computational complexity is similar. SVM are powerful tools, but their time and space requirements increase rapidly with the number of training vectors. The core of an SVM is a quadratic programming problem, which separates the support vectors from the rest of the training data. Standard SVM training reaches computational time and space of $O(n^3)$ and $O(n^2)$, respectively, where "n" is the size of

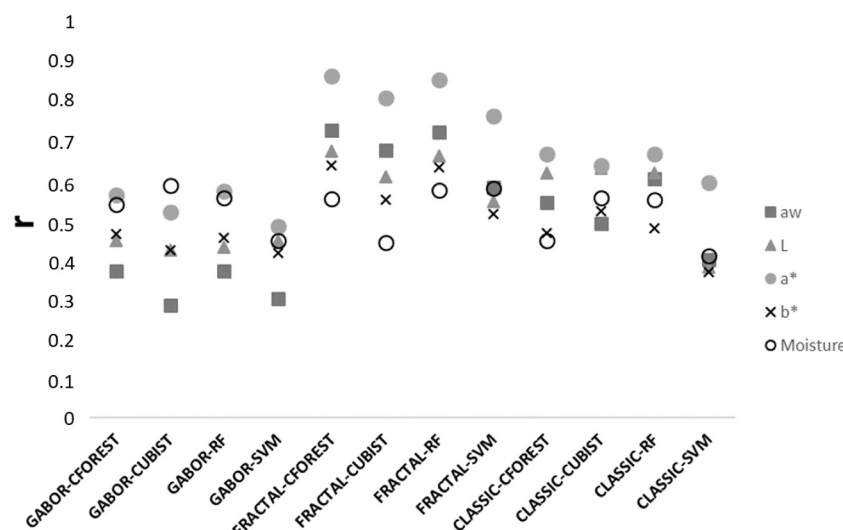
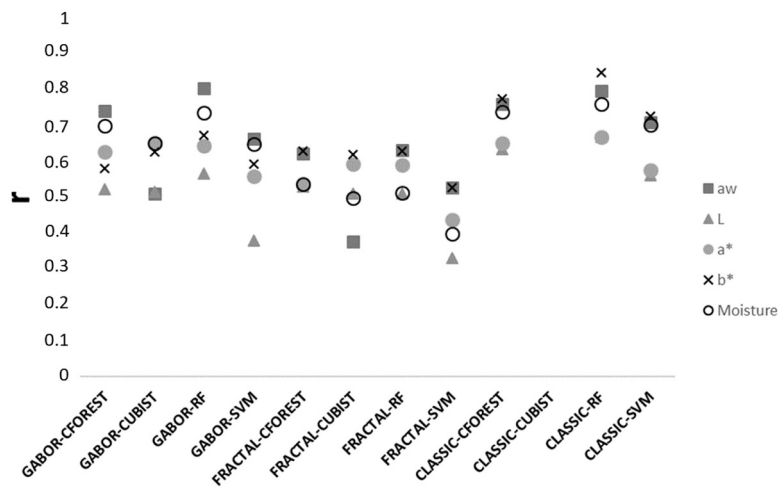
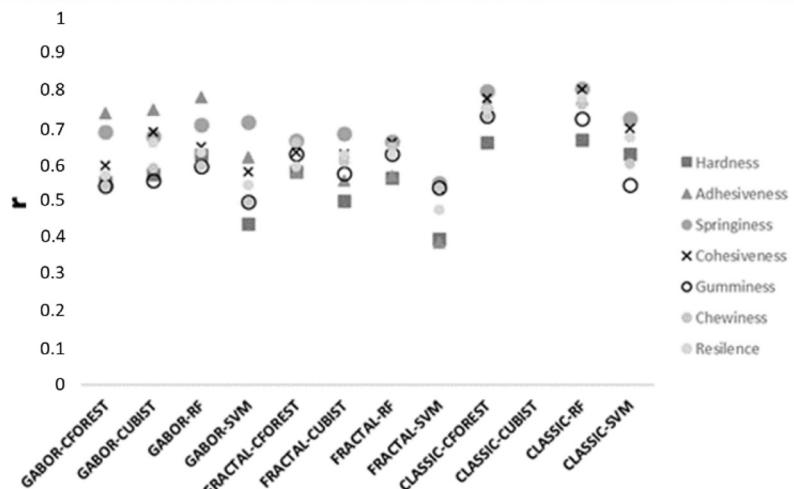


Fig. 4. Correlation coefficients (r) for prediction of physico-chemical parameters in fresh beef as a function of MRI from fresh samples by means of different combinations of MRI algorithms and regressors.

A)



B)



C)

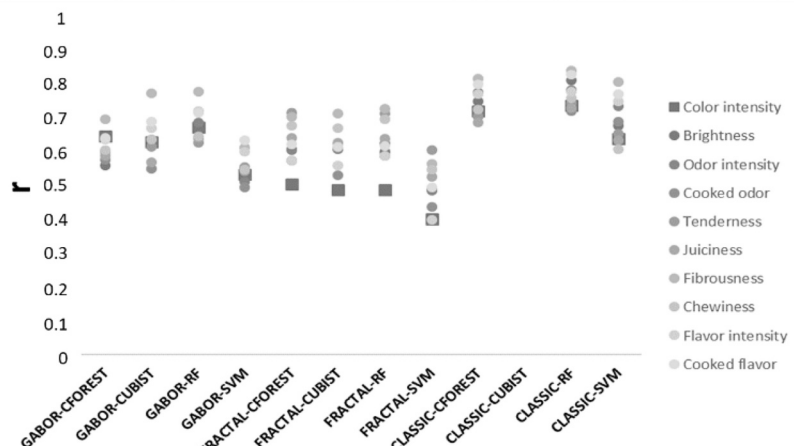


Fig. 5. Correlation coefficients (r) for prediction of physico-chemical (A), instrumental texture (B) and sensory parameters (C) of cooked FT beef samples as a function of MRI from raw FT samples by means of different algorithm-regressor combinations.

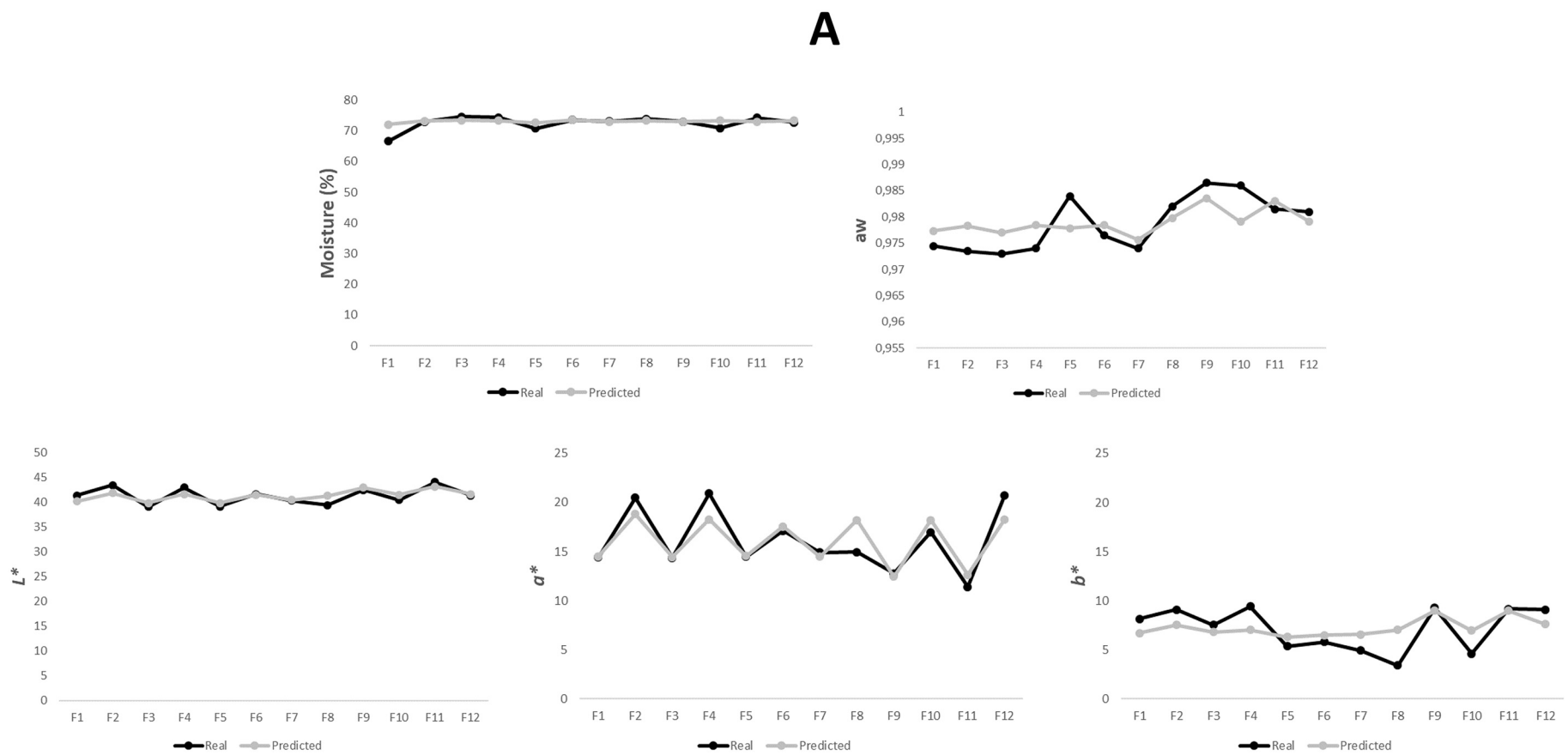
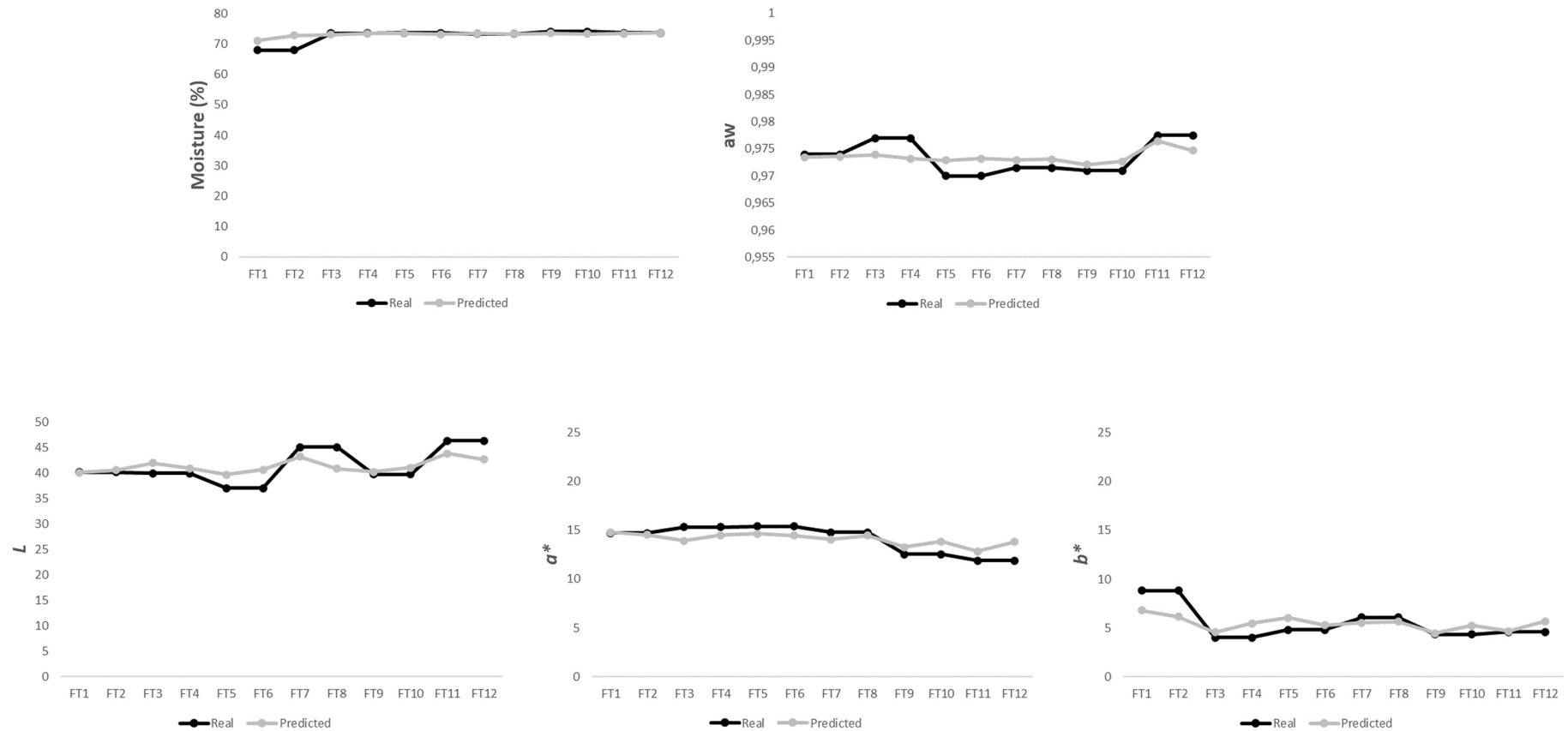


Fig. 6. Adjustment between real and predicted values for physico-chemical parameters in fresh (F) (A) and frozen-thawed (FT) (B) beef loins by means of optimum MRI algorithm-regressor combinations *.
* F1-F12 and FT1-FT12 are each one of the analysed samples.

B

the training set, therefore SVM is computationally unfeasible in very large data sets (Tsang, Kwok, & Cheung, 2005).

Thus, considering the computational costs and the results obtained by applying the quality classification measures, the most appropriate combination would be Fractal-RF.

3.2. Prediction of quality parameters of beef samples

Fig. 4 shows correlation coefficients for prediction equations of physico-chemical parameters of raw F and raw FT beef samples as a function of computational characteristics of MRI by means of different algorithm-regressor combinations. As can be observed, in general, the application of Fractal achieved higher correlation coefficients (0.44–0.86) in comparison to Classic (0.37–0.67) and Gabor algorithms (0.28–0.59). More specifically, it is noted that the highest correlation coefficient for a^* was obtained with Fractal, and for most quality characteristic, Fractal achieved higher correlation coefficients than Gabor. A previous study in pork loins has also found accurate prediction results when applying different Fractal algorithms to analyze MRI images (Caballero, Pérez-Palacios, et al., 2017). The values of correlation coefficients obtained by these authors were slightly higher than those found in the present study, and can be ascribed to the different validation procedure, which was carried out with partitions of the dataset in this work, whereas Caballero et al. (2017) applied the attribute selection method that has been described as a quite optimistic protocol (Ávila et al., 2019). In addition, Caballero, Pérez-Palacios, et al. (2017) and Caballero, Antequera, et al. (2017) pointed out differences in the correlation coefficients depending on the analysed parameter and the algorithm. They found higher correlation coefficients for fat percentage, salt content and colour coordinates when using Fractal in comparison to Classic algorithm, while the correlation coefficients for moisture and water activity were higher with Classic than with Fractal. In the present study, the parameters obtaining the highest correlation coefficients did not differ notably among algorithms: a^* when applying Fractal, a^* and moisture when using Gabor and a^* and L^* for Classic.

Regarding the regressor, marginally higher correlation coefficients were achieved when using CForest and RF in comparison to Cubist and SVM (**Fig. 4**). Thus, for the prediction of moisture, water activity and instrumental colour parameters of raw samples, the application of Fractal in combination with CForest or RF may be indicated. Considering correlation coefficients in detail, the same optimum algorithm-regressor combination for each individual parameter was found for most physico-chemical parameters: Fractal-CForest for water activity and instrumental colour coordinates, and Gabor-Cubist for moisture.

The prediction of quality parameters of cooked FT beef samples from MRI data of raw FT samples was also evaluated in the present study. **Fig. 5** describes the correlation coefficients of prediction equations for physico-chemical (**Fig. 5.A**), texture (**Fig. 5.B**) and sensory characteristics (**Fig. 5.C**) of cooked FT as a function of computational features of MRI from raw FT by means of different algorithm-regressor combinations. In this case, for physico-chemical, texture and sensory characteristics, the highest correlation coefficients were attained with Classic algorithm (0.56–0.85, 0.55–0.81 and 0.61–0.85, respectively), with lower values found when applying Gabor (0.38–0.80, 0.44–0.79 and 0.52–0.79, respectively) and Fractal (0.33–0.63, 0.39–0.69 and 0.40–0.73, respectively). As for the regressors, it may be pointed out that, in general, RF obtained the highest correlation coefficients, followed by CForest and SVM. Thus, the best algorithm-regressor combination for prediction physico-chemical, texture and sensory characteristics of cooked FT beef samples as a function of MRI from raw FT sample seems to be Classic-RF. As occurred in the prediction of physico-chemical parameters of raw samples, the chosen combination is the optimum for most of the analysed characteristics, with only a few exceptions: Gabor-RF for water activity and adhesiveness and Classic-CForest for springiness. Moreover, it is worth mentioning that this optimum combination for prediction of characteristics of cooked beef

(Classic-RF) is different from that proposed for the prediction of the physico-chemical parameters of fresh beef (Fractal-CForest). This is in concordance with a previous work focused on MRI to predict sensory attributes of dry-cured loins (Caballero et al., 2016), obtaining different results. These results are quite interesting and may indicate the need of adjusting the computer vision techniques, especially the algorithm to analyze the MRI, to the type of sample for achieving an accurate prediction of quality characteristics.

Finally, to validate the optimum algorithm-regressor combination selected for each type of sample, the adjustment between real and predicted values of the quality characteristics of beef samples was verified and the values for MAE, MAPE, RMSE and MSE were calculated. As an example, **Fig. 6** shows the values of moisture, water activity and instrumental colour coordinates of raw F (**Fig. 6.A**) and raw FT (**Fig. 6.B**) beef determined by physico-chemical analysis and predicted by MRI in each analysed sample. As can be seen, similar values were obtained with both procedures in most samples for all the parameters. Accurate values for MAE, MAPE, RMSE and MSE were also obtained, varying between 0.002 and 1.138, 0.002–1.138, 0.003–1.686 and 0.00001–2.842, respectively for raw F samples, and 0.002–1.339, 0.002–0.423, 0.003–2.022 and 0.00001–4.090, respectively for raw FT samples.

Looking to the future, results from this work may point out the applicability of MRI-computational analysis in the meat industry as a non-destructive methodology to classify and assess the quality of beef samples, however, the methodology should be previously optimized.

4. Conclusions

This is the first study showing the capability of MRI to identify raw F vs. raw FT beef and to determine physico-chemical, texture and sensory characteristics in these samples in a non-destructive way, being notable the accuracy of MRI-computer vision to differentiate between unfrozen and frozen-thawed beef samples.

The computational analysis of MRI, especially the algorithm to analyze the image, may be set as a function of the aim (classification or prediction) and of the type of sample (raw or cooked). The algorithm-regressor combinations of Fractal with CForest, RF or SVM seem to be the most effective to differentiate between fresh and frozen-thawed beef samples. For the prediction of quality parameters, Fractal-CForest or Fractal-RF may be applied in raw samples, while Classic-RF seems to be the optimum combination for cooked samples. It may point out the irrelevance of selecting an optimum algorithm-regressor combination for each analysed characteristic in this type of samples.

Funding

This work was supported by Junta de Extremadura: economic support for research group (GRU18138 and GRU18104). Trinidad Perez-Palacios thanks the Spanish Government (Ministerio de Ciencia e Innovación) the Ramón y Cajal contract (RYC-2017-21842).

Credit author statement

Trinidad Perez-Palacios: investigation; conceptualization; resources; writing - original draft; writing - review & editing; visualization.

Mar Ávila: investigation; formal analysis.

Juan Pedro Torres: investigation; formal analysis; data curation.

Alberto González-Mohino: investigation.

Teresa Antequera: term; conceptualization; resources; review; supervision; project administration.

Andrés Caro: term; conceptualization; resources; review; supervision; data curation; project administration.

Declaration of Competing Interest

The authors declare that they have no known competing financial

interests or personal relationships that could have appeared to influence the work reported in this paper.

Data availability

Data will be made available on request.

References

- Aggarwal, N., & Agrawal, R. K. (2012). First and second order statistics features for classification of magnetic resonance brain images. *Journal of Signal and Information Processing*, 3, 146–153. https://www.scirp.org/pdf/J SIP20120200017_13782492.pdf.
- Amayeh, G., Tavakkoli, A., & Bebis, G. (2019). Accurate and efficient computation of Gabor features in real-time applications. In *Presented at the 5th international symposium advances in visual computing, Las Vegas, USA*.
- Antequera, T., Caballero, D., Grassi, S., Uttaro, B., & Perez-Palacios, T. (2021). Evaluation of fresh meat quality by hyperspectral imaging (HSI), nuclear magnetic resonance (NMR) and magnetic resonance imaging (MRI): A review. *Meat Science*, 172, Article 108340. <https://www.sciencedirect.com/science/article/pii/S0309174020307725>.
- AOAC. (2000). Moisture in malt gravimetric method. In *Association of Official Analysis Chemists International, Official methods of analysis* (17th ed.). Association of Official Analytical Chemist.
- Ávila, M. M., Durán, M. L., Caballero, D., Antequera, T., Pérez-Palacios, T., Cernadas, E., & Fernández-Delgado, M. (2019). Magnetic resonance imaging, texture analysis and regression techniques to non-destructively predict the quality characteristics of meat pieces. *Engineering Applications of Artificial Intelligence*, 82, 110–125. <https://ur.booksc.eu/book/75066139/dd72cf>.
- Breiman, L. (2001). Random forests. *Machine Learning*, 45, 5–32. <https://link.springer.com/article/10.1023/A:1010933404324>.
- Caballero, D., Antequera, T., Caro, A., Amigo, J. M., Ersbøll, B. K., Dahl, A. B., & Pérez-Palacios, T. (2018). Analysis of MRI by fractals for prediction of sensory attributes: A case study in loin. *Journal of Food Engineering*, 227, 1–10. <https://www.sciencedirect.com/science/article/pii/S0260877418300542>.
- Caballero, D., Antequera, T., Caro, A., Ávila, M., Rodríguez, P. G., & Pérez-Palacios, T. (2017). Non-destructive analysis of sensory traits of dry-cured loins by MRI-computer vision techniques and data mining. *Journal of Food Science and Agriculture*, 97, 2942–2952. <https://onlinelibrary.wiley.com/doi/full/10.1002/jsfa.8132>.
- Caballero, D., Antequera, T., Caro, A., Durán, M. L., & Pérez-Palacios, T. (2016). Data mining on MRI-computational texture features to predict sensory characteristics in ham. *Food and Bioprocess Technology*, 9, 699–708. <https://link.springer.com/article/10.1007/s11947-015-1662-1>.
- Caballero, D., Caro, A., Amigo, J. M., Dahl, A. B., Ersbøll, B. K., & Pérez-Palacios, T. (2017). Development of a new fractal algorithm to predict quality traits of MRI loins. *Lecture Notes in Computer Science*, 10424, 208–218. https://link.springer.com/chapter/10.1007/978-3-319-64689-3_17.
- Caballero, D., Pérez-Palacios, T., Caro, A., Amigo, J. M., Dahl, A. B., Ersbøll, B. K., & Antequera, T. (2017). Prediction of pork quality parameters by applying fractals and data mining on MRI. *Food Research International*, 99, 739–747. <https://www.sciencedirect.com/science/article/pii/S0963996917303022>.
- Caballero, D., Pérez-Palacios, T., Caro, A., & Antequera, T. (2021). Use of magnetic resonance imaging to analyse meat and meat products non-destructively. *Food Reviews International*, 1912085. <https://www.tandfonline.com/doi/abs/10.1080/87559129.2021.1912085>.
- Cabrera, M. C., & Saadoun, A. (2014). An overview of the nutritional value of beef and lamb meat from South America. *Meat Science*, 98, 435–444. <https://pubmed.ncbi.nlm.nih.gov/25042240/>.
- Carballo, J., & Jiménez, F. (2001). *Refrigeración y congelación de carne y productos cárnicos*. In S. M. Bejarano (Ed.), *Enciclopedia de la carne y de los productos cárnicos* (pp. 475–509). Martín & Macías.
- Chang, C. C., & Lin, C. J. (2021). LIBSVM: A library for support vector machines. Retrieved from <https://www.csie.ntu.edu.tw/~cjlin/libsvm/>.
- Cheng, S., Wang, X., Li, R., Yang, H., Wang, H., Wang, H., & Tana, M. (2019). Influence of multiple freeze-thaw cycles on quality characteristics of beef semimembranosus muscle: With emphasis on water status and distribution by LF-NMR and MRI. *Meat Science*, 147, 44–52. <https://www.sciencedirect.com/science/article/pii/S030974018303127?via%3Dihub>.
- Colton, T. (1974). *Statistics in medicine*. Little Brown and Co.
- Dag, A., Topuz, K., Oztekin, A., Bulur, S., & Megahed, F. M. (2016). A probabilistic data-driven framework for scoring the preoperative recipient-donor heart transplant survival. *Decision Support Systems*, 86, 1–12. <https://dl.acm.org/doi/10.1016/j.dss.2016.02.007>.
- Evans, S. D., Nott, K. P., Kshirsagar, A. A., & Hall, L. D. (1998). The effect of freezing and thawing on the magnetic resonance imaging parameters of water in beef, lamb and pork meat. *International Journal of Food Science and Technology*, 33, 317–328. <https://ifst.onlinelibrary.wiley.com/doi/full/10.1046/j.1365-2621.1998.00165.x>.
- Fawcett, T. (2006). An introduction to ROC analysis. *Pattern Recognition Letters*, 27, 861–874. <https://www.sciencedirect.com/science/article/pii/S016786550500303X>.
- Frecka, J. C., Phinney, D. M., Yang, X., Knopp, M. V., Heldman, D. R., Wick, M. P., & Vodovotza, Y. (2019). Assessment of chicken breast meat quality after freeze/thaw abuse using magnetic resonance imaging techniques. *Journal of Food Science and Agriculture*, 99, 844–853. <https://pubmed.ncbi.nlm.nih.gov/30003554/>.
- Galloway, M. M. (1975). Texture classification using gray level dependence matrix. *Computational Vision Image Processing*, 4, 172–179. <https://www.sciencedirect.com/science/article/pii/S0146664X75800086>.
- González-Mohino, A., Antequera, T., Caballero, D., Mir-Bel, J., & Perez-Palacios, T. (2018). Near-infrared spectroscopy-based analysis to study sensory parameters on pork loins as affected by cooking methods and conditions. *Journal of Food Science and Agriculture*, 98, 4227–4236. <https://onlinelibrary.wiley.com/doi/full/10.1002/jsfa.8944>.
- Haralick, R. M., Shanmugam, K., & Dinstein, I. (1973). Textural features for image classification. *IEEE Transactions on Systems, Man, and Cybernetics*, 3, 610–621. <https://ieeexplore.ieee.org/document/4309314>.
- Hassine, K., Erbad, A., & Hamila, R. (2019). Important complexity reduction of random forest in multi-classification problem. In *Presented at the 15th international wireless communications & mobile computing conference (IWCMC), Tangier, Morocco*.
- Kohavi, R. (1995). A study of cross-validation and bootstrap for accuracy estimation and model selection. In *Presented at the international joint conference on artificial intelligence, Montreal, Canada*.
- Leygonie, C., Britz, T. J., & Hoffman, L. C. (2012). Impact of freezing and thawing on the quality of meat: Review. *Meat Science*, 91, 93–98. <https://www.sciencedirect.com/science/article/pii/S0309174012000149>.
- Lufkin, R. B. (1998). *The MRI manual*. Mosby-Year Book.
- Mandelbrot, B. B. (1982). *The fractal geometry of nature*. W.H. Freeman and Co.
- Oh, M., Kim, E. K., Jeon, B. T., Tang, Y., Kim, M. S., Seong, H. J., & Moon, S. H. (2016). Chemical compositions, free amino acid contents and antioxidant activities of Hanwoo (Bos taurus coreane) beef by cut. *Meat Science*, 119, 16–21. <https://pubmed.ncbi.nlm.nih.gov/27115864/>.
- ORDEN APA/2423/2002. (2022). *de 18 de septiembre, por la que se ratifica el Reglamento de la Indicación Geográfica Protegida «Ternera de Extremadura»*. BOE nº 237, 35083–35091.
- Perez-Palacios, T., Caballero, D., Antequera, T., Duran, M. L., Ávila, M., & Caro, A. (2017). Optimization of MRI acquisition and texture analysis to predict physicochemical parameters of loins by data mining. *Food and Bioprocess Technology*, 10, 750–758. <https://link.springer.com/article/10.1007%2Fs11947-016-1853-4>.
- Perez-Palacios, T., Ruiz, J., Martín, D., Barat, J. M., & Antequera, T. (2011). Pre-cooking effect on physicochemical, texture and sensory characteristics of Iberian ham. *Food Science and Technology International*, 17, 127–133. <https://journals.sagepub.com/doi/10.1177/1082013210381435>.
- Portanguen, S., Ikonic, P., Clerjon, S., & Kondjyan, A. (2014). Mechanisms of crust development at the surface of beef meat subjected to hot air: An experimental study. *Food and Bioprocess Technology*, 7, 3308–3318. <https://link.springer.com/article/10.1007%2Fs11947-014-1321-y>.
- Quinlan, R. (1993). Combining instance-based and model-based learning. In *Presented at the tenth international conference on machine learning, Amherst, Massachusetts*.
- Randen, T., & Husøy, J. H. (1999). Filtering for texture classification: A comparative study. *IEEE Transactions Pattern Analysis*, 21, 291–310. <https://ieeexplore.ieee.org/document/761261>.
- Sun, C., & Wee, G. (1982). Neighbouring gray level dependence matrix. *Computational Vision Image Processing*, 23, 341–352. <https://www.sciencedirect.com/science/article/pii/0734189X83900324>.
- Tsang, I. W., Kwok, J. T., & Cheung, P. (2005). Core vector machines: Fast SVM training on very large data sets. *Journal of Machine Learning Research*, 6, 363–392. <https://citeseerx.ist.psu.edu/viewdoc/download?doi=10.1.1.445.4342&rep=rep1&type=pdf>.
- Vafeiadis, T., Diamantaras, K. I., Sarigiannidis, G., & Chatzisavvas, K. C. (2015). A comparison of machine learning techniques for customer churn prediction. *Simulation Modelling Practice and Theory*, 55, 1–9. <https://www.sciencedirect.com/science/article/pii/S1569190X15000386>.

3.3. Artículo “An experimental protocol to determine quality parameters of dry-cured loins using low-field Magnetic Resonance Imaging”

• **Autores:** Daniel Caballero, Pablo García, Andrés Caro, Mar Ávila, Juan P. Torres, Teresa Antequera, Trinidad Pérez-Palacios

• **Publicación:** Journal of Food Engineering, Volume 313, Pages 110750, 2022

• **ISSN:** 0260-8774

• **DOI:** <https://doi.org/10.1016/j.jfoodeng.2021.110750>

• **Índice de impacto:**

IF (2022): 5.5 (30/142) Q1 in FOOD SCIENCE & TECHNOLOGY

IF (2022): 5.5 (26/140) Q1 in ENGINEERING, CHEMICAL

El objetivo de este estudio es proponer un protocolo experimental para determinar las características de calidad de lomos curados, de forma no destructiva mediante el uso de Imágenes de Resonancia Magnética (MRI) de campo bajo. El procedimiento de resonancia magnética se compone de tres etapas principales: adquisición de resonancia magnética, análisis de resonancia magnética (técnicas de visión por computadora) y análisis de datos (métodos de minería de datos). Se han implementado dos procedimientos dentro de un protocolo experimental, validados con muestras reales de la industria cárnica (lomos curados) mediante diferentes medidas de calidad. Los resultados de la validación pueden indicar el uso de los procedimientos implementados y el desarrollo de un protocolo experimental para determinar las características de calidad de los lomos mediante extracción de datos de visión por computador, resonancia magnética de campo bajo, de manera no destructiva, con alta precisión y reduciendo la dispersión de los valores. Esto trae la posibilidad de implementar esta metodología en plantas procesadoras de carne.



An experimental protocol to determine quality parameters of dry-cured loins using low-field Magnetic Resonance Imaging



Daniel Caballero^{a,b,*}, Pablo G. Rodríguez^b, Andrés Caro^b, María del Mar Ávila^b, Juan P. Torres^b, Teresa Antequera^c, Trinidad Pérez-Palacios^c

^a Chemometrics and Analytical Technology, Food Technology Department, Faculty of Science, University of Copenhagen, Rolighedsvej, 26, DK-1958, Frederiksberg C, Denmark

^b Media Engineering Group, Research Institute of Meat and Meat Products, University of Extremadura, Avda. Ciencias S/N, ES-10.003, Cáceres, Spain

^c Food Technology Department, Research Institute of Meat and Meat Products, University of Extremadura, Avda. Ciencias S/N, ES-10.003, Cáceres, Spain

ARTICLE INFO

Keywords:

Experimental protocol
Magnetic resonance imaging
Optimum procedures
Dry-cured loins
Quality parameters

ABSTRACT

The objective of this study was to achieve an experimental protocol (EP) to determine quality characteristics of dry-cured loins non-destructively by using low-field (LF) Magnetic Resonance Imaging (MRI). The MRI procedure is composed of three main stages: MRI acquisition, MRI analysis (computer vision techniques) and data analysis (data mining methods). Two procedures have been implemented within a EP and validated with real samples from the meat industry (dry-cured loins, n = 100) by means of different quality measures. The validation results may indicate the use of both implemented procedures and the development of an EP to determine quality characteristics of loins by LF MRI-computer vision-data mining in a non-destructive way, with high accuracy and reducing the dispersion of the values. This brings the possibility of implementing this methodology in meat processing plants.

1. Introduction

The evaluation of quality characteristics of meat and meat products are usually carried out by means of tedious and time and solvent consuming methods that usually involve the destruction of the samples. In this sense, the use of non-destructive techniques, such as computed tomography (CT) (Picouet et al., 2013; Vestergaard et al., 2015), near infrared spectroscopy (NIRs) (González-Mohino et al., 2018; Pérez-Palacios et al., 2019) or Magnetic Resonance Imaging (MRI) have been proposed as alternative-complementary techniques.

Among them, MRI has a set of characteristics (non-destructive, non-invasive, non-intrusive, innocuous and taking information from the

inner of the solid samples) that make it be so appropriate for the food analysis, though CT is ionizing, and minced samples are preferred when using NIRs (Caballero et al., 2021). In fact, several studies have been focused on the evaluation of the use of MRI to analyse meat and meat products. These works have been principally carried out using high field (HF) MRI scanners, which have a magnetic field higher than 2 T, giving very high-quality images. However, these devices are very expensive and require high maintenance costs (Feig, 2011; Ladd et al., 2018). Most studies by HF MRI scanners have analysed hams, there also being some publications on beef, pork and lamb samples (Caballero et al., 2021).

The methodology applied in these HF MRI studies for analysing meat and meat products differs in the acquisition sequences, the algorithms to

Abbreviations: CT, Computed Tomography; NIRs, Near Infrared Spectroscopy; MRI, Magnetic Resonance Imaging; HF, High Field; LF, Low Field; EP, Experimental protocol; GE, Gradient Echo; SE, Spin Echo; T3D, Turbo 3D; FOV, Field of view; TE, Echo time; TR, Repetition time; GLCM, Gray Level Co-occurrence Matrix; OPFTA, One Point of Fractal Texture Analysis; ROI, Region of Interest; ENE, Energy; ENT, Entropy; COR, Correlation; HC, Haralick's Correlation; IDM, Inverse Difference Moment; INE, Inertia; CS, Cluster Shade; CP, Cluster Prominence; CON, Contrast; DIS, Dissimilarity; UNI, Uniformity; HOM, Homogeneity; EFI, Efficiency; MLR, Multiple Linear Regression; KDD, Knowledge Discovery in Databases; WEKA, Waikato Environment for Knowledge Analysis; R, Correlation coefficient; MAE, Mean Absolute Error; RMSE, Root Mean Square Error; TSTD, True Standard Deviation; WAPE, Weighted Absolute Percentage Error; RF, Radiofrequency; GLRLM, Gray Level Run Length Matrix; NGLDM, Neighbouring Gray Level Dependence Matrix; CFA, Classical Fractal Algorithm; FTA, Fractal Texture Algorithm; IR, Isotonic Regression.

* Corresponding author. Chemometrics and Analytical Technology, Food Technology Department, Faculty of Science, University of Copenhagen, Rolighedsvej, 26, DK-1958, Frederiksberg C, Denmark.

E-mail address: dcaballero@unex.es (D. Caballero).

<https://doi.org/10.1016/j.jfoodeng.2021.110750>

Received 7 April 2021; Received in revised form 20 July 2021; Accepted 22 July 2021

Available online 29 July 2021

0260-8774/© 2021 Elsevier Ltd. All rights reserved.

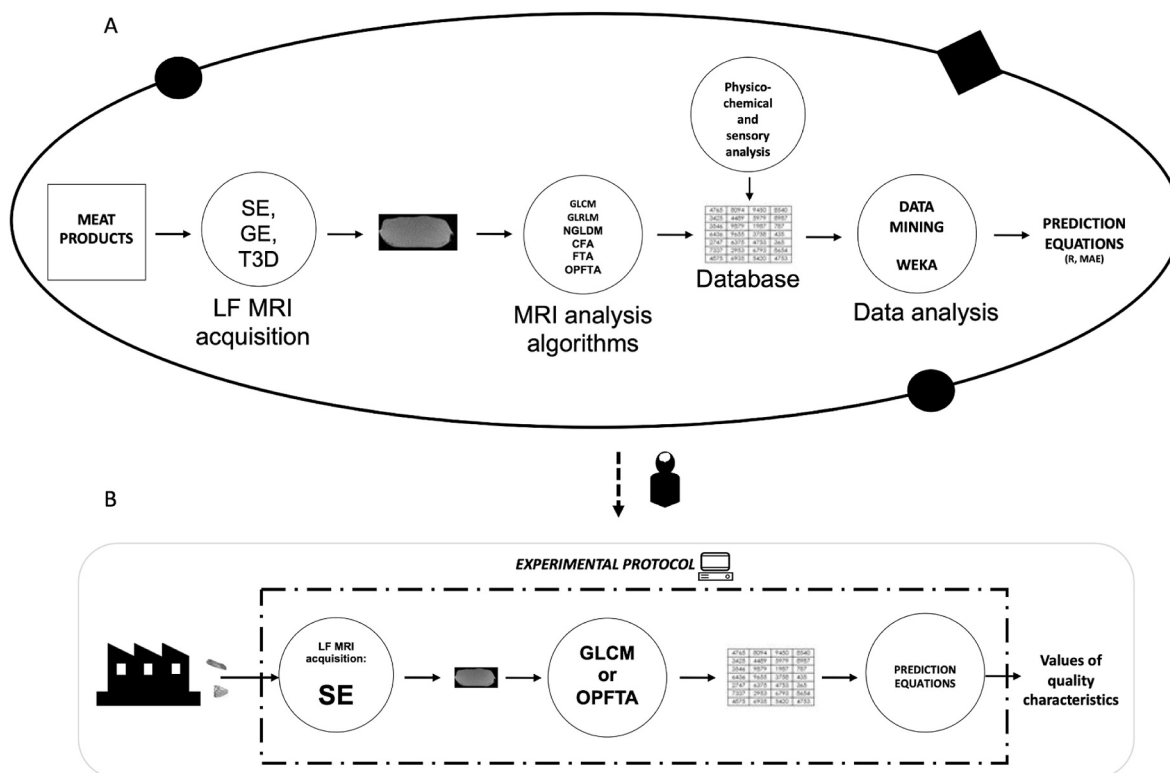


Fig. 1. Implementation (A) of the experimental protocol (B) evaluated in the present study.

analyse the image as well as on the data analysis technique. Main purposes of these works were to monitor the processing or cooking of the products, to classify different samples and to predict their quality characteristics. Accurate results have been shown in most cases.

Nowadays, the use of low field (LF) MRI scanners is increasing, with some recent publication on pork samples and dry-cured hams (Bernau et al., 2015; Torres et al., 2019). These scanners have a lower cost than HF ones and do not have maintenance costs. They generate magnetic field between 0.15 and 0.50 T (Ladd et al., 2018), and, consequently, the obtained images are of lower quality than those from HF MRI scanners. This aspect supposes a challenge to obtain an accurate analysis of the products and requires the optimization of the methodology, specially the procedures for the acquisition and analysis of the images. In fact, the activity of our research group in the last years have aimed to establish the optimum procedures for the LF MRI acquisition, the image analysis and the data analysis, to determine the quality characteristics of pork loins non-destructively (Ávila et al., 2018; Caballero et al., 2018a,b).

Nevertheless, despite the number of studies on MRI to analyse meat and meat products in a non-destructive way, there is no data about the development of any experimental protocol (EP) based on MRI, which can be applied for industrial use.

Considering all these aspects, the present study aimed to take a step forward by implementing the optimum procedure of LF MRI – computational analysis into an EP and evaluating its efficiency at industrial level.

2. Material and methods

2.1. Experimental design

The experimental design of the present work is composed of two parts. The first one dealt to compare the capability of the different techniques previously applied (for the image acquisition, image analysis and data analysis) to predict quality parameters of pork loins (Caballero et al., 2017a,b; 2018a,b; Pérez-Palacios et al., 2017). This comparison

led to the optimum combinations of techniques, which were selected to get the EP (Fig. 1). The EP was operationalized within the official analysis service for meat and meat products ("Animal Source Foodstuffs Innovation Services" or "SiPA") of the Faculty of Veterinary Science at University of Extremadura (Cáceres, Spain). Thus, the second experiment consisted on evaluating the accuracy of the proposed EP with real samples (dry-cured loins, n = 100) from the meat industry. For that, the samples were first analysed using the proposed EP, obtaining "predicted" values of physico-chemical and sensory characteristics. These samples were also analysed by means of physico-chemical and sensory methods to verify the predicted values.

2.2. Experimental protocol

The EP implemented in this study takes three consecutive stages: image acquisition, image analysis and application of prediction equations.

2.2.1. Image acquisition

MRI images are acquired using a LF MRI scanner (ESAOTE VET-MR E-SCAN XQ 0.18 T) with a hand/wrist coil, applying T1-weighted sequences of Spin Echo (SE). The acquisition sequence influenced significantly on the values of the computational features and, also on the prediction results. Overall, the highest correlation coefficients were achieved when using SE, followed by Gradient Echo (GE), and Turbo 3D (T3D) having the lowest values (Caballero et al., 2017a,b; 2018a,b). These effects have been ascribed to the low bandwidth and high signal to noise ratio of SE. Consequently, SE has been chosen as the acquisition sequence for the EP. In fact, most of the MRI studies on meat and meat products have applied SE (Pérez-Palacios et al., 2010a,b).

For the acquisition sequence with SE, the following parameters were used: Field of view (FOV): 150 × 150 mm², echo time (TE): 26 ms, slice thickness: 4 mm, flip angle: 90°, repetition time (TR): 630 ms, matrix size: 256 × 204, phase encode: 204, number of acquisitions: five per sample. Twenty-nine slices per sample were obtained and the MRI

acquisition took 50 min for each sample. The MRI acquisition was performed at 23 °C. All images were acquired in DICOM format with 512 × 512 resolution and 256 Gy levels.

2.2.2. Image analysis

The MRI images can be analysed by means of computer vision algorithms, to extract numerical features from the images. Algorithms based on textures (GLCM, GLRLM (Gray Level Run Length Matrix) and NGLDM (Neighbouring Gray Level Dependence Matrix)) and fractals (CFA (Classical Fractal Algorithm), FTA (Fractal Texture Algorithm) and OPFTA) have been tested to analyse the MRI images of pork loins (Caballero et al., 2018a). One algorithm based on textures (Gray Level Co-occurrence Matrix (GLCM)) and other on fractals (One Point Fractal Texture Algorithm (OPFTA)) were chosen for this EP.

2.2.2.1. Gray level CO-OCCURRENCE matrix. Firstly, the largest area rectangle inscribed in the contour of the loin muscle is selected (Molano et al., 2012). This is called region of interest (ROI), which is finally analysed by GLCM. GLCM (Haralick et al., 1973; Haralick and Shapiro, 1993) was computed by counting the number of times that each pair of gray levels occurred at a given distance “d” in all directions. In this matrix, each item $p(i, j)$ denotes the number of times that two neighbouring pixels separated by distance ($d = 1$ in this case) occur on the image, one with gray level “ i ” and the other with gray level “ j ”, in all 2D directions: 0°, 45°, 90°, 135°. These co-occurrences are accumulated into a single matrix, from which all the textural features are extracted. Ten computational texture features were obtained from this method proposed by Haralick et al. (1973): energy (ENE), entropy (ENT), correlation (COR), haralick's correlation (HC), inverse difference moment (IDM), inertia (INE), cluster shade (CS), cluster prominence (CP), contrast (CON) and dissimilarity (DIS). The equations that allow computing these features are the following:

$$ENE = \sum_{ij} P(i,j)^2 \quad (1)$$

$$ENT = - \sum_{ij} P(i,j) * \log(P(i,j)) \quad (2)$$

$$COR = \frac{\sum_{ij} (i - \mu_x) * (j - \mu_y) * P(i,j)}{\sigma_x * \sigma_y} \quad (3)$$

$$HC = \frac{\sum_{ij} ((i,j) * P(i,j)) - (\mu_x * \mu_y)}{\sigma_x * \sigma_y} \quad (4)$$

$$IDM = \sum_{ij} \frac{P(i,j)}{1 + (i-j)^2} \quad (5)$$

$$INE = \sum_{ij} (i-j)^2 * P(i,j) \quad (6)$$

$$CS = \sum_{ij} ((i - \mu_x) + (j - \mu_y))^3 * P(i,j) \quad (7)$$

$$CP = \sum_{ij} ((i - \mu_x) + (j - \mu_y))^4 * P(i,j) \quad (8)$$

$$CON = \sum_{ij} (i-j)^2 * P(i,j)^2 \quad (9)$$

$$DIS = \sum_{ij} |(i+1) - (j+1)| * P(i,j) \quad (10)$$

The normalized GLCM (P) represents the frequency or probability of co-occurrence of gray levels (i and j) in the image.

These texture statistics are sensitive for some kind of images. In particular, high values of ENE feature is corresponded to uniform

regions of the images. ENT feature is equivalent to non-uniform zones of the images. IDM feature implies homogeneity, whereas INE denotes contrast. More details about the semantic means of the features were defined in a previous study (Ávila et al., 2015).

2.2.2.2. One point fractal texture algorithms. OPFTA (Caballero et al., 2017c, 2018a,) is a novelty algorithm based on features obtained from fractal properties values. Initially, the images are divided into smaller rectangles and termed the region of interest (ROI). Then, the local exponents are computed for each ROI, these local exponents reflect the number of times that a pattern is repeated in each ROI depending of the size of boxes that they were calculated in each case. From all local exponent, one of them is selected with the box size equal to eight, since this value is the most representative (Caballero et al., 2017c). After that, one value for each ROI is gathered in order to create a matrix with the fractal values. Each cell of the matrix represents one ROI from the image. Seven features were computed on each matrix. These features were calculated based on second order statistics (Aggarwal and Agrawal, 2012; Peckinpaugh, 1991): uniformity (UNI), ENT, COR, homogeneity (HOM), INE, CON, and efficiency (EFI). The equations to calculate each feature from the values of the previously computed matrix are following indicated:

$$UNI = \sum_i \sum_j P(i,j)^2 \quad (11)$$

$$ENT = \sum_i \sum_j P(i,j) * \log(P(i,j)) \quad (12)$$

$$COR = \frac{\sum_i \sum_j \mu_x * \mu_y * P(i,j)}{\sigma_x * \sigma_y} \quad (13)$$

$$HOM = \sum_i \sum_j \frac{P(i,j)}{1 + (i-j)^2} \quad (14)$$

$$INE = \sum_i \sum_j (i-j)^2 * P(i,j) \quad (15)$$

$$CON = \sum_i \sum_j (i-j)^2 * P(i,j)^2 \quad (16)$$

$$EFI = \sum_i \sum_j \frac{\sigma_x}{\mu_x} + \frac{\sigma_y}{\mu_y} \quad (17)$$

Again, $P(i,j)$ stands for number of times gray tones i and j have been neighbours.

2.2.3. Prediction equations

Prediction equations obtained by using a predictive techniques of data mining (Multiple Linear Regression, MLR) were selected for the EP. Data mining is an important step of KDD (Knowledge Discovery in Databases), which is mainly related to the non-trivial process of finding knowledge and potentially useful information from data stored in repositories (Fayyad et al., 1996).

The free software WEKA 3.8 (Waikato Environment for Knowledge Analysis) (<http://www.cs.waikato.ac.nz/ml/weka/>) was used for carrying out the predictive techniques of data mining. The main advantage of the WEKA is that calibration and validation are achieved by using the same data sets, not being necessary to perform the validation with a different data set. This also allows the development of the prediction model. Cross validation of ten folds was used in this study.

2.2.3.1. Multiple linear regression. MLR is used to represent linear relationship between a dependent variable and several independent variables. This technique obtains a linear regression equation, which can be used to predict future values (Hastie et al., 2001). For that, MLR works on a database constructed with the values of the computational features

of MRI and real values of the quality characteristics of the products. This technique steps through the attributes removing the one with the smallest standardized coefficient until no improvement is observed in the estimation of the error. The estimation procedure was 10-fold cross validation (Dieterich, 1998), where the data were divided into 10 partitions of equal size. One subset was tested each time and the remaining data were used for fitting the model. The process was repeated sequentially until all subset were tested. Therefore, all data were used for both training and testing. However, although this method requires ten repetition analysis, this is a robust method (Grossman et al., 2010).

Thus, the equation that define the MLR model is:

$$y = \omega_0 + \sum_i \omega_i x_i, \quad (18)$$

where y is the dependent variable, ω_0 is the y -intercept (constant term), ω_i is the slope coefficients for each explanatory variable, and x_i are the explanatory variables.

Once obtained the equations, they should be made over periodically to assure their accuracy since the database is increasing continuously.

2.3. Evaluation of the experimental protocol

The correlation coefficient (R) is used for evaluating the goodness of the prediction and for its validation.

$$R = \sqrt{\frac{\sum_i (f_i - \bar{y})^2}{\sum_i (y_i - \bar{y})^2}} \quad (19)$$

where f_i is the predicted value, y_i is the real value and \bar{y} is the average value.

The mean absolute error (MAE) and root mean square error (RMSE) were used to evaluate the prediction results too (Ávila et al., 2019), which measures the difference between real and predicted values. They are given by the following equations:

$$MAE = \frac{1}{n} \sum_i |f_i - y_i| \quad (20)$$

$$RMSE = \sqrt{\frac{1}{n} \sum_i (f_i - y_i)^2} * 100 \quad (21)$$

where f_i is the predicted and y_i is the real value.

Real and predicted values were also compared by means of p-value, true standard deviation (TSTD), which evaluates the mean dispersion of the true measurements, and weighted absolute percentage error (WAPE) that measures the mean dispersion of the computer prediction values around the attribute (Ávila et al., 2019)

$$TSTD = \frac{1}{N} \sum_i \sqrt{\frac{1}{M_K - 1} \sum_j (d_{ijk} - \bar{d}_{ik})^2} \quad (22)$$

$$WAPE (\%) = \frac{100 \cdot \sum_i |f_i - y_i|}{\sum_i f_i} \quad (23)$$

where f_i and y_i are the predicted and the real values, N is the number of samples, M_K is the number of measurements carried out for each attribute K , d_{ijk} is the j th true measurements of sample i and for the attribute K , while \bar{d}_{ik} is the average over all the measurements for sample i and attribute K .

2.4. PHYSICO-CHEMICAL and sensory analysis

The physico-chemical analysis carried out in the loins of this study were: moisture (determined at 102 ± 2 °C by the official method (A.O.A.

C., 2000; reference 935.29)), lipid content (determined gravimetrically with chloroform/methanol (2:1, v/v), according to the method described in Pérez-Palacios et al. (2008)); water activity (with the system Lab Master-aw (NOVASINA AG, Switzerland) that was calibrated at 20–22 °C before use), instrumental color (with a Minolta CR-300 colorimeter (Minolta Camera Corp., Meter Division, Ramsey, NJ, determining lightness (L), redness (a^*), and yellowness (b^*), and standardized before use with a white tile). Salt content was determined volumetrically in dry-cured loins by the official method (A.O.A.C., 2000; reference 971.19). All determinations were done in triplicate.

The sensory analysis of the dry-cured loins was assessed by a trained panel of thirteen members using quantitative-descriptive analysis (Ruiz et al., 1998). Eleven traits of Iberian dry-cured loins (redness of lean, brightness of lean, marbling, odour intensity, hardness, juiciness, salty taste, flavor intensity, cured flavor, rancid flavor and flavor persistence) were assessed on a non-structured scale of 0–10. Analyses were performed in tasting rooms with the conditions specified in the UNE-EN ISO 8589:2010 regulations. All sessions were conducted at room temperature (22 °C) in rooms equipped with white fluorescent lighting (220–230 V, 35 W). The software used to record the scores in the sensory sessions was FIZZ Network (version 2.20, Biosystems, France). For each loin, two slices (1.5 mm) were given to the panellists. Slices were obtained using a commercial slicing machine and were served to the panellists on plates at room temperature. The panel sessions were held mid-morning, approximately 4 h after breakfast. Three samples randomly presented to the panellist were analysed in each session. Approximately 200 ml of water at room temperature was provided to the panellists. During each session, the panel average for each sample was recorded.

3. Results and discussion

3.1. Selection of the optimum procedures

Different LF MRI studies on pork loins (Caballero et al., 2017a,b; 2018a,b; Pérez-Palacios et al., 2017) have been evaluated in the present work, by comparing prediction results on physico-chemical and sensory characteristics as a function of the acquisition sequences of MRI, algorithms for the image analysis and techniques of data analysis. Three acquisition sequences have been used in the LF MRI studies in pork loin: SE, GE and T3D. In general, SE led to sharper and better-defined images than GE and T3D (Caballero et al., 2017a,b; 2018a,b) and the best prediction results (Caballero et al., 2017a,b; 2018a,b).

Algorithms to analyse MRI differ in the number of computational features and complexities. NGLDM is the simplest algorithm, with 5 computational features, following in increasing order by OPFTA (7), CFA (9) and FTA, GLCM and GLRLM (10). As for the complexity, it is lower in GLCM, GLRLM and OPFTA ($O(n^2)$) than in FTA ($O(n^2 * \log n)$) and NGLDM and CFA ($O(n^3)$) (Caballero et al., 2018a). Considering the results on prediction of the physico-chemical and sensory characteristics, GLCM and OPFTA achieved the highest correlation coefficients among the texture and fractal algorithms, respectively (Caballero et al., 2017a,b; 2018a,b; Pérez-Palacios et al., 2017). Thus, instead of not being the simplest algorithms, GLCM and OPFTA were selected for the EP.

MLR and Isotonic Regression (IR) have been tested as predictive techniques in the LF MRI studies on pork loins. In the case of applying texture algorithms for the image analysis, excellent correlation coefficients ($R > 0.75$) were achieved with both MLR and IR (Caballero et al., 2017b; Pérez-Palacios et al., 2017). However, more accurate prediction results were obtained with MLR than with IR when using fractal algorithms (Caballero et al., 2017a, 2018a,b). The MAE was also calculated in these studies, being lower when using MLR in both cases (texture and fractal algorithms). Besides, MLR is simpler (first degree equation) than IR (sixth degree equations) (Caballero et al., 2017a,b; 2018a,b; Pérez-Palacios et al., 2017). Accordingly, prediction equations

Table 1

Prediction equations (as a function of the computational features of GLCM or OPFTA) of the quality parameters of loins, obtained by Multiple Linear Regression and used in the experimental protocol.

	GLCM	OPFTA		
a_w	$= -0.034 * ENE$ $+ 0.012 * ENT -$ $0.059 * COR$ $+ 0.974 * HC +$ $0.073 * IDM + 0.197$ $* INE - 0.070 * CS -$ $0.036 * CP + 0.063$ $* CON - 0.295 * DIS$ $+ 0.919$	(24)	$= 0.368 * UNI +$ $0.334 * ENT +$ $0.020 * COR +$ $0.025 * HOM +$ $0.162 * INE - 0.135$ $* CON + 0.145 *$ $EFI + 0.566$	(25)
Moisture (%)	$= -11.038 * ENE +$ $6.316 * ENT - 7.109$ $* COR + 24.830 *$ $HC + 24.389 * IDM$ $+ 55.696 * INE -$ $20.659 * CS -$ $15.407 * CP +$ $10.157 * CON -$ $70.601 * DIS +$ 45.927	(26)	$= 49.568 * UNI +$ $64.839 * ENT +$ $4.683 * COR +$ $16.969 * HOM +$ $55.767 * INE -$ $30.923 * CON +$ $42.805 * EFI -$ 25.929	(27)
Instrumental color	$L^* = -6.759 * ENT -$ $16.836 * COR +$ $25.396 * HC +$ $0.964 * IDM +$ $28.971 * INE -$ $5.108 * CS + 2.132$ $* CP - 16.028 *$ $CON - 31.809 * DIS$ $+ 47.607$	(28)	$= 14.892 * ENT +$ $18.902 * HOM +$ $31.617 * INE -$ $29.366 * CON +$ $19.365 * EFI +$ 26.536	(29)
	$a = 2.223 * ENE -$ $2.416 * ENT +$ $1.514 * COR +$ $1.282 * HC - 3.919$ $* IDM + 9.143 *$ $INE + 2.848 * CS -$ $4.142 * CON +$ $10.490 * DIS +$ 13.516	(30)	$= -2.950 * HOM -$ $7.324 * INE +$ $7.488 * CON -$ $6.859 * EFI +$ 15.579	(31)
	$b = 2.311 * ENE -$ $0.763 * ENT +$ $0.916 * HC - 1.620$ $* IDM - 4.527 * INE$ $+ 1.991 * CS +$ $6.770 * CP + 7.878$ $* CON + 11.325 *$ $DIS + 4.256$	(32)	$= 12.883 * UNI +$ $3.205 * ENT -$ $4.705 * HOM -$ $6.591 * INE - 7.734$ $* EFI + 5.644$	(33)
Salt content (%)	$= 1.838 * COR -$ $2.226 * HC - 1.037$ $* IDM - 6.009 * INE$ $+ 1.574 * CS +$ $1.344 * CP + 7.336$ $* DIS + 0.821$	(34)	$= -8.898 * UNI -$ $7.546 * ENT -$ $0.506 * COR -$ $0.265 * HOM -$ $3.655 * INE +$ $3.281 * CON -$ $3.224 * EFI + 9.312$	(35)
Lipid content (%)	$= 11.641 * ENE -$ $10.390 * ENT +$ $7.151 * HC - 16.961$ $* IDM - 22.839 *$ $INE + 8.873 * CS +$ $12.602 * CP -$ $22.772 * CON +$ $27.982 * DIS +$ 17.497	(36)	$= -15.617 * ENT -$ $7.474 * HOM -$ $13.201 * INE -$ $22.415 * EFI +$ 36.191	(37)
Redness of lean	$= 1.784 * ENT -$ $2.828 * HC + 8.185$ $* IDM - 3.981 * INE$ $+ 3.855 * CP +$ $2.916 * CON +$ $5.247 * DIS + 3.805$	(38)	$= 4.403 * ENT -$ $1.131 * COR +$ $0.826 * HOM -$ $1.253 * INE +$ $1.711 * CON +$ $5.137 * EFI + 3.062$	(39)
Brightness of lean	$= 0.323 * ENT +$ $28.978 * COR +$ $1.917 * HC - 2.781$ $* IDM - 2.385 * INE$ $+ 4.523 * CP -$	(40)	$= 2.616 * UNI -$ $0.754 * INE - 6.529$ $* EFI + 4.764$	(41)

Table 1 (continued)

	GLCM	OPFTA		
Marbling of lean	$1.302 * CON +$ $3.328 * DIS + 2.657$ $= -3.966 * ENT +$ $6.765 * HC - 19.609$ $* IDM + 5.838 * INE$ $-3.113 * CP - 4.309$ $* CON - 12.017 *$ $DIS + 13.324$	(42)	$= 3.262 * UNI -$ $8.596 * ENT +$ $2.673 * COR -$ $1.556 * HOM +$ $1.797 * INE - 5.698$ $* CON - 11.163 *$ $EFI + 14.636$	(43)
Odour intensity	$= 38.889 * COR +$ $2.050 * HC - 3.797$ $* IDM + 2.473 * CP$ $-4.119 * CON +$ $3.563 * DIS + 5.346$	(44)	$= -1.657 * ENT +$ $0.689 * COR +$ $0.703 * HOM -$ $0.596 * INE +$ $0.792 * CON -$ $7.707 * EFI + 8.223$	(45)
Hardness of lean	$= -1.535 * ENE +$ $2.435 * ENT - 3.284$ $* HC + 9.761 * IDM$ $-2.479 * INE +$ $0.405 * CS + 2.030$ $* CP + 8.202 * DIS$ $+ 1.065$	(46)	$= -2.218 * UNI +$ $3.948 * ENT -$ $1.231 * COR +$ $1.130 * HOM -$ $1.128 * INE +$ $3.647 * CON +$ $3.244 * EFI + 1.675$	(47)
Juiciness	$= -1.321 * ENT +$ $3.156 * HC - 7.674$ $* IDM - 1.028 *$ $CON - 3.026 * DIS$ $+ 7.570$	(48)	$= 1.008 * UNI -$ $3.229 * ENT +$ $1.176 * COR -$ $1.511 * CON -$ $5.796 * EFI + 8.809$	(49)
Salty taste	$= 0.507 * ENT +$ $22.855 * COR +$ $1.606 * HC - 5.033$ $* INE + 5.735 * CP$ $+ 1.421 * CON +$ $4.014 * DIS + 2.307$	(50)	$= 4.354 * UNI +$ $2.113 * ENT -$ $1.231 * INE - 5.437$ $* EFI + 3.312$	(51)
Flavor intensity	$= -1.533 * ENE +$ $0.201 * ENT +$ $21.101 * COR +$ $1.424 * HC - 1.022$ $* IDM - 2.309 * INE$ $+ 2.129 * CP -$ $0.371 * CON +$ $2.901 * DIS + 5.203$	(52)	$= 1.513 * UNI -$ $5.347 * EFI + 6.761$	(53)
Flavor persistence	$= -2.047 * ENE +$ $0.395 * ENT +$ $22.681 * COR +$ $1.174 * HC - 2.458$ $* INE + 1.807 * CP -$ $0.553 * CON +$ $3.881 * DIS + 3.788$	(54)	$= 0.844 * UNI +$ $0.630 * CON -$ $5.164 * EFI + 5.698$	(55)
Cured flavor	$= 0.774 * ENT +$ $24.530 * COR +$ $0.887 * HC - 2.660$ $* INE + 5.047 * CP -$ $1.733 * CON +$ $5.183 * DIS + 3.401$	(56)	$= 1.143 * HOM -$ $0.501 * INE - 4.126$ $* EFI + 6.135$	(57)
Rancid flavor	$= 1.110 * ENE +$ $0.630 * ENT - 0.996$ $* HC + 2.124 * IDM$ $-1.113 * INE +$ $2.285 * CP + 0.788$ $* CON + 1.393 *$ $DIS + 0.763$	(58)	$= 0.487 * UNI +$ $1.506 * ENT -$ $0.320 * COR +$ $0.386 * HOM -$ $0.595 * INE +$ $2.156 * EFI + 0.477$	(59)

obtained by MLR were selected for the EP.

3.2. Implementation and validation the experimental protocol

Considering the above comparison work, the EP was implemented with two procedures: SE – GLCM – prediction equations obtained by MLR as a function of computational texture features of GLCM and SE – OPFTA - prediction equations obtained by MLR as a function of computational fractal features of OPFTA (Fig. 1B). Table 1 shows the prediction equations of the EP for both procedures. Once the EP was accomplished with the two optimum procedures, it was performed

Table 2

Quality measures of the prediction procedures (with GLCM or OPFTA) of the experimental protocol: correlation coefficient (R), weighted absolute percentage error (WAPE) and root mean square error of prediction (RMSEP).

	R	GLCM	OPFTA	WAPE	RMSEP
a_w		0.6747	0.010	0.009	0.8491
Moisture (%)		0.9114	0.050	0.205	0.8789
Instrumental color	L*	0.9076	0.181	0.181	0.9017
	a	0.6123	0.060	0.060	0.6961
	b	0.7064	0.096	0.096	0.8511
Salt content (%)		0.8909	0.094	0.024	0.8905
Lipids content (%)		0.8388	0.102	0.110	0.8489
Redness of lean		0.5697	0.076	0.048	0.6491
Brightness of lean		0.9471	0.123	0.079	0.9270
Marbling of lean		0.9097	0.123	0.081	0.9257
Odour intensity		0.9588	0.135	0.079	0.9591
Hardness of lean		0.7477	0.108	0.065	0.9183
Juiciness		0.7692	0.108	0.054	0.9249
Salty taste		0.9560	0.124	0.059	0.9513
Flavor intensity		0.9442	0.067	0.048	0.9791
Flavor persistence		0.9259	0.076	0.058	0.9764
Cured flavor		0.9491	0.097	0.055	0.9777
Rancid flavor		0.8588	0.181	0.032	0.9137

Table 3

Comparison between physico-chemical (P-C) and predicted results from the GLCM and OPFTA procedures of the experimental protocol^a.

	P-C	GLCM	OPFTA	p (P-C vs GLCM)	p (P-C vs OPFTA)
a_w	0.875 ± 0.009	0.875 ± 0.011	0.879 ± 0.016	0.557	0.068
Moisture (%)	40.119 ± 3.407	39.394 ± 4.381	40.976 ± 3.537	0.182	0.075
Instrumental color	L	45.179 ± 3.148	45.036 ± 3.973	0.772 ± 3.478	0.211
	a ^a	14.705 ± 0.576	14.329 ± 0.537	0.316 ± 0.294	0.067
	b ^a	8.713 ± 0.557	9.402 ± 1.093	0.752 ± 0.699	0.209
Salt content (%)	2.503 ± 0.385	2.431 ± 0.447	2.480 ± 0.409	0.211	0.604
Lipid content (%)	10.580 ± 1.198	11.257 ± 1.569	10.027 ± 0.867	0.362	0.707

^a Values are expressed as mean ± standard deviation; p-value < 0.05 indicates significant differences.

within the official analysis service of the Faculty of Veterinary Science at University of Extremadura (Cáceres, Spain) and evaluated with real samples, as explained in the experimental design subsection (Fig. 1B).

Table 2 shows values for R, WAPE and RMSE that evaluate the prediction results of the two procedures of the EP (by using GLCM or OPFTA). R values are higher than 0.75 for most quality parameters of loins, which indicates a very good to excellent correlation (Colton, 1974), when applying both GLCM and OPFTA. Besides, the WAPE and the RMSE are lower than 0.02% and 0.3%, respectively, in all the cases. Instead of the adequacy of these quality measures for both procedures, it can be observed a higher number of predicted parameters with R > 0.75 and WAPE < 0.01 when using OPFTA. This fact shows the suitability of these optimized procedures in the EP.

Giving a step forward, results from physico-chemical and sensory analyses have been statistically compared with those predicted by GLCM and OPFTA procedures. Mean values and standard deviation of physico-chemical and sensory parameters from traditional analyses and predicted by GLCM and OPFTA procedures are shown in Table 3 and Fig. 2, respectively, which also expose the p-values between real and predicted values. No significant differences ($p > 0.05$) were found between real and predicted results in all cases. It is also noted in Table 3 and Fig. 2, some differences in the standard deviation of the results, being, overall, higher in the GLCM predicted values than in the real and OPFTA predicted.

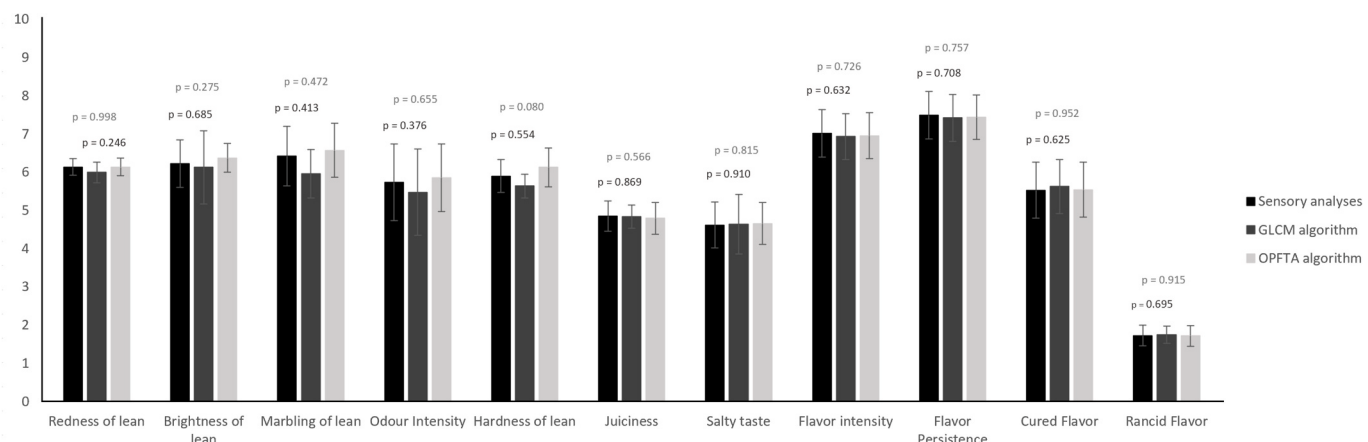


Fig. 2. Mean values (columns), standard deviation (error bars) and p-values between values real and GLCM predicted (dark grey) and real and OPFTA predicted (light grey) of the loin attributes obtained from the sensory analysis and predicted by the GLCM and OPFTA procedures of the experimental protocol.

Table 4

Dispersion of the results from the physico-chemical and sensory analysis (Mean Absolute Error, MAE) and predicted by GLCM and OPFTA (True Standard Deviation, TSTD).

	TSTD	MAE	
		GLCM	OPFTA
a_w	0.014	0.009	0.010
Moisture (%)	3.913	1.998	1.995
Instrumental color	<i>L</i>	3.611	0.039
	<i>a*</i>	0.760	0.040
	<i>b*</i>	0.684	0.107
Salt content (%)	0.4453	0.236	0.201
Lipids content (%)	1.4671	1.075	0.776
Redness of lean	0.5443	0.468	0.400
Brightness of lean	1.4465	0.767	0.576
Marbling of lean	1.7544	0.788	0.610
Odour intensity	2.1552	0.773	0.656
Hardness of lean	0.9234	0.638	0.432
Juiciness	0.9012	0.523	0.363
Salty taste	1.3192	0.574	0.402
Flavor intensity	1.3212	0.472	0.294
Flavor persistence	1.3352	0.568	0.316
Cured flavor	1.5853	0.538	0.352
Rancid flavor	0.6585	0.312	0.251

In view of this fact, TSTD and MAE were measured (Table 4). The TSTD evaluates the mean dispersion of the true measurements, and MAE evaluates the mean dispersion of the predicted values around the characteristics, which is the average over the true measurements. In all quality parameters, TSTD values are higher than MAE of GLCM and OPFTA procedures, indicating a lower dispersion in the computer prediction than in the true measurements. This finding was also shown by Ávila et al. (2019), which ascribed to the low number of measurements for the physico-chemical and sensory characteristics. This aspect may also influence in the results of the present study since each sample ($n = 100$) was evaluated in triplicate by means of physico-chemical and sensory analysis, while twenty-nine MRI images are obtained and computationally analysed for each loin. It is also observed in Table 4, slightly higher MAE values for quality parameters predicted by GLCM than by OPFTA. This finding corroborates the values of R, WAPE and RMSE (Table 2) previously discussed and may be affected by the relationship between the quality parameters of loins and the computational features.

5. Conclusions

An experimental protocol has been developed for the non-destructive analysis of quality parameters of meat products by MRI-computer vision-data mining. The comparison of different techniques for the MRI acquisition, the MRI analysis and the data analysis to predict quality parameters of pork loins have led to two optimum procedures (SE – GLCM – prediction equations obtained by MLR as a function of computational texture features of GLCM and SE – OPFTA - prediction equations obtained by MLR as a function of computational fractal features of OPFTA) to be implemented in an experimental protocol. The validation of these two procedures in a high number of samples from the meat industry by several quality measures allows to indicate the use of any of them to determine quality characteristics of loins by LF MRI in a non-destructive way, with high accuracy and reducing the dispersion of the values. These results bring the possibility of implementing this methodology in meat processing plants. For that, some improvements in the image acquisition (time reduction) and image and data analysis (software development to provide on-line results) should be done.

Author contributions

DANIEL CABALLERO, Conceptualization; Formal analysis; Funding acquisition; Investigation; Methodology; Software; Validation;

Visualization; Writing – original draft. PABLO G. RODRÍGUEZ, Conceptualization; Funding acquisition; Investigation; Methodology; Supervision. ANDRÉS CARO, Data curation; Formal analysis; Funding acquisition; Investigation; Methodology; Project administration; Supervision; Validation; Visualization; Writing – review & editing. MARÍA DEL MAR ÁVILA, Data curation; Formal analysis; Funding acquisition; Investigation; Methodology; Project administration; Supervision; Validation; Visualization; Writing – review & editing. JUAN P. TORRES, Formal analysis; Methodology; Software. TERESA ANTEQUERA, Formal analysis; Funding acquisition; Investigation; Methodology; Resources; Supervision; Validation; Writing – original draft; Writing – review & editing. TRINIDAD PÉREZ-PALACIOS, Conceptualization; Formal analysis; Funding acquisition; Investigation; Methodology; Resources; Supervision; Validation; Visualization; Writing – original draft; Writing – review & editing.

Declaration of competing interest

All authors have participated in (a) conception and design, or analysis and interpretation of the data; (b) drafting the article or revising it critically for important intellectual content; and (c) approval of the final version.

Acknowledgments

Daniel Caballero thanks the “Junta de Extremadura” for the post-doctoral grant (PO17017). The authors wish to acknowledge the funding received from the FEDER-MICCIN Infrastructure Research Project (UNEX-10-1E-402), Junta de Extremadura economic support for research group (GRU18138 and GRU18104) and for the Regional Government Board – Research Project (IB16089). We also wish to thank the Animal Source Foodstuffs Innovation Services (SiPA) (Cáceres, Spain) from the University of Extremadura.

References

- Aggarwal, N., Agrawal, R.K., 2012. First and second order statistics features for classification of magnetic resonance brain images. *J. Signal Inf. Process.* 3, 574–850.
- Association of Official Analytical Chemists (A.O.A.C.), 2000. In: *Official Methods of Analysis* of AOAC International, vols. 1 and 2. AOAC International, Gaithersburg, Maryland, U.S.A.
- Ávila, M.M., Caballero, D., Durán, M.L., Caro, A., Pérez-Palacios, T., Antequera, T., 2015. Including 3D-textures in a computer vision system to analyze quality traits of loin. *Lect. Notes Comput. Sci.* 9163, 456–465.
- Ávila, M.M., Caballero, D., Antequera, T., Durán, M.L., Caro, A., Pérez-Palacios, T., 2018. Applying 3D textura algorithms on MRI to evaluate quality traits of loin. *J. Food Eng.* 222, 258–266.
- Ávila, M.M., Durán, M.L., Caballero, D., Antequera, T., Pérez-Palacios, T., Cernadas, E., Fernández-Delgado, M., 2019. Magnetic Resonance Imaging, texture analysis and regression techniques to non-destructively predict the quality characteristics of meat pieces. *Eng. Appl. Artif. Intell.* 82, 110–125.
- Bernau, M., Kremer, P.V., Lauterbach, E., Tholen, E., Petersen, B., Pappenberger, E., Scholz, A.M., 2015. Evaluation of carcass composition of intact boars using linear measurements from performance testing, dissection, dual energy X-ray absorptiometry (DXA) and magnetic resonance imaging (MRI). *Meat Sci.* 104, 58–66.
- Caballero, D., Pérez-Palacios, T., Caro, A., Amigo, J.M., Dahl, A.B., Ersboll, B.K., Antequera, T., 2017a. Prediction of pork quality parameters by applying fractals and data mining on MRI. *Food Res. Int.* 99, 739–747.
- Caballero, D., Antequera, T., Caro, A., Ávila, M.M., Rodríguez, P.G., Pérez-Palacios, T., 2017b. Non-destructive analysis of sensory traits of dry-cured loins by MRI-computer vision techniques and data mining. *J. Sci. Food Agric.* 97, 2942–2952.
- Caballero, D., Caro, A., Amigo, J.M., Dahl, A.B., Ersboll, B.K., Pérez-Palacios, T., 2017c. Development of a new fractal algorithm to predict quality traits of MRI loins. *Lect. Notes Comput. Sci.* 10424, 208–218.
- Caballero, D., Caro, A., Dahl, A.B., Ersboll, B.K., Amigo, J.M., Pérez-Palacios, T., Antequera, T., 2018a. Comparison of different image analysis algorithms on MRI to predict physico-chemical and sensory attributes of loin. *Chemometr. Intell. Lab. Syst.* 180, 54–63.
- Caballero, D., Antequera, T., Caro, A., Amigo, J.M., Ersboll, B.K., Dahl, A.B., Pérez-Palacios, T., 2018b. Analysis of MRI by fractals for Prediction of sensory attributes: a case of study in loin. *J. Food Eng.* 227, 1–10.
- Caballero, D., Pérez-Palacios, T., Caro, A., Antequera, T., 2021. Use of Magnetic Resonance Imaging to analyse meat and meat products non-destructively. *Food Rev. Int.* <https://doi.org/10.1080/87559129.2021.1912085>.

- Colton, T., 1974. Statistical in Medicine. Little Brown and Co., New York, New York, U.S.A, pp. 1–372.
- Dietterich, T., 1998. Approximate statistical tests for comparing supervised classification learning algorithms. *Neural Comput.* 10 (7), 1895–1923.
- Fayyad, U., Piatetsky-Shapiro, L.G., Smyth, P., 1996. From data mining to knowledge discovery in databases. *Am. Ass. Artifi. Intel.* 17, 37–54.
- Feig, S., 2011. Comparison of costs and benefits of breast cancer screening with mammography, ultrasonography, and MRI. *Obstet. Gynecol. Clin. N. Am.* 38 (1), 179–196.
- González-Mohino, A., Antequera, T., Ventanas, S., Caballero, D., Mir-Bel, J., Pérez-Palacios, T., 2018. Near-infrared spectroscopy-based analysis to study sensory parameters on pork loins as affected by cooking methods and conditions. *J. Sci. Food Agric.* 98, 4227–4236.
- Grossman, R., Seni, G., Elder, J., Agarwal, N., Liu, H., 2010. Ensemble methods in data mining: improving accuracy through combining predictions. *Synthesis lectures on data mining and knowledge discovery* 2 (1), 1–126.
- Haralick, R.M., Shanmugam, K., Dinstein, I., 1973. Textural features for image classification. *IEEE Trans. Syst. Man Cyber.* 3 (6), 610–621.
- Haralick, R.M., Shapiro, L.G., 1993. Computer and Robot Vision. Addison-Wesley, Chicago, Illinois, U.S.A, pp. 453–508.
- Hastie, T., Tibshirani, R., Friedman, J., 2001. The Elements of Statistical Learning: Data Mining Inference and Prediction. Springer-Verlag, New York, New York, U.S.A, pp. 43–100.
- Ladd, M.E., Bachert, P., Meyerspeer, M., Moser, E., Nagel, A.M., Norris, D.G., Schmitter, S., Speck, O., Straub, S., Zaiss, M., 2018. Pros and cons of ultra-high-field MRI/MRS for human application. *Prog. Nucl. Magn. Reson. Spectrosc.* 109, 1–50.
- Molano, R., Rodríguez, P.G., Caro, A., Durán, M.L., 2012. Finding the largest area rectangle of arbitrary orientation in a closed contour. *Appl. Math. Comput.* 218 (19), 9866–9874.
- Peckinpaugh, S., 1991. An improved method for computing gray-level co-occurrence matrix based texture measured. *Comput. Vis. Graph Image Process* 53, 574–580.
- Pérez-Palacios, T., Ruiz, J., Martín, D., Muriel, E., Antequera, T., 2008. Comparison of different methods for total lipid quantification. *Food Chem.* 110, 1025–1029.
- Pérez-Palacios, T., Antequera, T., Durán, M.L., Caro, A., Rodríguez, P.G., Ruiz, J., 2010a. MRI-based analysis, lipid composition and sensory traits for studying Iberian dry-cured hams from pigs fed with different diets. *Food Res. Int.* 43, 248–254.
- Pérez-Palacios, T., Antequera, T., Molano, R., Rodríguez, P.G., Palacios, R., 2010b. Sensory traits Prediction in dry-cured hams from fresh product via MRI and lipid composition. *J. Food Eng.* 101, 152–157.
- Pérez-Palacios, T., Caballero, D., Antequera, T., Durán, M.L., Ávila, M.M., Caro, A., 2017. Optimization of MRI acquisition and texture analysis to predict physico-chemical parameters of loins by data mining. *Food Bioprocess Technol.* 10, 750–758.
- Pérez-Palacios, T., Caballero, D., González-Mohino, A., Mir-Bel, J., Antequera, T., 2019. Near infrared reflectance spectroscopy to analyse texture related characteristics of sous vide pork loin. *J. Food Eng.* 263, 417–423.
- Picouet, P.A., Gou, P., Fulladosa, E., Santos-Garcés, E., Arnau, J., 2013. Estimation of NaCl diffusivity by computed tomography in the semimembranosus muscle during salting of fresh and frozen/thawed hams. *LWT Food Sci. Technol.* 51, 275–280.
- Ruiz, J., Ventanas, J., Cava, R., Timón, M.L., García, C., 1998. Sensory characteristics of Iberian ham: influence of processing time and slice location. *Food Res. Int.* 31, 53–58.
- Torres, J.P., Ávila, M.M., Caro, A., Pérez-Palacios, T., Caballero, D., 2019. Non-destructive Prediction of quality parameters of dry-cured Iberian ham by applying Computer vision and low-field MRI. *Lect. Notes Comput. Sci.* 11867, 498–507.
- Vestergaard, C., Erbou, S.G., Thauland, T., Adler-Nissen, J., Berg, B., 2015. Salt distribution in dry-cured ham measured by computed tomography and image analysis. *Meat Sci.* 69, 9–15.

Capítulo 4

4. Resultados y discusión

4.1 Resultados del artículo “A Computer-Aided Inspection System to Predict Quality Characteristics in Food Technology”

Según los experimentos realizados para la redacción del primer artículo “A Computer-Aided Inspection System to Predict Quality Characteristics in Food Technology” se obtuvieron los siguientes resultados.

La participación de los regresores en el modelo final puede ser interesante para la comunidad científica. Luego, se presentará, en primer lugar una relación de los regresores, ordenados según el grado de correlación con las técnicas tradicionales obtenido en los experimentos.

Este proceso de jerarquización premia a los regresores con coeficientes de correlación “r” mayores que la media de las correlaciones de todos los algoritmos, siempre que el regresor considerado presente una correlación mayor que 0.5 (correlación moderada a excelente). La [Fig 4.1] muestra el porcentaje de votos recibidos por cada regresor en todos los experimentos, separado por lotes (cerdo o ternera).

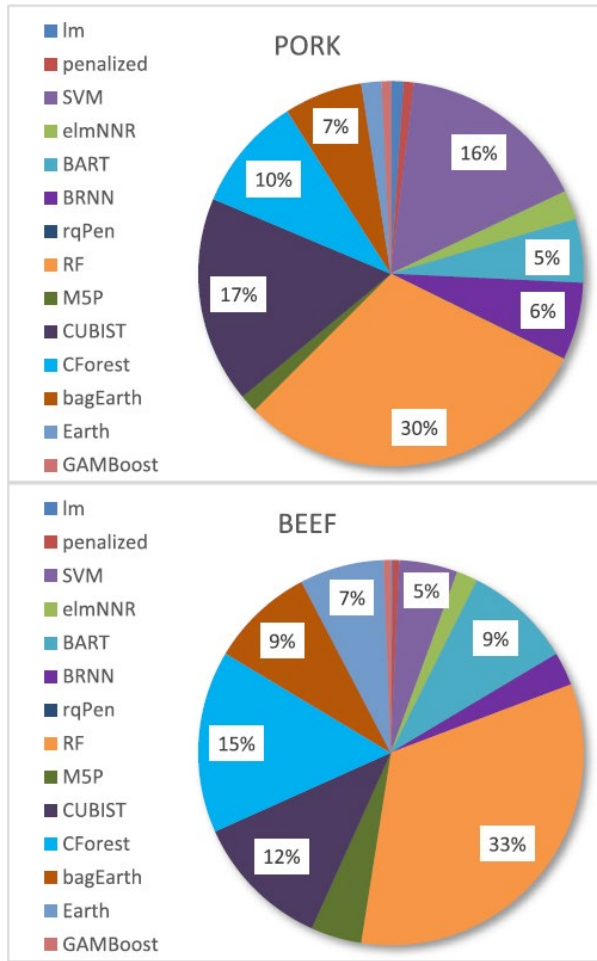


Figura 4.1. Porcentaje de votos de cada regresor.

En el caso de las muestras de cerdo, RF recibió el 30% de votos, siendo la opción mayoritaria. CUBIST (17%) y SVM (16%) respectivamente también presentan aproximadamente $\frac{1}{3}$ de los votos. Del resto, CFOREST recibió un 10% de los votos, y M5P un 7%. El resto de los regresores obtuvieron una representación muy pequeña.

Los resultados para las muestras de ternera fueron muy similares. Un tercio de los votos fueron para el RF, siendo CFOREST (15%) la segunda mejor opción. CUBIST bajó un poquito, obteniendo un 12%. Ligeramente por debajo del 10% se encuntran los regresores bagEARTH (9%), BART (9%) y EARTH (7%). Debe resaltarse que el SVM tuvo una importancia sólo del 5%.

La tabla [4.1] muestra la calificación de los 7 mejores regresores, de los 14 totales usados en el artículo, como su influencia de acuerdo a los votos recibidos (para cerdo, ternera y

ambos tipos mezclados). Como se puede ver, tan solo con la mitad de los regresores, aproximadamente el 90% de la participación se obtiene en el modelo de aprendizaje final, basándose en los votos.

Tabla 4.1. Ranking de regresores.

Cerdo		Ternera		Cerdo y ternera	
Regresor	%	Regresor	%	Regresor	%
RF	30,21%	RF	33,21%	RF	31,71%
Cubist	17,35%	CForest	15,31%	Cubist	14,44%
SVM	16,05%	Cubist	11,54%	CForest	12,47%
CForest	9,64%	BART	9,06%	SVM	10,48%
BagEarth	6,56%	BagEarth	8,73%	BagEarth	7,65%
BRNN	6,45%	EARTH	7,06%	BART	7,20%
BART	5,34%	SVM	4,91%	BRNN	4,63%
TOTAL	91,60%	TOTAL	89,82%	TOTAL	88,58%

En la Tabla [4.2] (para cerdo) y en la Tabla [4.3] (para ternera) se muestran la media de las correlaciones obtenidas cuando los regresores de la tabla [4.1] son utilizados para calcular todos los atributos de cada uno de los cuatro algoritmos de extracción de características usados en estos experimentos (algoritmos de texturas clásicos, Gabor, Wavelet y algoritmos de fractales). Las medias de las correlaciones obtenidas no son muy buenas. De acuerdo a las indicaciones de Colton [58], no existe casi ninguna correlación que pueda ser considerada en el rango “muy bueno-excelente”. Algunas de las características del mismo algoritmo alcanzan valores altos, pero otros obtienen valores bajos, lo que significa que la media no será tan alta como sería deseable. Las distribuciones numéricas no son homogéneas para todas las características del mismo modelo, lo que penaliza el uso de un único método para las predicciones. Esto prueba que no es una buena opción considerar el mismo regresor para calcular todas las características de acuerdo con el mismo algoritmo extractor. En su lugar, es conveniente estudiar la mejor combinación regresor-algoritmo extractor de características, atributo por atributo.

Tabla 4.2. Coeficientes de correlación para lomos de cerdo.

	Algoritmo	RF	Cubist	SVM	CForest	bagEarth	BRNN	BART
Fresco	Clásicos	0.6274	0.6200	0.5715	0.5822	0.5454	0.4912	0.5509
	Gabor	0.6657	0.6491	0.6595	0.6613	0.5989	0.5867	0.5815
	Wavelet	0.5163	0.5055	0.4190	0.4899	0.5068	0.4515	0.4977
	Fractales	0.7995	0.8362	0.5193	0.6256	0.4994	0.4442	0.5997
Descong.	Clásicos	0.6603	0.5922	0.6740	0.5970	0.5371	0.5188	0.5550
	Gabor	0.5827	0.5399	0.5729	0.5781	0.4931	0.4921	0.4683
	Wavelet	0.3629	0.3806	0.2635	0.3332	0.3782	0.1687	0.3379
	Fractales	0.5767	0.5148	0.5148	0.5282	0.4407	0.5767	0.4744
Cocinado	Clásicos	0.6433	0.5895	0.5857	0.5962	0.5381	0.5178	0.5495
	Gabor	0.5600	0.5203	0.5459	0.5269	0.4984	0.4378	0.4780
	Wavelet	0.3307	0.3814	0.2010	0.2796	0.3631	0.2495	0.2972
	Fractales	0.5968	0.3814	0.3814	0.5754	0.4975	0.4059	0.5314
Curado	Clásicos	0.6185	0.5865	0.6437	0.5947	0.5315	0.5340	0.5723
	Gabor	0.6856	0.6668	0.6959	0.6719	0.5342	0.5253	0.5911
	Wavelet	0.4751	0.4738	0.3391	0.4052	0.4226	0.2532	0.3985
	Fractales	0.2896	0.2584	0.2841	0.2896	0.2419	0.3044	0.2635

Tabla 4.3. Coeficientes de correlación para lomos de ternera.

	Algoritmo	RF	Cubist	SVM	CForest	bagEarth	BRNN	BART
Fresco	Clásicos	0.7179	0.6766	0.6852	0.6563	0.6704	0.6414	0.6383
	Gabor	0.6294	0.5940	0.5923	0.5607	0.5603	0.4806	0.6026
	Wavelet	0.5636	0.5607	0.5378	0.5496	0.5238	0.4982	0.4597
	Fractales	0.6266	0.6310	0.5991	0.6021	0.5381	0.5874	0.5132
Descong	Clásicos	0.7718	0.7503	0.7646	0.7328	0.6712	0.5492	0.6507
	Gabor	0.6907	0.6679	0.6171	0.6047	0.5746	0.5262	0.6028
	Wavelet	0.5286	0.5100	0.5545	0.5191	0.5391	0.5381	0.3063
	Fractales	0.6373	0.6360	0.6123	0.5946	0.4648	0.5739	0.4788
Cocinado	Clásicos	0.7474	0.7149	0.7249	0.6941	0.7114	0.6747	0.6489
	Gabor	0.6896	0.6413	0.5954	0.5898	0.6038	0.5560	0.5701
	Wavelet	0.5094	0.4567	0.4499	0.496	0.4913	0.4145	0.2924
	Fractales	0.5532	0.5560	0.5119	0.5024	0.3500	0.5074	0.4278

La correlación final del sistema siguiendo este enfoque es de 0.712379883 para los lomos de cerdo y 0.745761477 para los lomos de ternera, calculado como una media de las mejores combinaciones mostradas en las Tabla [4.2 y 4.3].

Como se especifica en el artículo, todas las combinaciones de regresores-algoritmos extractores de características representan un total de 6180 modelos diferentes. En el contexto de proponer una solución para la industria cárnica, integrar todos esos modelos en un sistema “ensemble” puede suponer un gran desafío. De este modo, para superar las limitaciones, solo

se integran 110 modelos en la propuesta del sistema “ensamble”. Específicamente, los modelos que proporcionaron los mejores resultados.

La Tabla [4.4] muestra las mejores combinaciones para los 110 modelos entrenados, basados en las clasificaciones propuestas en la metodología.

Tabla 4.4. Mejores combinaciones de regresores-algoritmo extractor.

CERDO								
	Fresco		Descongelado		Cocinado		Curado	
Wa	RF	FR	BRNN	GA	RF	CL	svm	GA
L*	Cubist	FR	RF	CL	RF	CL	svm	GA
a*	Cubist	FR	RF	CL	RF	GA	svm	GA
b*	Cubist	FR	svm	CL	Cubist	CL	svm	GA
MO	Cubist	FR	svm	CL	CForest	FR	svm	GA
LI	RF	FR	svm	CL	RF	FR	RF	GA

TERNERA								
	Fresco		Descongelado		Cocinado			
Wa	RF	CL	RF	CL	BRNN	CL		
L*	CForest	FR	RF	CL	RF	CL		
a*	RF	CL	RF	CL	bagEarth	CL		
b*	RF	CL	RF	CL	RF	CL		
MO	svm	GA	CForest	CL	M5P	CL		
LI	RF	CL	CForest	CL	RF	CL		

a)

CERDO					TERNERA					
	Descongelado		Cocinado		Curado		Descongelado		Cocinado	
HD	svm	GA	RF	GA	svm	GA	RF	CL	RF	CL
AD	svm	CL	svm	GA	Cubist	GA	RF	CL	BRNN	CL
ST	svm	CL	RF	FR	RF	GA	RF	CL	RF	CL
CS	RF	CL	RF	FR	svm	GA	RF	CL	RF	CL
SP	svm	GA	svm	CL	svm	GA	RF	CL	CForest	CL
CH	bart	FR	RF	CL	svm	GA	RF	CL	RF	CL
RE	RF	GA	RF	FR	svm	GA	RF	CL	RF	CL

b)

	CI	BR	OI	CO	TD	JC	FB	CH	FI	CF
CERDO	svm	Cubist	RF	svm	svm	RF	RF	RF	RF	RF
	CL	CL	FR	CL	CL	GA	GA	GA	FR	CL
TERNERA	RF	RF	RF	RF	RF	RF	RF	RF	RF	RF
	CL	CL	CL	CL	CL	CL	CL	CL	CL	CL

c)

CI	BR	MB	PO	OI	HD	JC	FB	CH	ST	CF	PF	FI
svm	svm	svm	RF	Cubist	svm	svm	svm	svm	svm	RF	RF	RF
GA	GA	GA	GA	GA	GA	GA	GA	GA	GA	GA	GA	GA

d)

La figura [4.2.a] muestra que el algoritmo RF es el mejor regresor para más de la mitad de las características de calidad, siendo SVM la segunda opción más repetida para aproximadamente un tercio de las características. CUBIST y CForest son la tercera y cuarta opción respectivamente.

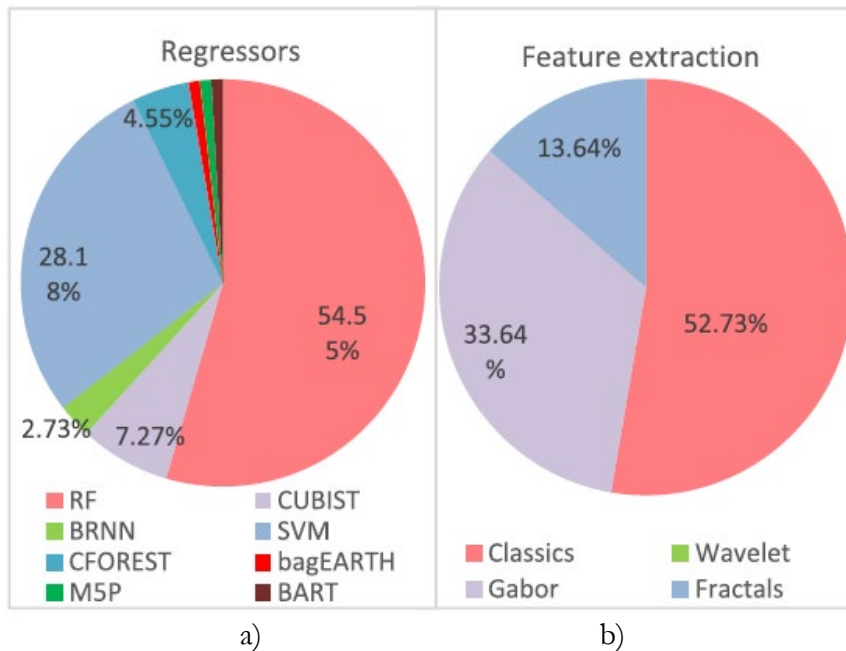


Figura 4.2. Distribución de los mejores regresores(a) y los mejores extractores(b).

Respecto a los algoritmos extractores de características (fig 4.2.b), los algoritmos clásicos son usados en la mitad de las características, mientras un tercio de las características utilizadas son basadas en filtros de Gabor. Los fractales son la tercera opción y cabe señalar que las Wavelets no son utilizadas en ninguna combinación.

La fig.[4.3.a] muestra la participación de cada regresor y algoritmo extractor en los diferentes subconjuntos de categorías de calidad. RF es el regresor más usado y SVM es el segundo para predecir los tres conjuntos de características: físico-químicas (PC), texturas instrumentales (IT) y sensoriales (SA). Hasta 7 regresores diferentes están involucrados en la predicción de las características físico-químicas (PC), lo que implica características con distribuciones heterogéneas. Por lo tanto, algunas características son predichas utilizando métodos basados en árboles (RF, CUBIST, M5P), otros con SVM y algunos otros con modelos “ensemble” (CFOREST, bagEARTH). Para las características de texturas instrumentales (IT), la mayoría de las predicciones se realizan utilizando el algoritmo RF y SVM, mientras que raramente se usan otros regresores. Finalmente, para los atributos

sensoriales (SA), la mayoría de las predicciones se realizaron usando árboles (principalmente RF, y CUBIST), siendo la tercera mejor opción el uso de SVM. Destacar que los modelos Bayesianos (BRNN y BART) solo son útiles para unas pocas características PC e IT.

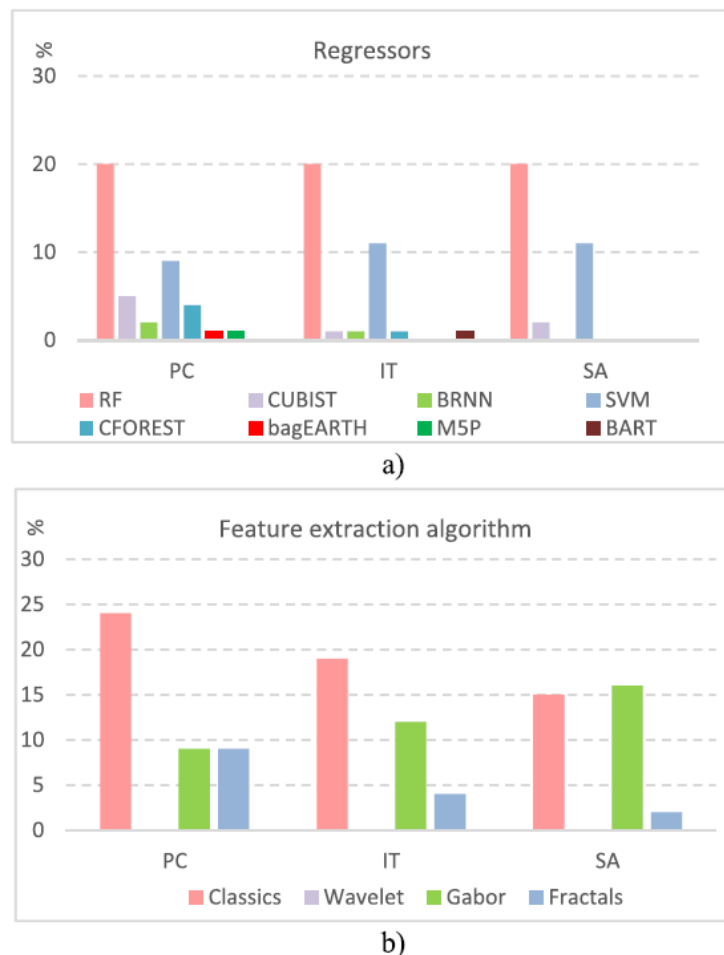


Figura 4.3. Distribución de los mejores regresores(a) y los mejores extractores(b), de acuerdo a los grupos de extractores.

En cuanto a los algoritmos extractores (fig 4.3.b), los algoritmos de texturas clásicos alcanzan los mejores resultados para más de la mitad de las características físico-químicas (PC) y texturas instrumentales (IT), siendo las Gabor y las características de fractales las mejores para la otra mitad. En las cualidades sensoriales, Gabor es el más repetido, seguido de cerca por los algoritmos clásicos. Otra vez, las características extraídas de las Wavelets no son utilizadas para ninguna predicción.

Finalmente, la tabla 4.5 muestra las correlaciones obtenidas por las combinaciones de los mejores regresores y algoritmos extractores de características, para cada una de las cualidades de calidad predichas.

Tabla 4.5. Correlaciones para las mejores combinaciones.

Tipo		Wa	L*	a*	b*	MO	LI
Cerdo	Fresco	0.8603	0.8308	0.9289	0.8515	0.8737	0.7883
	Descongelado	0.6744	0.7103	0.6649	0.6774	0.7277	0.6711
	Cocinado	0.6238	0.6770	0.6336	0.6437	0.6640	0.6752
	Curado	0.7070	0.7646	0.6651	0.6700	0.6839	0.6954
Ternera	Fresco	0.7489	0.7518	0.8814	0.6840	0.7291	0.6244
	Descongelado	0.6691	0.7375	0.8504	0.7761	0.8232	0.7946
	Cocinado	0.8516	0.6685	0.6800	0.8470	0.7682	0.7426

a)

Tipo		HD	AD	ST	CS	SP	CH	RE
Cerdo	Descongelado	0.6786	0.7406	0.7683	0.7441	0.6648	0.6334	0.6372
	Cocinado	0.5902	0.7012	0.7711	0.7185	0.6421	0.6849	0.7527
	Curado	0.7510	0.7129	0.7875	0.7266	0.7261	0.7274	0.7040
Ternera	Descongelado	0.8698	0.7237	0.7992	0.8591	0.8610	0.8512	0.7518
	Cocinado	0.6726	0.8530	0.8139	0.8104	0.7393	0.7692	0.7901

b)

Tipo	CI	BR	OI	CO	TD	JC	FB	CH	FI	CF
Cerdo	0.525	0.657	0.634	0.658	0.587	0.655	0.613	0.645	0.707	0.679
Ternera	0.744	0.820	0.791	0.727	0.753	0.738	0.849	0.767	0.785	0.836

c)

CI	BR	MB	PO	OI	HD	JC	FB	CH	ST	CF	PF	FI
0.740	0.728	0.721	0.681	0.722	0.751	0.781	0.754	0.727	0.750	0.669	0.687	0.725

d)

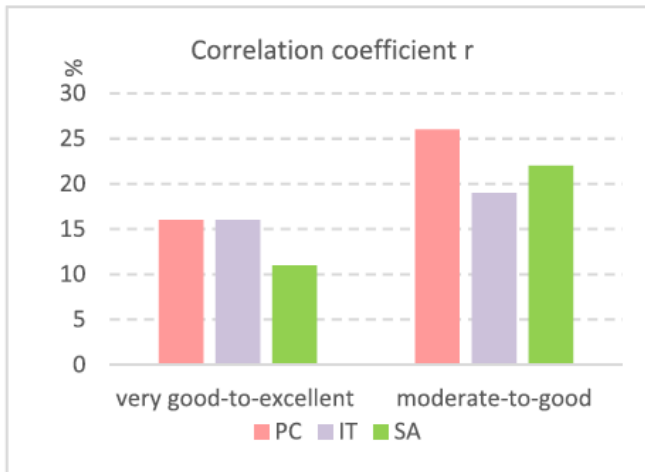


Figura 4.4. Correlaciones para las mejores combinaciones.

La fig [4.4] muestra la calidad de las predicciones, destacando que casi la mitad de las características (específicamente el 40% de ellas) obtienen una predicción de “muy bueno a excelente”, obteniéndose también altos porcentajes en la categoría “moderado-a-bueno”. Para las características de texturas instrumentales (IT) se obtiene la mayor precisión en conjunto, seguidas por las características físico-químicas (PC). Las características sensoriales (SA) obtienen las peores correlaciones, aunque obtienen buenos resultados. No obstante, en los experimentos desarrollados, la mayoría de las características se predicen con una gran precisión.

La correlación final del sistema siguiente este enfoque es 0.7346 para lomos de cerdo y 0.7746 para los lomos de ternera, calculado como la media de las mejores combinaciones mostradas en las tablas [4.2 y 4.3]. Las correlaciones han sido mejoradas desde 0.7124 a 0.7346 para los lomos de cerdo, y desde 0.7458 a 0.7746 para lomos de ternera, considerando una selección atributo a atributo de las mejores combinaciones, en lugar de considerar las mejores combinaciones agrupadas por algoritmo extractor.

A modo de ejemplo, la Tabla [4.6] muestra los resultados obtenidos por las diferentes métricas de rendimiento considerando para ese caso los lomos frescos de cerdo y ternera

Tabla 4.6. Correlaciones para las mejores combinaciones.

Carne	Métrica	Wa	L*	a*	b*	MO	LI
Cerdo Fresco	R	0.8898	0.9491	0.9435	0.8974	0.8489	0.7620
	RMSE	0.0020	0.6900	0.4448	0.4828	0.6794	0.7857
	MAE	0.0013	0.5106	0.3128	0.3281	0.5153	0.6083
	MAPE	0.0014	0.0116	0.0308	0.0937	0.0073	0.0974
Ternera Fresca	R	0.7264	0.6911	0.8641	0.6381	0.7730	0.6506
	RMSE	0.0034	1.1521	1.4890	1.6137	1.2970	1.6860
	MAE	0.0025	0.8871	0.9781	1.1381	0.9496	1.1136
	MAPE	0.0025	0.0213	0.0576	0.1662	0.0130	0.3383

4.2 Resultados del artículo “An experimental protocol to determine quality parameters of dry-cured loins using low-field Magnetic Resonance Imaging”

En el segundo artículo se pueden considerar los siguientes resultados.

En los experimentos realizados, se evalúan diferentes estudios realizados sobre MRI de bajo campo en lomos de cerdo [60, 59, 62, 5], comparando los resultados de las predicciones físico-químicas y características sensoriales como una función de la secuencia de adquisición MRI, algoritmos para el análisis de imágenes y técnicas de análisis de datos. En los experimentos se emplean tres secuencias de adquisición en bajo campo (LF) MRI en lomos de cerdo: SE, GE y T3D. En general, SE lleva a imágenes más finas y mejor definidas que GE y T3D [60, 59, 62, 6, 61] y genera mejores predicciones [60, 59, 6, 61].

Los algoritmos para analizar imágenes MRI difieren en el número de características computacionales y complejidades. NGLDM es el algoritmo más simple con 5 características computacionales, seguido en orden de complejidad por el OPFTA (7), CFA (9) y FTA, GLCM y GLRLM (10). En lo referente a las complejidades, es más baja en el GLCM, GLRLM y OPFTA ($O(n^2)$) que en el FTA ($O(n^2 * \log n)$) y CFA ($O(n^3)$) [6, 61]. Considerando los resultados de las predicciones de las características de análisis físico-químicos y sensoriales, GLCM y OPFTA obtuvieron el coeficiente de correlación más alto entre los algoritmos de texturas y fractales, respectivamente [60, 59, 62, 5]. Por esto, en lugar de los algoritmos más simples, GLCM y OPFTA fueron los seleccionados para EP.

Como técnicas predictivas, MLR y las regresiones isotónicas (IR) son las seleccionadas en los estudios realizados para dispositivos MRI de bajo campo (LF MRI) en lomos de cerdo. En el caso de aplicar algoritmos de texturas para el análisis de imágenes, se obtuvieron correlaciones excelentes ($r > 0.75$) tanto con MLR como con IR [59, 5]. Sin embargo, se obtuvieron resultados más precisos para las predicciones utilizando MLR que con IR cuando se usaron los algoritmos de fractales [60, 59, 62, 6, 61]. El MAE fue también calculado en estos estudios, siendo más bajo cuando se utilizaba MLR en ambos casos (texturas y algoritmos de fractales). También, MLR es más simple (ecuación de primer grado) que IR (ecuaciones de sexto grado) [60, 59, 62, 6, 61, 5]. Respectivamente, para el protocolo experimental (EP) se seleccionaron las ecuaciones de predicción obtenidas por MLR.

Como se aprecia en la figura 4.5, el protocolo experimental (EP) se implementó con dos procesos: A) SE - GLCM - ecuaciones de predicción obtenidas por MLR en función de las características de textura computacional de GLCM. B) SE - OPFTA - ecuaciones de predicción obtenidas por MLR en función de las características fractales computacionales de OFTA.

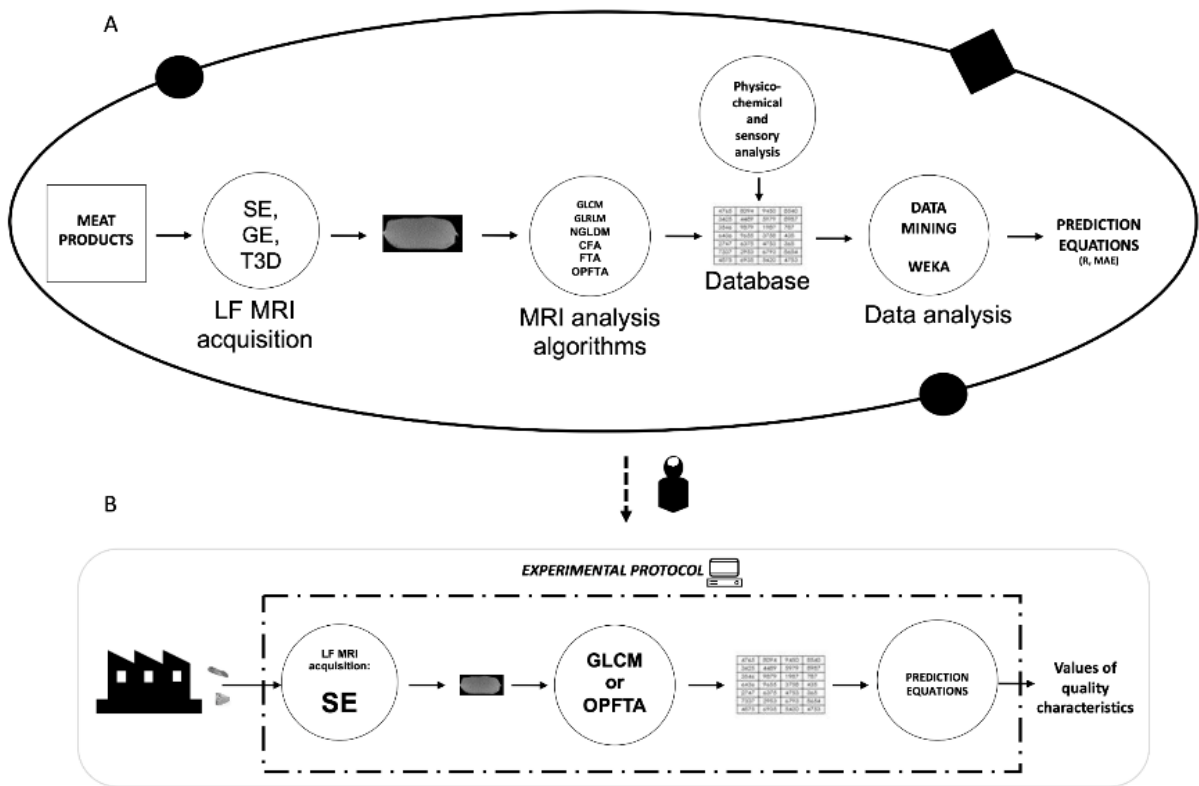


Figura 4.5. Implementación del protocolo experimental evaluado en este estudio.

La Tabla. 4.7 muestra la desviación estándar de los parámetros físicoquímicos y sensoriales de los análisis tradicionales y de los pronosticados por los procedimientos GLCM y OPFTA. Por su parte, la Tabla 4.8 muestra los valores de R, WAPE y RMSE que evalúan los resultados de las predicciones de los dos procesos para el protocolo experimental (usando GLCM o OPFTA). Se aprecia que se obtienen valores de R superiores a 0.75 para la mayoría de los parámetros de calidad de los lomos, lo que indica una correlación de muy buena a excelente [58], al aplicar tanto GLCM como OPFTA. Además, la WAPE y los RMSE son menores de 0.02% y 0.3%, respectivamente, en todos los casos. Se puede observar un mayor número de parámetros con R > 0.75 y WAPE < 0.01 cuando se utiliza OPFTA.

Tabla 4.7. Comparación entre valores fisicoquímicos y los valores predichos de GLCM y OPFTA.

		P-C	GLCM	OPFTA	p(P-C vs GLCM)	p(P-C vs OPFTA)
Actividad del agua		0.875 ± 0.009	0.875 ± 0.011	0.879 ± 0.016	0.557	0.068
Humedad (%)		40.119 ± 3.407	39.394 ± 4.381	40.976 ± 3.537	0.182	0.075
Color instrumental	L*	45.179 ± 3.148	45.036 ± 3.973	45.753 ± 3.478	0.772	0.211
	a	14.705 ± 0.576	14.329 ± 0.537	14.821 ± 0.294	0.316	0.067
	b	8.713 ± 0.557	9.402 ± 1.093	8.502 ± 0.699	0.752	0.209
Contenido sal (%)		2.503 ± 0.385	2.431 ± 0.447	2.480 ± 0.409	0.211	0.604
Contenido graso (%)		10.580 ± 1.198	11.257 ± 1.569	10.027 ± 0.867	0.362	0.707

Los resultados de los análisis físico-químicos y sensoriales se han comparado estadísticamente con los predichos por los procedimientos GLCM y OPFTA. Como se ha comentado, los valores medios y la desviación estándar de los parámetros fisicoquímicos y sensoriales de los análisis tradicionales y pronosticados por los procedimientos GLCM y OPFTA se muestran en la Figura 4.6 y la Tabla. 4.7, respectivamente, que también exponen los valores p entre los valores reales y predichos. No se encontraron diferencias significativas ($p > 0,05$) en los resultados predichos en todos los casos.

Tabla 4.8. Comparación entre valores fisicoquímicos y los valores predichos de GLCM y OPFTA.

		GLCM			OPFTA		
		R	WAPE	RMSEP	R	WAPE	RMSEP
Actividad del agua		0.6747	0.010	0.009	0.8491	0.011	0.010
Humedad (%)		0.9114	0.050	0.205	0.8789	0.050	0.204
Color instrumental	L*	0.9076	0.181	0.181	0.9017	0.175	0.175
	a	0.6123	0.060	0.060	0.6961	0.041	0.041
	b	0.7064	0.096	0.096	0.8511	0.049	0.049
Contenido sal (%)		0.8909	0.094	0.024	0.8905	0.080	0.021
Contenido graso (%)		0.8388	0.102	0.110	0.8489	0.073	0.079
Rojo del magro		0.5697	0.076	0.048	0.6491	0.048	0.041
Brillo del magro		0.9471	0.123	0.079	0.9270	0.093	0.059
Marmoleo del magro		0.9097	0.123	0.081	0.9257	0.095	0.062
Intensidad del olor		0.9588	0.135	0.079	0.9591	0.114	0.067
Dureza del magro		0.7477	0.108	0.065	0.9183	0.073	0.044
Jugosidad		0.7692	0.108	0.054	0.9249	0.075	0.037
Sabor salado		0.9560	0.124	0.059	0.9513	0.087	0.041
Intensidad del sabor		0.9442	0.067	0.048	0.9791	0.042	0.030
Persistencia del sabor		0.9259	0.076	0.058	0.9764	0.042	0.032
Sabor curado		0.9491	0.097	0.055	0.9777	0.063	0.036
Sabor rancio		0.8588	0.181	0.032	0.9137	0.146	0.026

La Tabla 4.9 muestra las ecuaciones de predicción del protocolo experimental para ambos procedimientos. Una vez implementado el protocolo experimental con los dos procedimientos óptimos, se probó su ejecución dentro del servicio de análisis oficial de la Facultad de Veterinaria de la Universidad de Extremadura (Cáceres, España), donde fue evaluado con muestras reales, como se explica en el subapartado de diseño experimental (Fig. 4.5B).

Tabla 4.9. Ecuaciones de predicción de los parámetros de calidad para lomos usando el regresor LM.

	GLCM	OPFTA
Actividad del agua	= -0.034 * ENE + 0.012 * ENT - 0.059 * COR + 0.974 * HC + 0.073 * IDM + 0.197 * INE - 0.070 * CS - 0.036 * CP + 0.063 * CON - 0.295 * DIS + 0.919	= 0.368 * UNI + 0.334 * ENT + 0.020 * COR + 0.025 * HOM + 0.162 * INE - 0.135 * CON + 0.145 * EFI + 0.566
Humedad (%)	= -11.038 * ENE + 6.316 * ENT - 7.109 * COR + 24.830 * HC + 24.389 * IDM + 55.696 * INE - 20.659 * CS - 15.407 * CP + 10.157 * CON - 70.601 * DIS + 45.927	= 49.568 * UNI + 64.839 * ENT + 4.683 * COR + 16.969 * HOM + 55.767 * INE - 30.923 * CON + 42.805 * EFI - 25.929
Color instrumental	L*	= -6.759 * ENT - 16.836 * COR + 25.396 * HC + 0.964 * IDM + 28.971 * INE - 5.108 * CS + 2.132 * CP - 16.028 * CON - 31.809 * DIS + 47.607
	a	= 2.223 * ENE - 2.416 * ENT + 1.514 * COR + 1.282 * HC - 3.919 * IDM + 9.143 * INE + 2.848 * CS - 4.142 * CON + 10.490 * DIS + 13.516
	b	= 2.311 * ENE - 0.763 * ENT + 0.916 * HC - 1.620 * IDM - 4.527 * INE + 1.991 * CS + 6.770 * CP + 7.878 * CON + 11.325 * DIS + 4.256
Contenido sal (%)	= 1.838 * COR - 2.226 * HC - 1.037 * IDM - 6.009 * INE + 1.574 * CS + 1.344 * CP + 7.336 * DIS + 0.821	= -8.898 * UNI - 7.546 * ENT - 0.506 * COR - 0.265 * HOM - 3.655 * INE + 3.281 * CON - 3.224 * EFI + 9.312
Contenido graso (%)	= 11.641 * ENE - 10.390 * ENT + 7.151 * HC - 16.961 * IDM - 22.839 * INE + 8.873 * CS + 12.602 * CP - 22.772 * CON + 27.982 * DIS + 17.497	= -15.617 * ENT - 7.474 * HOM - 13.201 * INE - 22.415 * EFI + 36.191
Rojo del magro	= 1.784 * ENT - 2.828 * HC + 8.185 * IDM - 3.981 * INE + 3.855 * CP + 2.916 * CON + 5.247 * DIS + 3.805	= 4.403 * ENT - 1.131 * COR + 0.826 * HOM - 1.253 * INE + 1.711 * CON + 5.137 * EFI + 3.062
Brillo del magro	= 0.323 * ENT + 28.978 * COR + 1.917 * HC - 2.781 * IDM - 2.385 * INE + 4.523 * CP - 1.302 * CON + 3.328 * DIS + 2.657	= 2.616 * UNI - 0.754 * INE - 6.529 * EFI + 4.764
Marmoleo del magro	= -3.966 * ENT + 6.765 * HC - 19.609 * IDM + 5.838 * INE - 3.113 * CP - 4.309 * CON - 12.017 * DIS + 13.324	= 3.262 * UNI - 8.596 * ENT + 2.673 * COR - 1.556 * HOM + 1.797 * INE - 5.698 * CON - 11.163 * EFI + 14.636
Intensidad del olor	= 38.889 * COR + 2.050 * HC - 3.797 * IDM + 2.473 * CP - 4.119 * CON + 3.563 * DIS + 5.346	= -1.657 * ENT + 0.689 * COR + 0.703 * HOM - 0.596 * INE + 0.792 * CON - 7.707 * EFI + 8.223
Dureza del magro	= -1.535 * ENE + 2.435 * ENT - 3.284 * HC + 9.761 * IDM - 2.479 * INE + 0.405 * CS + 2.030 * CP + 8.202 * DIS + 1.065	= -2.218 * UNI + 3.948 * ENT - 1.231 * COR + 1.130 * HOM - 1.128 * INE + 3.647 * CON + 3.244 * EFI + 1.675
Jugosidad	= -1.321 * ENT + 3.156 * HC - 7.674 * IDM - 1.028 * CON - 3.026 * DIS + 7.570	= 1.008 * UNI - 3.229 * ENT + 1.176 * COR - 1.511 * CON - 5.796 * EFI + 8.809

Sabor salado	$= 0.507 * ENT + 22.855 * COR + 1.606 * HC - 5.033 * INE + 5.735 * CP + 1.421 * CON + 4.014 * DIS + 2.307$	$= 4.354 * UNI + 2.113 * ENT - 1.231 * INE - 5.437 * EFI + 3.312$
Intensidad del sabor	$= - 1.533 * ENE + 0.201 * ENT + 21.101 * COR + 1.424 * HC - 1.022 * IDM - 2.309 * INE + 2.129 * CP - 0.371 * CON + 2.901 * DIS + 5.203$	$= 1.513 * UNI - 5.347 * EFI + 6.761$
Persistencia del sabor	$= - 2.047 * ENE + 0.395 * ENT + 22.681 * COR + 1.174 * HC - 2.458 * INE + 1.807 * CP - 0.553 * CON + 3.881 * DIS + 3.788$	$= 0.844 * UNI + 0.630 * CON - 5.164 * EFI + 5.698$
Sabor curado	$= 0.774 * ENT + 24.530 * COR + 0.887 * HC - 2.660 * INE + 5.047 * CP - 1.733 * CON + 5.183 * DIS + 3.401$	$= 1.143 * HOM - 0.501 * INE - 4.126 * EFI + 6.135$
Sabor rancio	$= 1.110 * ENE + 0.630 * ENT - 0.996 * HC + 2.124 * IDM - 1.113 * INE + 2.285 * CP + 0.788 * CON + 1.393 * DIS + 0.763$	$= 0.487 * UNI + 1.506 * ENT - 0.320 * COR + 0.386 * HOM - 0.595 * INE + 2.156 * EFI + 0.477$

La figura 4.6 muestra los valores medios, desviación estándar y la significancia (*p*-value) entre los valores reales y GLCM y real y OPFTA. Considerando esta figura 4.6 y Tabla 4.7, se pueden observar algunas diferencias en la desviación estándar de los resultados, siendo, en general, mayor en los valores predichos del GLCM que en los predichos reales y OPFTA.

En vista de este hecho, se midieron el TSTD y el MAE (Tabla 4.10). El TSTD evalúa la dispersión media de las mediciones verdaderas y el MAE evalúa la dispersión media de los valores predichos alrededor de las características, que es el promedio de las mediciones verdaderas. En todos los parámetros de calidad, los valores del TSTD son superiores a los del MAE de los procedimientos GLCM y OPFTA, lo que indica una menor dispersión en la predicción por computador que en las mediciones reales. Este hallazgo también fue demostrado por [63], que lo atribuyó al bajo número de mediciones de las características físico-químicas y sensoriales. Este aspecto también puede influir en los resultados del presente estudio ya que cada muestra ($n = 100$) fue evaluada por triplicado mediante análisis físico-químico y sensorial, mientras que para cada lomo se obtienen y analizan computacionalmente veintinueve imágenes de resonancia magnética. También se observa en la Tabla 4.10 valores MAE ligeramente superiores para los parámetros de calidad predichos por GLCM que por OPFTA. Este hallazgo corrobora los valores de R, WAPE y RMSE (Tabla 4.8) discutidos previamente y puede verse afectado por la relación entre los parámetros de calidad de los lomos y las características computacionales.

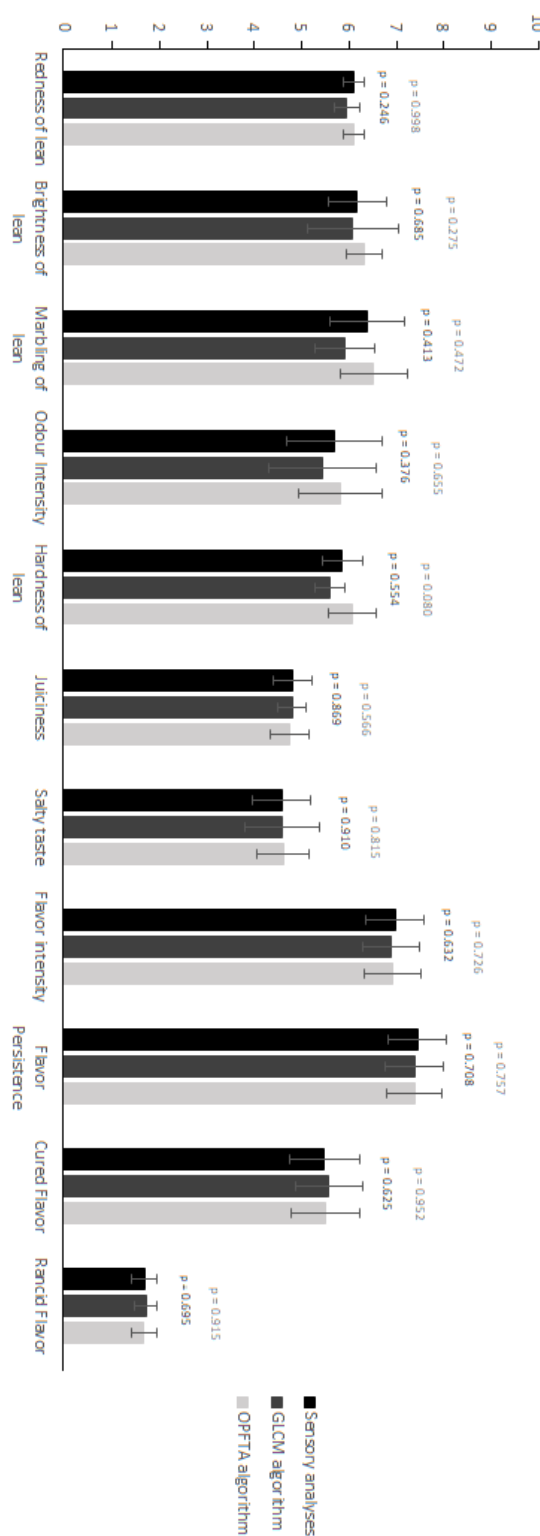


Figura 4.6. Valores medios, desviación estándar y p-values entre los valores reales y GLCM y real y OPFTA.

Tabla 4.10. Ecuaciones de predicción de los parámetros de calidad para lomos usando el regresor LM.

		TSTD	MAE	
			GLCM	OPFTA
Actividad del agua		0.014	0.009	0.010
Humedad (%)		3.913	1.998	1.995
Color instrumental	L*	3.611	0.039	0.038
	a	0.760	0.040	0.027
	b	0.684	0.107	0.055
Contenido sal (%)		0.4453	0.236	0.201
Contenido graso (%)		1.4671	1.075	0.776
Rojo del magro		0.5443	0.468	0.400
Brillo del magro		1.4465	0.767	0.576
Marmoleo del magro		1.7544	0.788	0.610
Intensidad del olor		2.1552	0.773	0.656
Dureza del magro		0.9234	0.638	0.432
Jugosidad		0.9012	0.523	0.363
Sabor salado		1.3192	0.574	0.402
Intensidad del sabor		1.3212	0.472	0.294
Persistencia del sabor		1.3352	0.568	0.316
Sabor curado		1.5853	0.538	0.352
Sabor rancio		0.6585	0.312	0.251

4.3 Resultados del artículo “MRI-computer vision on fresh and frozen-thawed beef: Optimization of methodology for classification and quality prediction”

A continuación, se presentan y discuten los resultados correspondientes al tercer artículo. Este trabajo se orienta a la clasificación de muestras de ternera frescas (F) y congeladas y descongeladas (FT), mediante parámetros físico-químicos (humedad, actividad del agua, L*, a*, b*) y técnicas de visión por computador con MRI. Se trata de estudiar las consecuencias que produce en la carne el efecto de congelar la carne y posteriormente descongelarla, para ver si es posible diseñar una metodología que distinga carne fresca de carne que ha sido congelada previamente.

La figura 4.7 muestra el biplot del análisis de componentes principales (PCA) de parámetros fisicoquímicos de muestras frescas (F) y congeladas-descongeladas (FT). Se observa que dos componentes principales representaron el 70,76% de la varianza total (50,37% para PC1 y 20,39% para PC2). Las muestras frescas (F) y las congeladas-descongeladas (FT) se ubican en los cuatro cuadrantes, no estando bien separadas. Esto puede explicarse por la ausencia de diferencias significativas ($p > 0,05$) en los parámetros fisicoquímicos entre los lotes de muestras frescas (F) y descongeladas (FT) (Tabla 1). Sin embargo, caben mencionar las diferencias notables en los valores medios de humedad y L* entre muestras frescas y descongeladas, aunque no difirien significativamente, lo que puede explicarse por la alta desviación estadística en estos dos parámetros. De hecho, previamente también se han descrito diferencias en el porcentaje de humedad y algunas coordenadas de color entre jamones frescos y congelados-descongelados [64] y se atribuyeron a la liberación de agua durante el proceso de descongelación. Este aspecto también puede estar relacionado con la variabilidad en los valores de humedad y L*, debido a que no es fácil retener el agua del interior en la superficie de las muestras congeladas-descongeladas.

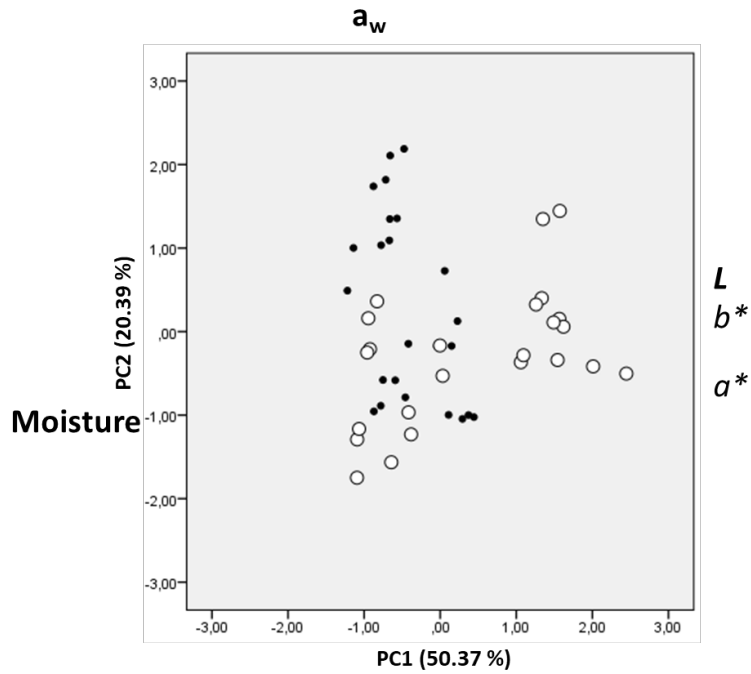


Figura 4.7. Biplot del análisis de componentes principales de los parámetros físico-químicos.

La figura 4.8 muestra imágenes de resonancia magnética de muestras frescas (F) y congeladas-descongeladas (FT) sin procesar. El color gris claro ilustra la parte magra del trozo de carne, mientras que el color gris oscuro representa la grasa. Es difícil discernir alguna diferencia visual entre las imágenes F y FT sin procesar. Como máximo, se puede señalar un color gris más claro del magro en las muestras crudas FT en comparación con las crudas F. Esto puede explicarse por la liberación de agua durante la congelación-descongelación, ya que las secuencias ponderadas en T1 de la resonancia magnética detectan hidrógeno y otras características como la fluidez de las grasas y la retención de agua, que aumentan el tiempo de relajación en T1 [65].

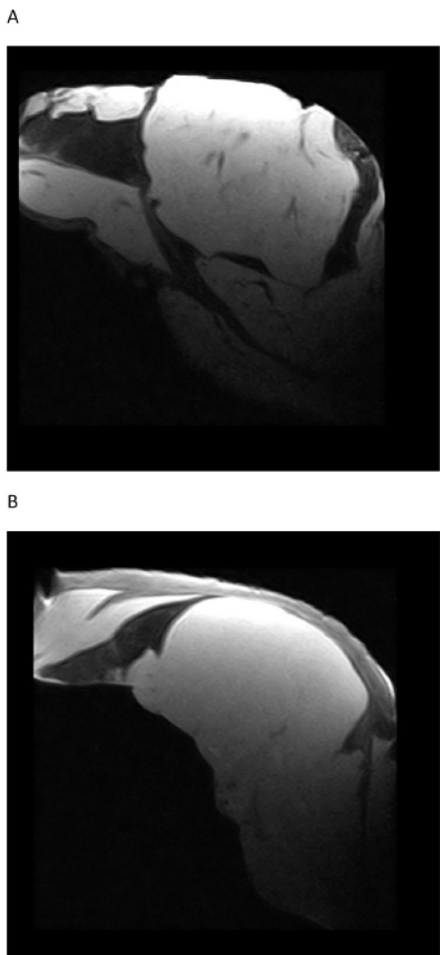


Figura 4.8. Imágenes MRI de un lomo de ternera fresco (A) y descongelado (B).

La Tabla 4.11 describe las medidas de calidad (precisión, recall y F-score) de los resultados de clasificación entre muestras frescas (F) y descongeladas (FT) mediante diferentes combinaciones de algoritmos de extracción de características (Gabor, Fractal y Clásicos) y regresores (RF, CFOREST y SVM). Los valores más altos de precisión, recall y F-score se encontraron al aplicar algoritmos de fractales en combinación con cualquiera de los regresores. Los mejores resultados se obtuvieron con el regresor RF (1.000 en todos los casos). Los algoritmos Clásicos y Gabor ofrecieron valores más bajos para estas medidas de clasificación de calidad. Estos resultados señalan la capacidad del análisis computacional (Fractal-RF) para diferenciar muestras de ternera fresca (F) de muestras de ternera descongelada (FT). Los altos valores de precisión, recall y F-score obtenidos con fractales pueden indicar que las muestras de carne descongelada (FT) tienen una influencia mucho mayor en el patrón de repeticiones de la resonancia magnética que en los niveles de gris o la distribución espacial analizadas por los algoritmos Clásicos y Gabor, respectivamente. Según

[60], en lomos de cerdo, las medidas instrumentales de color están más relacionadas con el patrón de repeticiones que con los niveles de gris, mientras que estos últimos están más fuertemente relacionados con los parámetros relacionados con la humedad.

Tabla 4.11. Resultados de la clasificación de los lomos frescos y descongelados por diferentes combinaciones de algoritmos.

		CLASICO		FRACTAL		GABOR	
		Fresco	Descongelado	Fresco	Descongelado	Fresco	Descongelado
CFOREST	Precision	0.683	0.745	0.988	1.000	0.682	0.738
	Recall	0.755	0.672	1.000	0.988	0.758	0.652
	F-score	0.717	0.707	0.994	0.994	0.718	0.693
RF	Precision	0.685	0.776	1.000	1.000	0.684	0.752
	Recall	0.748	0.736	1.000	1.000	0.789	0.665
	F-score	0.715	0.751	1.000	1.000	0.732	0.710
SVM	Precision	0.657	0.778	0.964	1.000	0.780	0.648
	Recall	0.788	0.644	1.000	0.963	0.528	0.854
	F-score	0.717	0.704	0.982	0.981	0.630	0.737

Además de las medidas de clasificación de calidad, también se considera el coste computacional para seleccionar la combinación más adecuada de algoritmo extracción de característica y regresor. El costo computacional de los diferentes algoritmos fractales es $O(N^3)$ para CFA, $O(N^2 \log n)$ para FTA y $O(N^2)$ para OPFTA. Los algoritmos clásicos son métodos estadísticos basados en la relación entre pares de píxeles, píxeles vecinos y también miden tramos de niveles de gris en una imagen. Combinados, estos algoritmos tienen un coste computacional de $O(N^3)$ [61]. Las características de Gabor se basan en las respuestas del filtro Gabor a una imagen de entrada determinada. Las respuestas de la imagen se calculan para un conjunto de filtros sintonizados en varias orientaciones y frecuencias. La técnica más sencilla para realizar la operación de filtrado es implementar la convolución en el dominio espacial. La complejidad de la convolución depende directamente del tamaño de la máscara de convolución (en este caso, la máscara es el filtro Gabor). La complejidad de calcular la respuesta del filtro para un punto es $O(M^2)$, donde M es el ancho y el alto de la máscara. Si

el filtrado se realiza en toda la imagen de tamaño $N \times N$, la complejidad se vuelve $O(M^2 N^2)$ [66].

Al analizar el coste computacional de los 3 regresores, RF implica un costo de tiempo de $O(M m n \log(n))$, siendo “M” el número de árboles, “m” el número de características y “n” el número de muestras en el conjunto de entrenamiento [28]. Como CForest es un tipo de implementación de RF, la complejidad computacional es similar. Los requisitos temporales y espaciales de los SVM aumentan rápidamente con la cantidad de vectores de entrenamiento. El núcleo de un SVM es un problema de programación cuadrática, que separa los vectores de soporte del resto de los datos de entrenamiento. El entrenamiento SVM estándar alcanza un tiempo y espacio computacional de $O(n^3)$ y $O(n^2)$, respectivamente, donde “n” es el tamaño del conjunto de entrenamiento, por lo tanto, SVM es computacionalmente inviable en conjuntos de datos muy grandes [30].

Así, considerando los costes computacionales y los resultados obtenidos al aplicar las medidas de clasificación de calidad, la combinación más adecuada sería Fractal-RF.

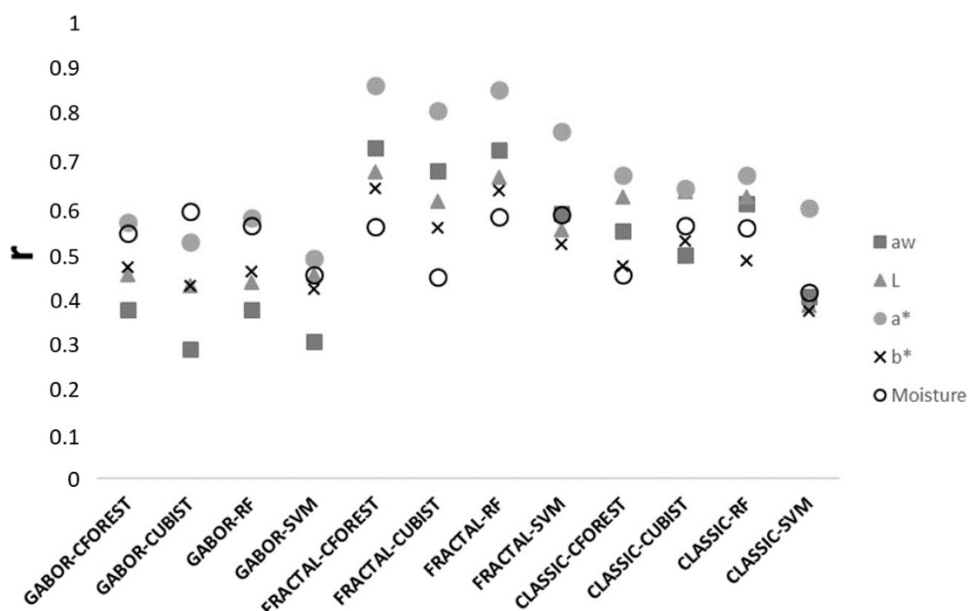


Figura 4.9. Coeficientes de correlación para las predicciones de parámetros fisicoquímicos en lomos frescos de ternera.

La Fig. 4.9 muestra los coeficientes de correlación para las ecuaciones de predicción de parámetros fisicoquímicos de muestras de carne de ternera fresca y descongelada. Como se puede observar, en general, la aplicación de Fractal logró coeficientes de correlación más

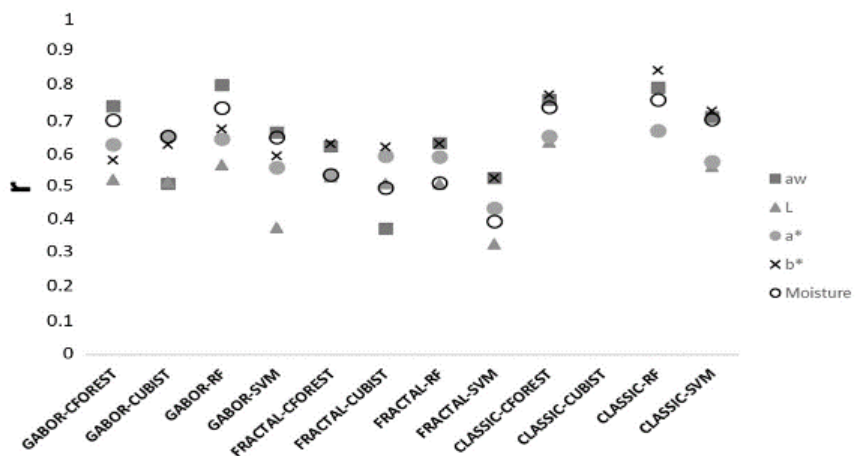
altos (0.44 - 0.86) en comparación con los algoritmos Clásico (0.37 - 0.67) y Gabor (0.28 - 0.59). Más específicamente, se observa que el coeficiente de correlación más alto para a^* se obtuvo con Fractal, y para la mayoría de las características de calidad, Fractal logró coeficientes de correlación más altos que Gabor. Un estudio previo en lomos de cerdo también ha encontrado resultados de predicción precisos al aplicar diferentes algoritmos Fractal para analizar imágenes de resonancia magnética [60]. Los valores de los coeficientes de correlación obtenidos por estos autores fueron ligeramente superiores a los encontrados en el presente estudio, y pueden atribuirse al diferente procedimiento de validación que se llevó a cabo con particiones del conjunto de datos en este trabajo, mientras que [60] aplicaron el método de selección de atributos que ha sido descrito como un protocolo bastante optimista [67]. Además, [60] y [59] señalaron diferencias en los coeficientes de correlación según el parámetro analizado y el algoritmo. Encontraron coeficientes de correlación más altos para el porcentaje de grasa, el contenido de sal y las coordenadas de color cuando usaron Fractal en comparación con los algoritmos Clásicos, mientras que los coeficientes de correlación para la humedad y la actividad del agua fueron mayores con Clásicos que con Fractal. En el presente estudio, los parámetros que obtuvieron los coeficientes de correlación más altos no difirieron notablemente entre los algoritmos: a^* al aplicar Fractal, a^* y humedad al usar Gabor y a^* y L^* para Clásicos.

Con respecto al regresor, se lograron coeficientes de correlación ligeramente más altos cuando se utilizó CForest y RF en comparación con Cubist y SVM (Fig. 4.9). Así, para la predicción de la humedad, la actividad del agua y los parámetros instrumentales de color de muestras frescas, puede estar indicada la aplicación de Fractal en combinación con CForest o RF. Considerando en detalle los coeficientes de correlación, se encontró la misma combinación óptima de regresores algorítmicos para cada parámetro individual para la mayoría de los parámetros fisicoquímicos: Fractal-CForest para la actividad del agua y coordenadas instrumentales de color, y Gabor-Cubist para la humedad.

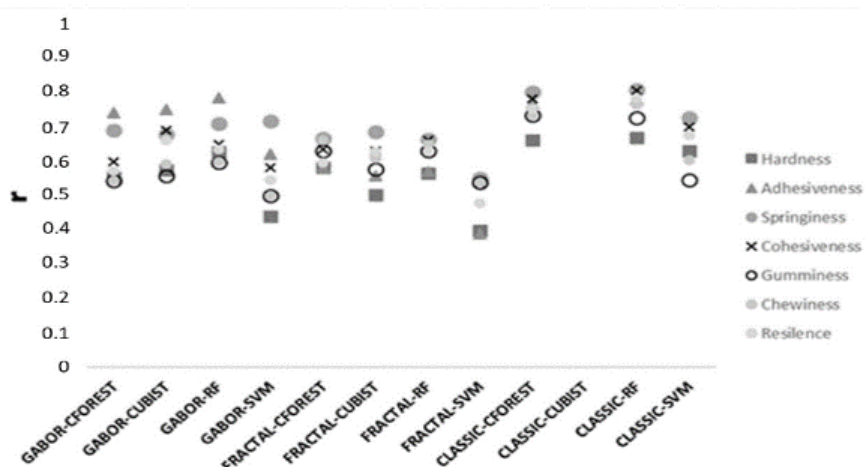
En el presente estudio también se evaluó la predicción de los parámetros de calidad de muestras de carne de ternera descongelada y cocinada, a partir de imágenes de resonancia magnética de muestras frescas. La Fig. 4.10 describe los coeficientes de correlación de las ecuaciones de predicción para las características fisicoquímicas (Fig. 4.10.A), textura (Fig. 4.10.B) y sensoriales (Fig. 4.10.C) de ternera descongelada y cocinada en función de las características extraídas de las imágenes MRI mediante los algoritmos de extracción de

características a partir de ternera fresca, mediante diferentes combinaciones algoritmo extractor-regresor. En este caso, para las características fisicoquímicas, de textura y sensoriales, los coeficientes de correlación más altos se obtuvieron con el algoritmo Clásicos (0.56–0.85, 0.55–0.81 y 0.61–0.85, respectivamente), encontrándose valores más bajos al aplicar Gabor (0.38–0.80, 0.44–0.79 y 0.52–0.79, respectivamente) y Fractal (0.33–0.63, 0.39–0.69 y 0.40–0.73, respectivamente). En cuanto a los regresores, cabe señalar que, en general, RF obtuvo los mayores coeficientes de correlación, seguido de CForest y SVM. Por lo tanto, la mejor combinación de algoritmo extractor-regresor para la predicción de características fisicoquímicas, de textura y sensoriales de muestras de carne de ternera descongelada y cocinada en función muestras de ternera descongelada parece ser la RF clásica. Por lo tanto, la mejor combinación de algoritmo extractor-regresor para la predicción de características fisicoquímicas, de textura y sensoriales de muestras de carne de ternera descongelada y cocida es Clásicos-RF. Al igual que ocurrió en la predicción de parámetros físico-químicos de muestras frescas, la combinación elegida es la óptima para la mayoría de las características analizadas, con sólo algunas excepciones: Gabor-RF para actividad de agua y adhesividad y Clásicos-CForest para elasticidad. Además, cabe mencionar que esta combinación óptima para la predicción de características de carne de ternera cocinada (Clásicos-RF) es diferente a la propuesta para la predicción de parámetros físico-químicos de carne vacuna fresca (Fractal-CForest). Esto concuerda con un trabajo previo enfocado en resonancia magnética para predecir atributos sensoriales de lomos curados [68], obteniendo resultados diferentes. Estos resultados son bastante interesantes y pueden indicar la necesidad de ajustar las técnicas de visión por ordenador, especialmente el algoritmo para analizar las imágenes de resonancia magnética, al tipo de muestra para lograr una predicción precisa de las características de calidad.

A)



B)



C)

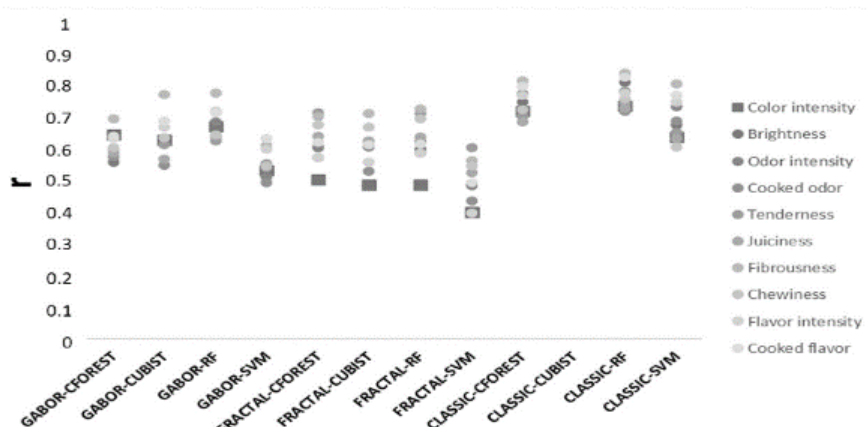


Figura 4.10. Coeficientes de correlación para las predicciones de parámetros fisicoquímicos, textura instrumental y parámetros sensoriales en lomos de ternera cocinados.

Capítulo 5

5. Conclusiones

Una vez presentados los objetivos y materiales empleados en la realización de las investigaciones de la presente Tesis Doctoral, y después de la presentación del diseño experimental, la metodología seguida (en los tres artículos que forman el compendio), tras la presentación y discusión de resultados, a continuación, se presentan las conclusiones.

La primera conclusión es que se ha podido realizar una predicción de todas las características de calidad de los productos cárnicos usados en los experimentos (lomos de cerdos alimentados con pienso, lomos de cerdos alimentados con bellota, lomos de ternera y los mismos productos tras ser congelados y descongelados). Las predicciones se han alcanzado con altas correlaciones entre los valores obtenidos en los experimentos realizados en esta Tesis con respecto a los valores obtenidos mediante técnicas tradicionales, realizados por expertos en Tecnología de los Alimentos.

Se han podido realizar predicciones de todos los grupos de características de calidad habitualmente empleados en Tecnología de los Alimentos. Esto es, las predicciones realizadas son válidas tanto para el grupo de características físico-químicas, como para las características de texturas de Tecnología de los Alimentos e igualmente también son válidas para el grupo de características sensoriales de calidad.

Se han realizado experimentos considerando algoritmos de extracción de características basados en 3 algoritmos clásicos de texturas, en filtros Gabor, en Wavelet y en 3 algoritmos

de fractales, combinados con 14 algoritmos de aprendizaje automático. De entre todas las combinaciones posibles entre algoritmos de extracción de características y algoritmos de aprendizaje automático, para cada una de las características de calidad se propone la mejor combinación posible, que sería aquella en que se obtienen las correlaciones más altas entre los métodos presentados en esta Tesis y los métodos tradicionales de Tecnología de los Alimentos.

Finalmente, y como conclusiones colaterales, también se ha propuesto un protocolo para determinar la mejor configuración de dispositivos MRI para el óptimo funcionamiento de los algoritmos de extracción de características en conjunción de los algoritmos de aprendizaje automático, así como la consideración de los máximos volúmenes de interés (VOI) sobre los que centrar la extracción de características.

Referencias

- [1] Shrestha, L., Crichton, S., Kulig, B., Kiesel, B., Hensel, Ol, Sturm, B., “Comparative analysis of methods and model prediction performance evaluation for continuous online non-invasive quality assessment during drying of apples from two cultivars”, Thermal Science and Engineering Progress, vol. 18, pp. 100461, 2020.
- [2] Fowler, S. M., Wheeler, D., Morris, S., Mortimer, S. I., Hopkins, D. L., “Partial least squares and machine learning for the prediction of intramuscular fat content of lamb loin”, Meat Science, vol. 177, pp. 108505, 2021.
- [3] Cortez, P., Portelinha, M., Quinteiro, S., Pilão, V., Costa, A., “Lamb Meat Quality Assessment by Support Vector Machines”, Neural Processing Letters, vol. 24, pp. 41–51, 2016.
- [4] Neto, H.A., Tavares, W.L.F., Ribeiro, D.C.S.Z., Alves, R.C.O., Fonseca, L.M., Campos, S.V.A., “On the utilization of deep and ensemble learning to detect milk adulteration”, BioData Mining, vol. 12, pp. 1-13, 2019.
- [5] Pérez-Palacios, T., Caballero, D., Antequera, T., Durán, M.L., Ávila, M.M., Caro, A., “Optimization of MRI acquisition and texture analysis to predict physico-chemical parameters of loins by data mining”, Food Bioproc. Tech., vol. 10, pp. 750-758, 2017.
- [6] Caballero, D., Caro, A., Dahl, A. B., ErsbØll, B. K., Amigo, J. M., Pérez-Palacios, T., Antequera, T., “Comparison of different image analysis algorithms on MRI to predict physico-chemical and sensory attributes of loin”, Chemometrics and Intelligent Laboratory Systems, vol. 180, pp. 54–63, 2018.
- [7] Khulal, U., Zhao, J., Hu, W., Chen, Q., “Intelligent evaluation of total volatile basic nitrogen (TVB-N) content in chicken meat by an improved multiple level data fusion model”, Sensors and Actuators B: Chemical, vol. 238, pp. 337–345, 2017.
- [8] Li, H., Chen, Q., Zhao, J., Wu, M., “Nondestructive detection of total volatile basic nitrogen (TVB-N) content in pork meat by integrating hyperspectral imaging and colorimetric sensor combined with a nonlinear data fusion”, LWT- Food Science and Technology, vol. 63, pp. 268–274, 2015.

- [9] Zhao, M., Esquerre, C., Downey, G., O'Donnell, C. P., "Process analytical technologies for fat and moisture determination in ground beef - a comparison of guided microwave spectroscopy and near infrared hyperspectral imaging", *Food Control*, vol. 73, pp. 1082–1094, 2017.
- [10] Fantazzini, P., Gombia, M., Schembri, P., Simoncini, N., Virgili, R., "Use of magnetic resonance imaging for monitoring parma dry-cured ham processing", *Meat Science*, vol. 82 (2), pp. 219–227, 2009.
- [11] Antequera, T., Caro, A., Rodríguez, G., Pérez-Palacios, T., "Monitoring the ripening process of Iberian ham by computer vision on magnetic resonance imaging", *Meat Science*, vol. 76, pp. 561–567, 2007.
- [12] Manzocco, L., Anese, M., Marzona, S., Innocente, N., Lagazio, C., Nicoli, M.C., "Monitoring dry-curing of S. Daniele ham by magnetic resonance imaging", *Food Chem.*, vol. 141 (3), pp. 2246–2252, 2013.
- [13] Pérez-Palacios, T., Caballero, D., Caro, A., Rodríguez, P.G., Antequera, T., "Applying data mining and computer vision techniques to MRI to estimate quality traits in Iberian hams" *J. Food Eng.*, vol. 131, pp. 82–88, 2014.
- [15] Bernau, M., Kremer, P. V., Lauterbach, E., Tholen, E., Petersen, B., Pappenberger, E., Scholz, A. M., "Evaluation of carcass composition of intact boars using linear measurements from performance testing, dissection, dual energy x-ray absorptiometry (DXA) and magnetic resonance imaging (MRI)", *Meat Science*, vol. 104, pp. 58–66, 2015.
- [16] Lee, S., Lohumi, S., Lim, H. S., Gotoh, T., Cho, B. K., Jung, S., "Determination of intramuscular fat content in beef using magnetic resonance imaging", *Journal of the Faculty of Agriculture*, vol. 60(1), pp. 157–162, 2015.
- [17] Caballero, D., Pérez-Palacios, T., Caro, A., Ávila, M., Antequera, T., "Optimization of the image acquisition procedure in low-field MRI for non-destructive analysis of loin using predictive models", *PeerJ Comput. Sci.*, vol. 7:e583, <http://doi.org/10.7717/peerjcs>, 2021.
- [18] Haralick, R. M., Shanmugam, K., Dinstein, I., "Textural features for image classification. IEEE Trans", *Mobile Comput.*, vol. 3 (6), pp. 610–621, 1973.

- [19] Haralick, R.M., Shapiro, L.G., Computer and Robot Vision, Addison-Wesley, Chicago, Illinois, U.S.A, 1993.
- [20] Sonka, M., Hlavac, V., Boyle, R., Image Processing, Analysis and Machine Vision. International Thomsom Publishing, ITP, Stanford, California, U.S.A., 1999.
- [21] Sun, C., Wee, G., “Neighbouring gray level dependence matrix”, Comput. Vis. Graph Image Process, vol. 23, pp. 341–352, 1982.
- [22] Galloway, M.M., “Texture classification using gray level run length”, Comput. Graph. Image Process., vol. 4, pp. 172–179, 1975.
- [23] Siew, L. H., Hodgson, R.M., Wood, E.J., “Texture measures for carpet wear assessment”, IEEE Transactions on Pattern, Anal. Mach. Intell., vol. 10 (1), pp. 92–10, 1988.
- [24] Minhas, S., Javed, M. Y., “Iris feature extraction using Gabor filter”, International Conference on Emerging Technologies, pp. 252-255, 2009.
- [25] Mallat, S., “A theory for multiresolution signal descomposition: the wavelet representation”, IEEE Trans. on Pattern Analysis and Machine Intelligence, vol. 11(7), pp. 674–693, 1989.
- [26] Mandelbrot, B. B., The Fractal Geometry of Nature, McMillan Learning, 1982.
- [27] Breiman, L., Random Forests. Machine Learning, vol. 45, pp. 5-32, 2001.
- [28] Hassine, K., Erbad, A., Hamila, R., “Important Complexity Reduction of Random Forest in Multi-Classification Problem”, 15th International Wireless Communications & Mobile Computing Conference (IWCMC), pp. 226-231, 2019.
- [29] Chang, C.C., Lin, C.J., LIBSVM: a library for Support Vector Machines. [Online]. Available:
- [30] Tsang, I. W., Kwok, J. T., Cheung, P., “Core Vector Machines: Fast SVM Training on Very Large Data Sets”, Journal of Machine Learning Research, vol. 6, pp. 363-392, 2005.
- [31] Lorena, A.C., Jacintho, L.F.O., Siqueira, M.F., DeGiovanni, R., Lohmann, L.G., de Carvalho, A.C.P.L.F., Yamamoto, M., “Comparing machine learning classifiers in potential distribution modelling”, Expert Systems with Applications, vol. 38-5, pp. 5268-5275, 2011.

- [32] Chambers, J. M., “Chapter 4. Linear models” in Statistical Models in S, Eds J. M. Chambers and T. J. Hastie, Wadsworth & Brooks/Cole, 1992.
- [33] Goeman J.J., “L-1 Penalized Estimation in the Cox Proportional Hazards Model”, Biometrical Journal, vol. 52-1, pp. 70-84, 2010.
- [34] Kapelner, A., Bleich, J., “bartMachine: Machine Learning with Bayesian Additive Regression Trees”, Journal of Statistical Software, vol. 70-4, pp. 1-40, 2016.
- [35] Chipman, H.A., George, E., McCulloch, R.E., “BART: Bayesian Additive Regressive Trees”, The Annals of Applied Statistics, vol. 4(1), pp. 266—298, 2010.
- [36] MacKay, D. J. C., “Bayesian interpolation”, Neural Computation, vol. 4-3, pp. 415-447, 1992.
- [37] Foresee, F.D., Hagan, M. T., “Gauss-Newton approximation to Bayesian regularization”, Proceedings of the International Joint Conference on Neural Networks, pp. 1930–1935, 1997.
- [38] Nguyen, D., Widrow, B., “Improving the learning speed of 2-layer neural networks by choosing initial values of the adaptive weights”, Proceedings of the IJCNN, vol. 3, pp. 21-26, 1990.
- [39] Koenker, R., Mizera, I., “Convex optimization in R”, Journal of Statistical Software, vol. 60, pp. 1-23, 2014.
- [40] Wang, Y., Witten, I. H., “Induction of model trees for predicting continuous classes”, Proceedings of the European Conference on Machine Learning, 1997.
- [41] Quinlan, R., “Learning with continuous classes”, Proceedings of the Australian Joint Conference on Artificial Intelligence, pp. 343-348, 1992.
- [42] Quinlan, R., “Combining instance-based and model-based learning”, Proceedings of the Tenth International Conference on Machine Learning, pp. 236-243, 1993.
- [43] Friedman, J.H., “Multivariate Adaptive Regression Splines (with discussion)”, Annals of Statistics, vol. 19-1, pp. 1-141, 1991.
- [44] Friedman, J.H., Fast MARS. Stanford University Department of Statistics, Technical Report 110, 1993.

- [45] Kaggle, Computational Complexity of Machine Learning Models. [Online]. Available: <https://www.kaggle.com/general/263127>. Accessed on: Jun-2022.
- [46] Parviainen, E., Riihimäki, J., “A Connection between Extreme Learning Machine and Neural Network Kernel”, Knowledge Discovery, Knowledge Engineering and Knowledge Management, Springer, vol. 272, pp. 122-135, 2013.
- [47] Walker, J.S., A Primer on Wavelets and their Scientific Applications, Chapman and Hall, CRC, 2008.
- [48] Laine, A., Fan, J., “Texture classification by wavelet packet signatures”, IEEE Trans. Pattern Anal., vol. 15(11), pp. 1186–1191, 1993.
- [49] Randen, T., Husoy, J.H., “Filtering for texture classification: A comparative study”, IEEE Trans. Pattern Anal., vol. 21(4), pp. 291–310, 1999.
- [50] Aggarwal, N., Agrawal, R. K., “First and second order statistics features for classification of magnetic resonance brain images”, Journal of Signal and Information Processing, vol. 3, pp. 146–153, 2012.
- [51] Peckingpaugh, S., “An improved method for computing gray-level co-occurrence matrix-based texture measured”, Computer Vision, Graphics and Image Processing, vol. 53, pp. 574–580, 1991.
- [52] Amayeh, G., Tavakkoli, A, Bebis, G., “Accurate and Efficient Computation of Gabor Features in Real-Time Applications”, Advances in Visual Computing, 5th International Symposium, ISVC, Proceedings, Part I, pp. 243-252, 2019.
- [53] Tutz G, Binder H. Generalized additive modeling with implicit variable selection by likelihood-based boosting. Biometrics. 2006 Dec;62(4):961-71.
- [54] Paul H. C. Eilers, Brian D. Marx "Flexible smoothing with B-splines and penalties," Statistical Science, Statist. Sci. 11(2), 89-121, (May 1996)
- [55] Pérez-Palacios, T., Ruiz, J., Martin, D., Muriel, E., Antequera, T., “Comparison of different methods for total lipid quantification”, Food Chemistry, vol. 110, pp. 1025–1029, 2008.

- [56] TTC (Texture Technologies Company), Overview of Texture Profile Analysis. [Online]. Available: <https://texturetechnologies.com/resources/texture-profile-analysis#settings-and-standards>. Accessed on: Jun-2022.
- [57] González-Mohino, A., Antequera, T., Ventanas, S., Caballero, D., Mir-Bel, J., Pérez-Palacios, T., “Near-infrared spectroscopy-based analysis to study sensory parameters on pork loins as affected by cooking methods and conditions”, *J. Sci. Food Agric.*, vol. 98-11, pp. 4227–4423, 2018.
- [58] Colton, T., *Statistical in Medicine*, Little Brown and Co., New York, NJ, 1974.
- [59] Caballero, D., Antequera, T., Caro, A., Ávila, M.d.M., G Rodríguez, P. and Pérez-Palacios, T. (2017), Non-destructive analysis of sensory traits of dry-cured loins by MRI–computer vision techniques and data mining. *J. Sci. Food Agric.*, 97: 2942-2952.
- [60] D. Caballero et al., “Prediction of pork quality parameters by applying fractals and data mining on MRI”, *Food Res. Int.*, vol. 99, pp. 739–747, septiembre de 2017.
- [61] D. Caballero et al., “Analysis of MRI by fractals for prediction of sensory attributes: A case study in loin”, *J. Food Eng.*, vol. 227, pp. 1–10, Junio de 2018.
- [62] Caballero, D., Caro, A., Amigo, J.M., Dahl, A.B., Ersbøll, B.K., Pérez-Palacios, T. (2017). Development of a New Fractal Algorithm to Predict Quality Traits of MRI Loins. In: Felsberg, M., Heyden, A., Krüger, N. (eds) *Computer Analysis of Images and Patterns. CAIP 2017. Lecture Notes in Computer Science()*, vol 10424.
- [63] M. M. Ávila et al., “Magnetic Resonance Imaging, texture analysis and regression techniques to non-destructively predict the quality characteristics of meat pieces”, *Eng. Appl. Artif. Intell.*, vol. 82, pp. 110–125, Junio de 2019.
- [64] Pérez-Palacios T, Ruiz J, Martín D, Barat JM, Antequera T. Pre-cure freezing effect on physicochemical, texture and sensory characteristics of Iberian ham. *Food Sci Technol Int.* 2011 Apr;17(2):127-33.
- [65] L. R. B, Ed., *The MRI manual*, 2a ed. St. Louis: Mosby, 1998.

- [66] Amayeh, G., Tavakkoli, A., Bebis, G. (2009). Accurate and Efficient Computation of Gabor Features in Real-Time Applications. In: Bebis, G., et al. Advances in Visual Computing. ISVC 2009. Lecture Notes in Computer Science, vol 5875. Springer, Berlin, Heidelberg.
- [67] M. M. Ávila et al., "Magnetic Resonance Imaging, texture analysis and regression techniques to non-destructively predict the quality characteristics of meat pieces", Eng. Appl. Artif. Intell., vol. 82, pp. 110–125, Junio de 2019.
- [68] Caballero, D., Antequera, T., Caro, A. et al. Data Mining on MRI-Computational Texture Features to Predict Sensory Characteristics in Ham. Food Bioprocess Technol 9, 699–708 (2016).
- [69] J. P. Torres, A. Caro, M. D. M. Ávila, T. Pérez-Palacios, T. Antequera and P. G. Rodríguez, "A Computer-Aided Inspection System to Predict Quality Characteristics in Food Technology," in IEEE Access, vol. 10, pp. 71496-71507, 2022
- [70] T. Perez-Palacios, M. Ávila, T. Antequera, J. P. Torres, A. González-Mohino y A. Caro, "MRI-computer vision on fresh and frozen-thawed beef: Optimization of methodology for classification and quality prediction", Meat Sci., vol. 197, p. 109054, Marzo de 2023.
- [71] D. Caballero et al., "An experimental protocol to determine quality parameters of dry-cured loins using low-field Magnetic Resonance Imaging", J. Food Eng., vol. 313, p. 110750, Enero de 2022.
- [72] R. Molano et al., "Finding the Largest Volume Parallelepipedon of Arbitrary Orientation in a Solid," in IEEE Access, vol. 9, pp. 103600-103609, 2021
- [73] Daniel Caballero, Trinidad Pérez-Palacios, Andrés Caro & Teresa Antequera (2023) Use of Magnetic Resonance Imaging to Analyse Meat and Meat Products Non-destructively, Food Reviews International, 39:1, 424-440
- [74] Pérez-Palacios, T., Antequera, T., Durán, M. L., Caro, A., Rodríguez, P. G., & Ruiz, J. (2010). MRI-based analysis, lipid composition and sensory traits for studying Iberian dry-cured hams from pigs fed with different diets. In Food Research International (Vol. 43, Issue 1, pp. 248–254). Elsevier BV.

- [75] Pérez-Palacios, T., Antequera, T., Molano, R., Rodríguez, P. G., & Palacios, R. (2010). Sensory traits prediction in dry-cured hams from fresh product via MRI and lipid composition. In *Journal of Food Engineering* (Vol. 101, Issue 2, pp. 152–157). Elsevier BV.
- [76] Pérez-Palacios, T., Caballero, D., Antequera, T., Durán, M. L., Ávila, M., & Caro, A. (2017). Optimization of MRI Acquisition and Texture Analysis to Predict Physico-chemical Parameters of Loins by Data Mining. In *Food and Bioprocess Technology* (Vol. 10, Issue 4, pp. 750–758). Springer Science and Business Media LLC.
- [77] Perez-Palacios, T., Caballero, D., González-Mohíno, A., Mir-Bel, J., & Antequera, T. (2019). Near Infrared Reflectance spectroscopy to analyse texture related characteristics of sous vide pork loin. In *Journal of Food Engineering* (Vol. 263, pp. 417–423). Elsevier BV.
- [78] Bernau, M., Kremer, P. V., Lauterbach, E., Tholen, E., Petersen, B., Pappenberger, E., & Scholz, A. M. (2015). Evaluation of carcass composition of intact boars using linear measurements from performance testing, dissection, dual energy X-ray absorptiometry (DXA) and magnetic resonance imaging (MRI). In *Meat Science* (Vol. 104, pp. 58–66). Elsevier BV.
- [79] Ávila, M.M., Caballero, D., Durán, M.L., Caro, A., Pérez-Palacios, T., Antequera, T. (2015). Including 3D-textures in a Computer Vision System to Analyze Quality Traits of Loin. In: Nalpantidis, L., Krüger, V., Eklundh, JO., Gasteratos, A. (eds) *Computer Vision Systems. ICVS 2015. Lecture Notes in Computer Science()*, vol 9163. Springer, Cham.
- [80] Ávila, M., Caballero, D., Antequera, T., Durán, M. L., Caro, A., & Pérez-Palacios, T. (2018). Applying 3D texture algorithms on MRI to evaluate quality traits of loin. In *Journal of Food Engineering* (Vol. 222, pp. 258–266). Elsevier BV.
- [81] Dietterich, T. G. (1998). Approximate Statistical Tests for Comparing Supervised Classification Learning Algorithms. In *Neural Computation* (Vol. 10, Issue 7, pp. 1895–1923). MIT Press - Journals.
- [82] Fayyad, U., Piatetsky-Shapiro, G., & Smyth, P. (1996). From Data Mining to Knowledge Discovery in Databases. *AI Magazine*, 17(3), 37.

- [83] Feig S. Comparison of costs and benefits of breast cancer screening with mammography, ultrasonography, and MRI. *Obstet Gynecol Clin North Am.* 2011 Mar;38(1):179-96, ix.
- [84] Seni, G., & Elder, J. F. (2010). Ensemble Methods in Data Mining. In *Synthesis Lectures on Data Mining and Knowledge Discovery*. Springer International Publishing.
- [85] Hastie, T., Tibshirani, R., & Friedman, J. (2009). *The Elements of Statistical Learning*. In *Springer Series in Statistics*. Springer New York.
- [86] Ladd ME, Bachert P, Meyerspeer M, Moser E, Nagel AM, Norris DG, Schmitter S, Speck O, Straub S, Zaiss M. Pros and cons of ultra-high-field MRI/MRS for human application. *Prog Nucl Magn Reson Spectrosc.* 2018 Dec;109:1-50.
- [87] Picouet, P. A., Gou, P., Fulladosa, E., Santos-Garcés, E., & Arnau, J. (2013). Estimation of NaCl diffusivity by computed tomography in the Semimembranosus muscle during salting of fresh and frozen/thawed hams. In *LWT - Food Science and Technology* (Vol. 51, Issue 1, pp. 275–280). Elsevier BV.
- [88] Torres, J.P., Ávila, M., Caro, A., Pérez-Palacios, T., Caballero, D. (2019). Non-destructively Prediction of Quality Parameters of Dry-Cured Iberian Ham by Applying Computer Vision and Low-Field MRI. In: Morales, A., Fierrez, J., Sánchez, J., Ribeiro, B. (eds) *Pattern Recognition and Image Analysis. IbPRIA 2019. Lecture Notes in Computer Science()*, vol 11867. Springer, Cham.
- [89] Ruiz, J., Ventanas, J., Cava, R., Timón, M. L., & García, C. (1998). Sensory characteristics of Iberian ham: influence of processing time and slice location. In *Food Research International* (Vol. 31, Issue 1, pp. 53–58). Elsevier BV.
- [90] Vestergaard, C., Erbou, S. G., Thauland, T., Adler-Nissen, J., & Berg, P. (2005). Salt distribution in dry-cured ham measured by computed tomography and image analysis. In *Meat Science* (Vol. 69, Issue 1, pp. 9–15). Elsevier BV.
- [91] J. C. S. Núñez, A. C. Lindo and P. G. Rodríguez, "A Preventive Secure Software Development Model for a Software Factory: A Case Study," in *IEEE Access*, vol. 8, pp. 77653-77665, 2020

- [92] Sancho, J. C., Caro, A., Ávila, M., & Bravo, A. (2020). New approach for threat classification and security risk estimations based on security event management. In Future Generation Computer Systems (Vol. 113, pp. 488–505). Elsevier BV.
- [93] Dag, A., Topuz, K., Oztekin, A., Bulur, S., & Megahed, F. M. (2016). A probabilistic data-driven framework for scoring the preoperative recipient-donor heart transplant survival. In Decision Support Systems (Vol. 86, pp. 1–12). Elsevier BV.
- [94] Antequera, T., Caballero, D., Grassi, S., Uttaro, B., & Perez-Palacios, T. (2021). Evaluation of fresh meat quality by Hyperspectral Imaging (HSI), Nuclear Magnetic Resonance (NMR) and Magnetic Resonance Imaging (MRI): A review. In Meat Science (Vol. 172, p. 108340). Elsevier BV.
- [95] Cabrera, M. C., & Saadoun, A. (2014). An overview of the nutritional value of beef and lamb meat from South America. In Meat Science (Vol. 98, Issue 3, pp. 435–444). Elsevier BV.
- [96] Carballo, J., & Jiménez, F. (2001). Refrigeración y congelación de carne y productos cárnicos. Enciclopedia de la carne y de los productos cárnicos, 1, 475-509.
- [97] Cheng S, Wang X, Li R, Yang H, Wang H, Wang H, Tan M. Influence of multiple freeze-thaw cycles on quality characteristics of beef semimembranous muscle: With emphasis on water status and distribution by LF-NMR and MRI. *Meat Sci*. 2019 Jan;147:44-52.
- [98] Cheng S, Wang X, Li R, Yang H, Wang H, Wang H, Tan M. Influence of multiple freeze-thaw cycles on quality characteristics of beef semimembranous muscle: With emphasis on water status and distribution by LF-NMR and MRI. *Meat Sci*. 2019 Jan;147:44-52.
- [99] Dag, A., Topuz, K., Oztekin, A., Bulur, S., & Megahed, F. M. (2016). A probabilistic data-driven framework for scoring the preoperative recipient-donor heart transplant survival. In Decision Support Systems (Vol. 86, pp. 1–12). Elsevier BV.
- [100] Evans, S. D., Nott, Kevin. P., Kshirsagar, A. A., & Hall, L. D. (1998). The effect of freezing and thawing on the magnetic resonance imaging parameters of water in beef, lamb and pork meat. In International Journal of Food Science & Technology (Vol. 33, Issue 3, pp. 317–328). Wiley.

- [101] Fawcett, T. (2006). An introduction to ROC analysis. In Pattern Recognition Letters (Vol. 27, Issue 8, pp. 861–874). Elsevier BV.
- [102] Frecka JC, Phinney DM, Yang X, Knopp MV, Heldman DR, Wick MP, Vodovotz Y. Assessment of chicken breast meat quality after freeze/thaw abuse using magnetic resonance imaging techniques. J Sci Food Agric. 2019 Jan 30;99(2):844-853.
- [103] Kohavi, R. (1995). A Study of Cross-Validation and Bootstrap for Accuracy Estimation and Model Selection. International Joint Conference on Artificial Intelligence.
- [104] Leygonie, C., Britz, T. J., & Hoffman, L. C. (2012). Impact of freezing and thawing on the quality of meat: Review. In Meat Science (Vol. 91, Issue 2, pp. 93–98). Elsevier BV.
- [105] Portanguen, S., Ikonic, P., Clerjon, S. et al. Mechanisms of Crust Development at the Surface of Beef Meat Subjected to Hot Air: An Experimental Study. Food Bioprocess Technol 7, 3308–3318 (2014).
- [106] Vafeiadis, T., Diamantaras, K. I., Sarigiannidis, G., & Chatzisavvas, K. Ch. (2015). A comparison of machine learning techniques for customer churn prediction. In Simulation Modelling Practice and Theory (Vol. 55, pp. 1–9). Elsevier BV.
- [107] Ávila, Mar & Caballero, Daniel & Fernández, Manuel & Torres Muñoz, Juan & Caro, Andres. (2018). Evaluation of different texture algorithms-regressors combinations to determine Iberian loin characteristics by MRI.
- [108] Teresa Antequera, Daniel Caballero, Juan Pedro Torres, Mar Ávila, Trinidad Pérez-Palacios. (2022). High-field vs. Low-field MRI scanners to analyse sensory attributes of dry-cured hams [Poster Presentation]. International Conference on the applications of magnetic resonance in food science (MRFOOD). Pág. 65.
- [109] Trinidad Perez-Palacios, Andrés Caro, Juan Pedro Torres, Mar Ávila, Teresa Antequera. (2022). Low Field MRI and computer vision to detect and characterize defective dry-cured hams [Poster Presentation]. International Conference on the applications of magnetic resonance in food science (MRFOOD). Pág. 66.